CFMR
COMITÉ FRANÇAIS DE MÉCANIQUE DES ROCHES

When Gas Builds Up, Do Clay-Rich Rocks (Re)Fracture?

Insights From Hydro-Mechanical Modelling for Nuclear Waste Repositories

Gilles CORMAN & Frédéric COLLIN

May 28, 2026 • Mines Paris (France)

This project has received funding from the European Union's Horizon 2020 research and innovation programme under grant agreement n° 847593.

eurad
European Joint Programme on Radioactive Waste Management

LIÈGE université

Introduction

A story of energy

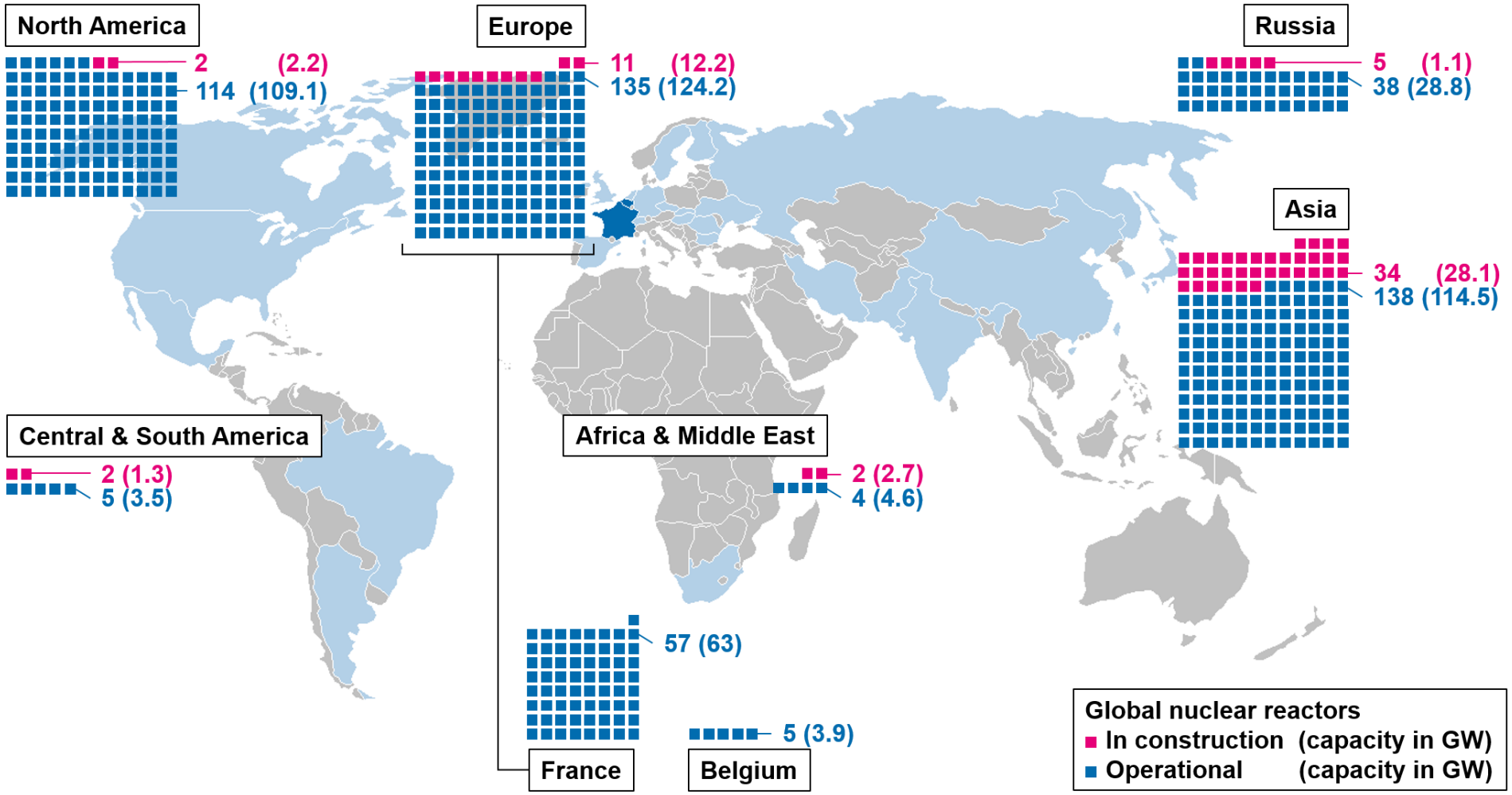

Data collected from [IAEA, 2025]

- 56 reactors under construction
- 441 operational reactors

9% of the global electric capacity *(2025)*

↓

Production of **long-lasting & high-level radioactive waste**, harmful to the biosphere

↓

Deep geological repository

Deep geological repository

© Fanghong

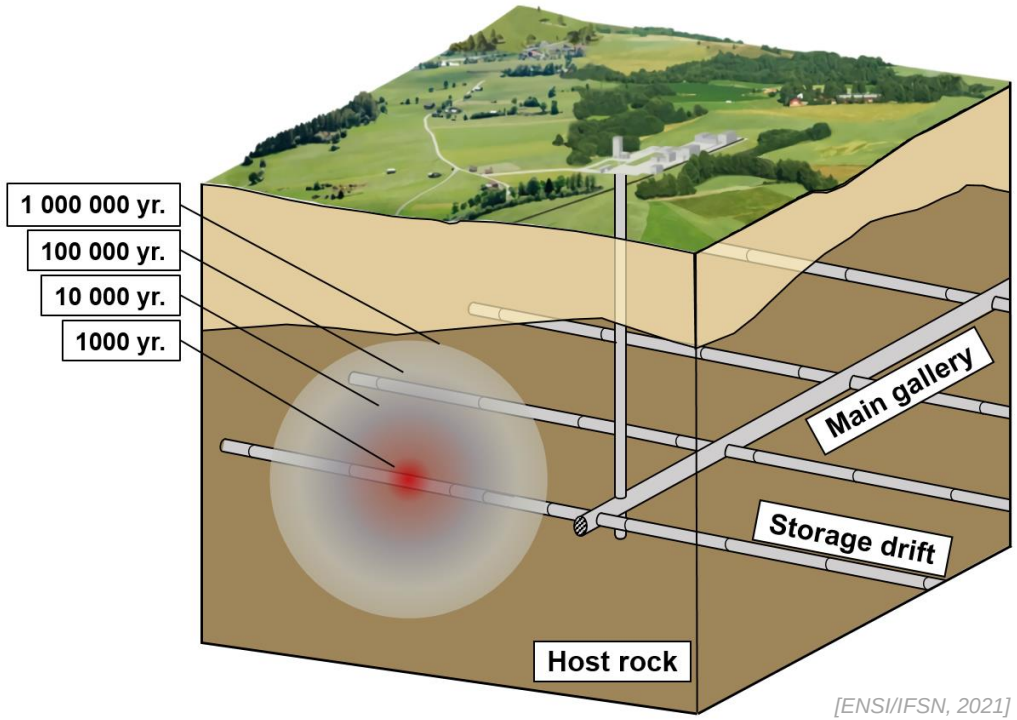

[ENSI/IFSN, 2021]

Deep geological repository

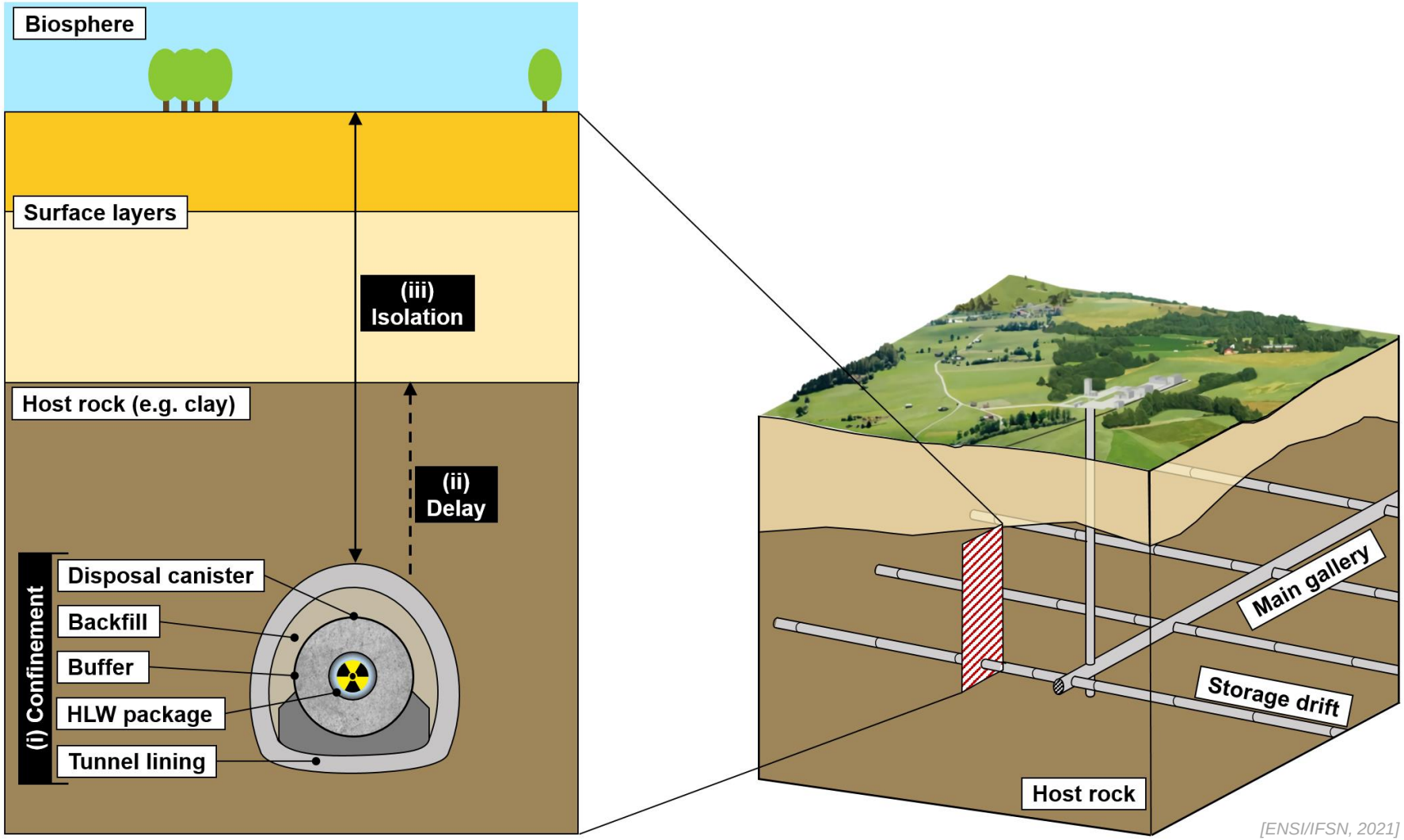

[ENSI/IFSN, 2021]

Deep geological repository

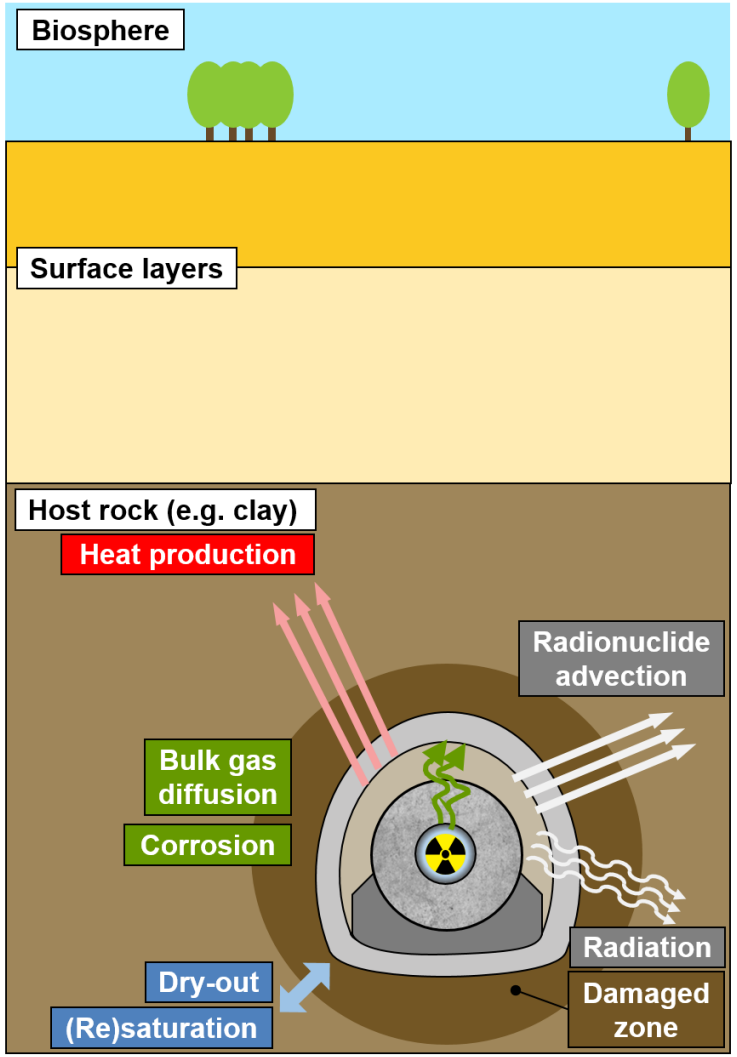

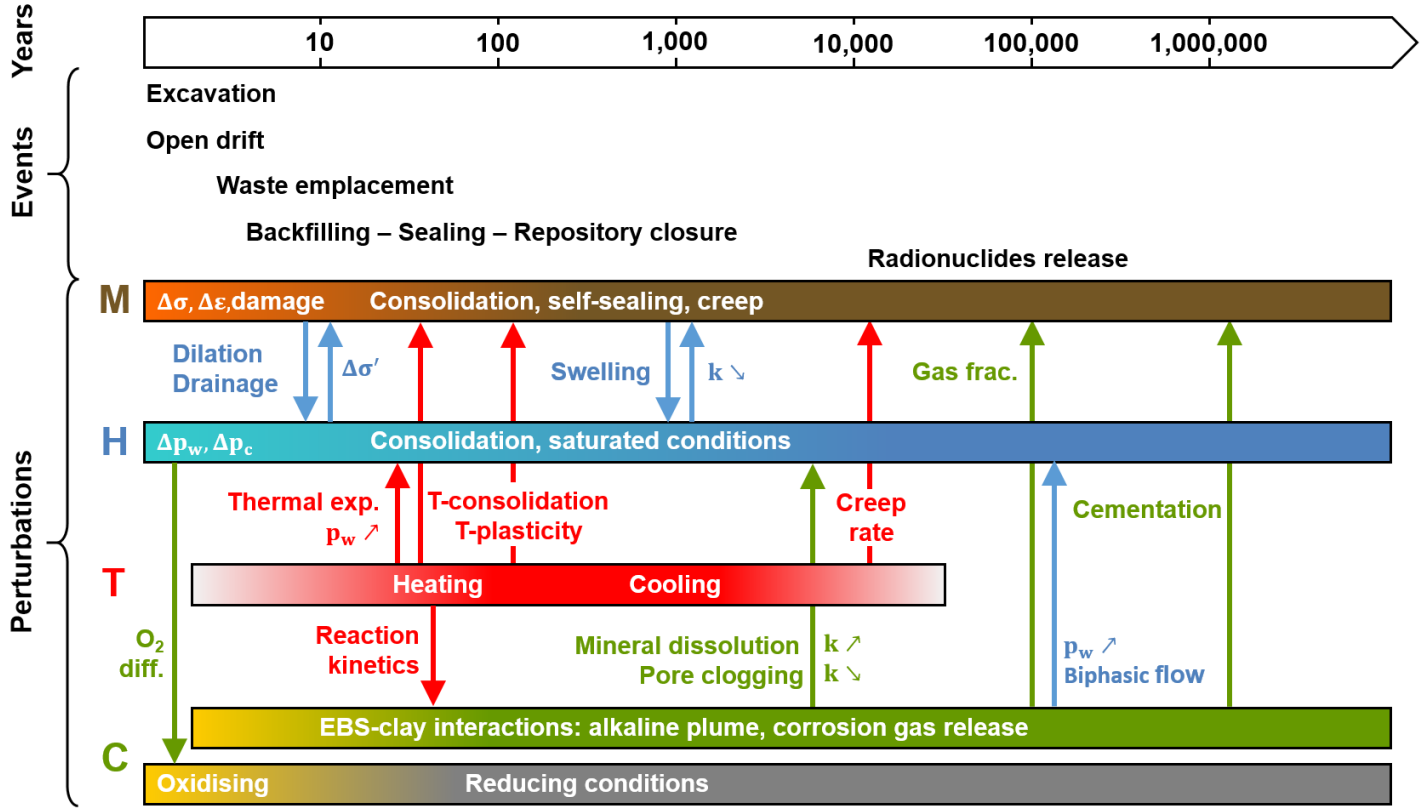

[Sillen, 2012]

Deep geological repository

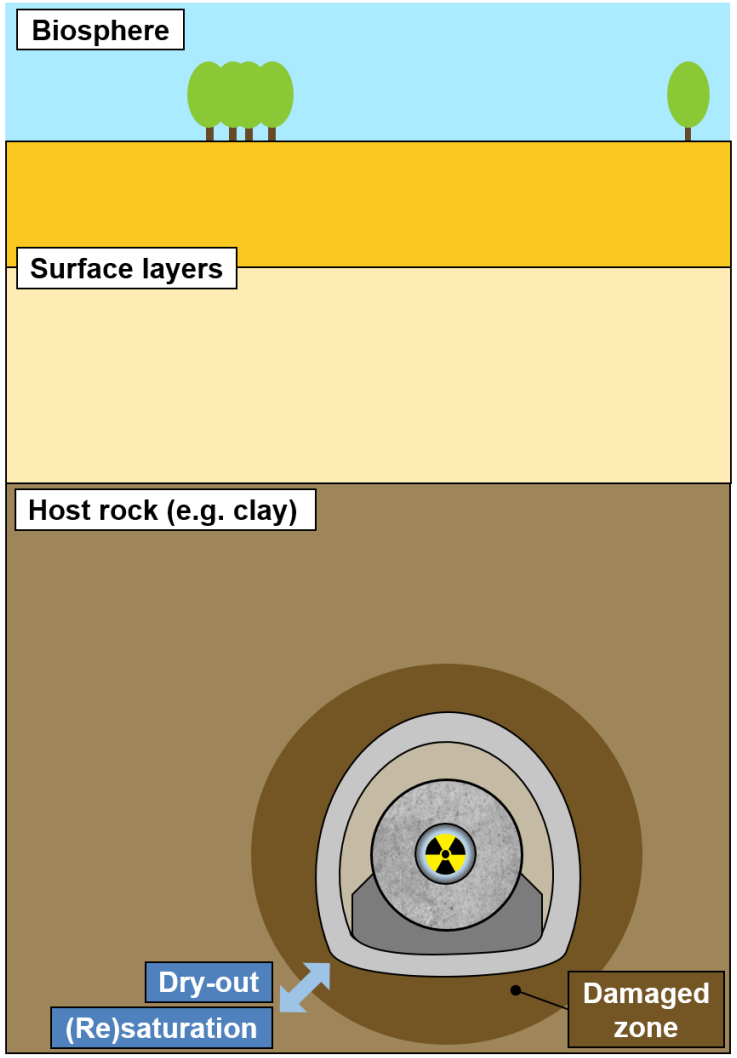

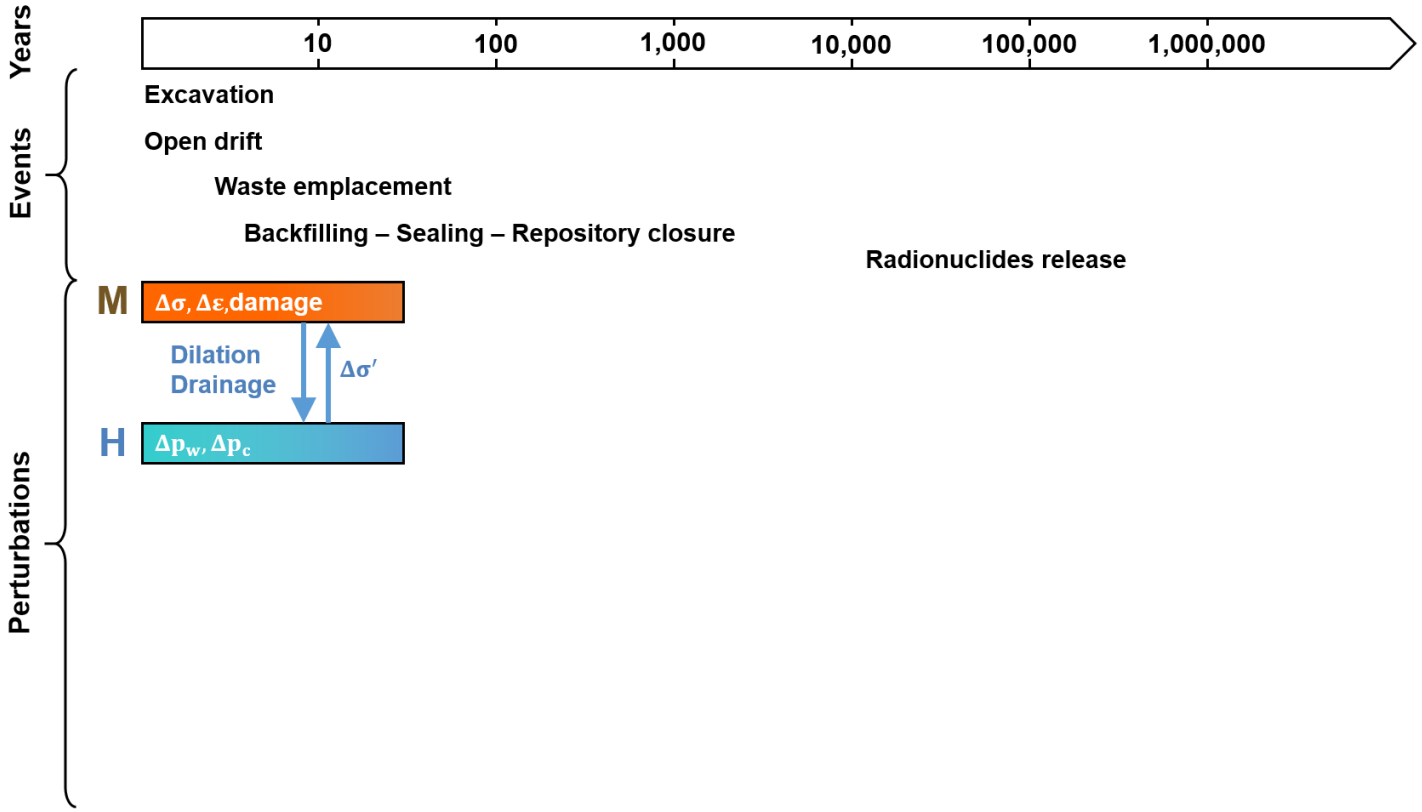

[Sillen, 2012]

Deep geological repository

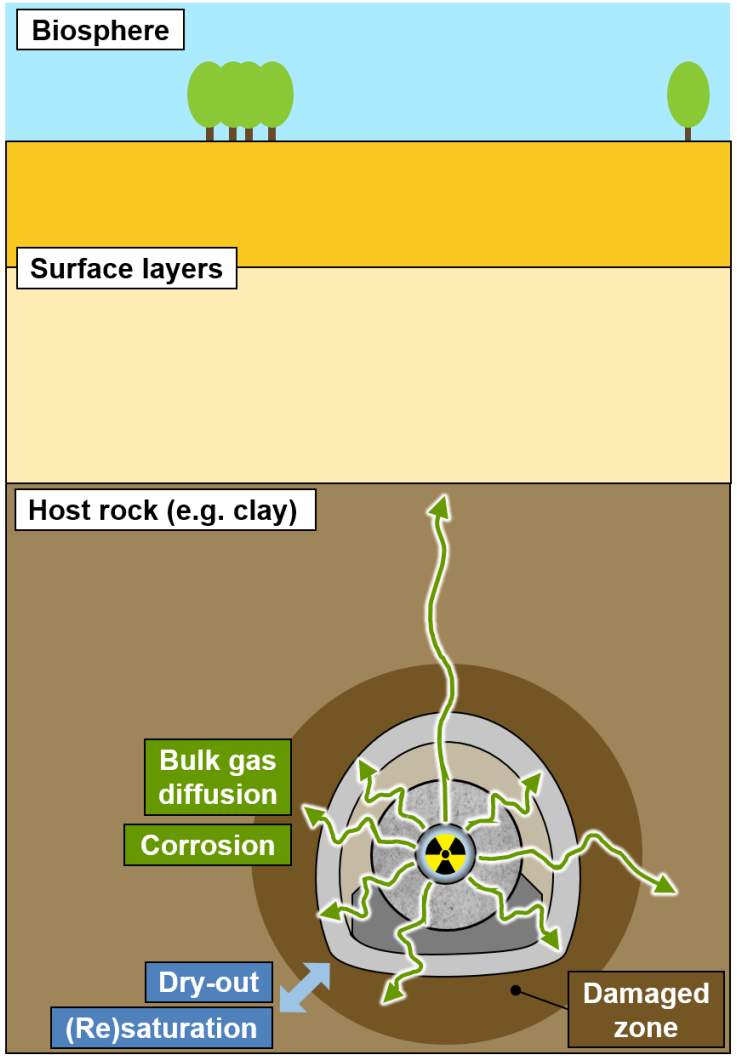

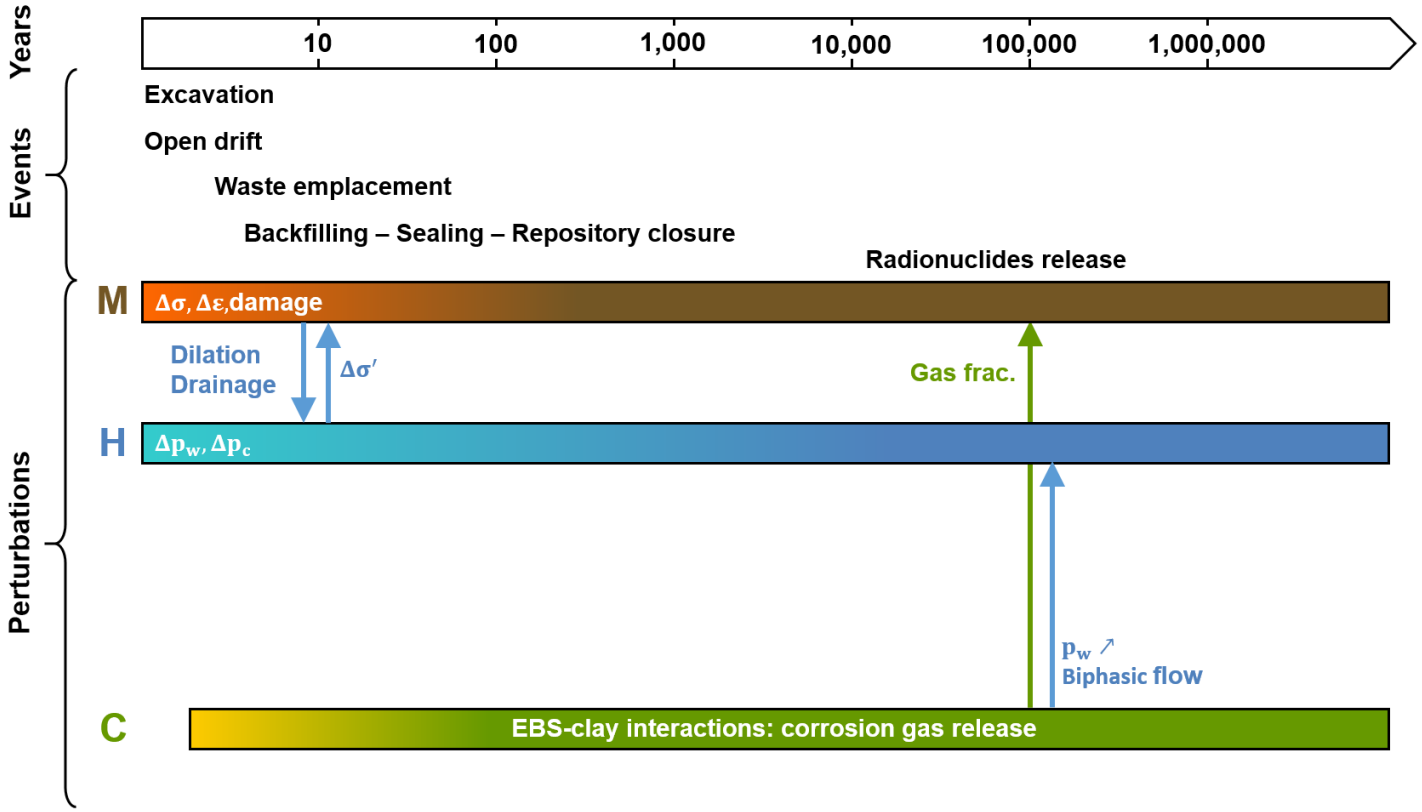

[Sillen, 2012]

Work objectives

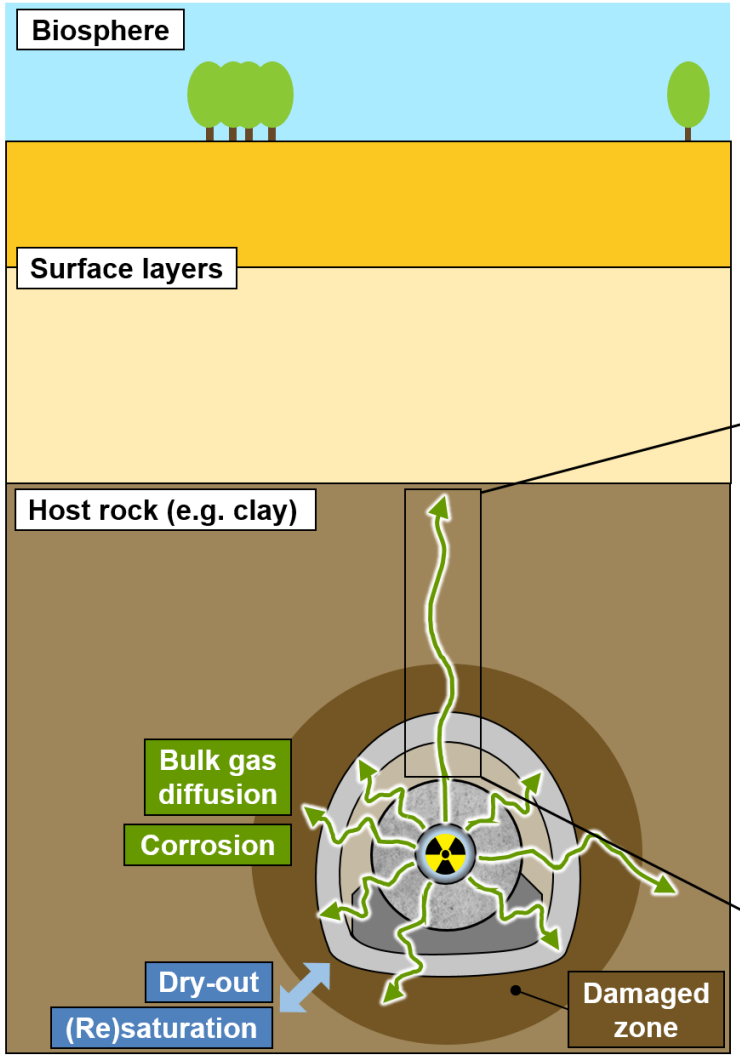

When gas builds up, do clay-rich rocks (re)fracture? ?

Numerical models of gas transport modes

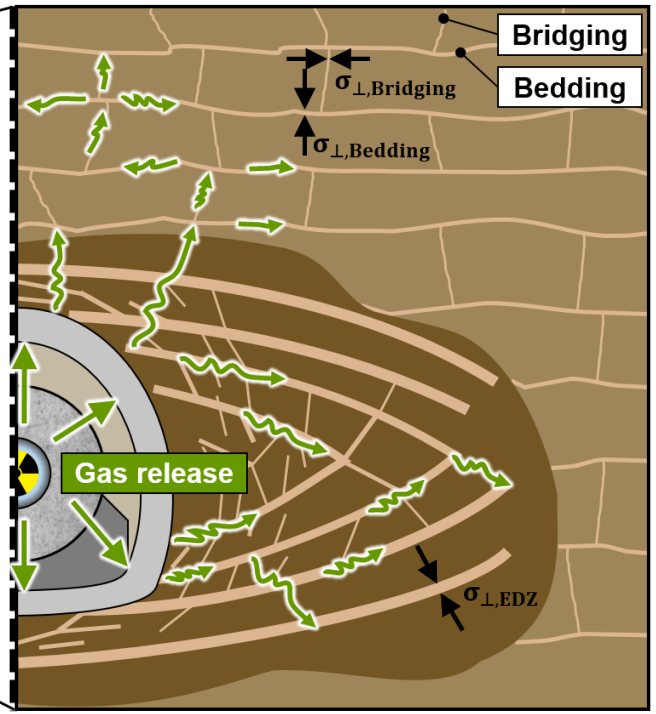

Zones of interest

Sound rock [Corman et al., 2025]

Excavation Damaged Zone (EDZ)

[Corman et al., 2022]

Introduction

01 **Characterisation of gas transport processes**

02 **Modelling gas transport in the EDZ**

03 **Modelling gas transport in sound rocks**

Conclusion

Experimental insights for HM modelling

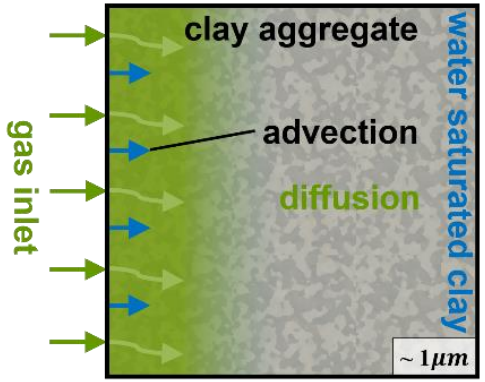

(i) Advection and diffusion of dissolved gas

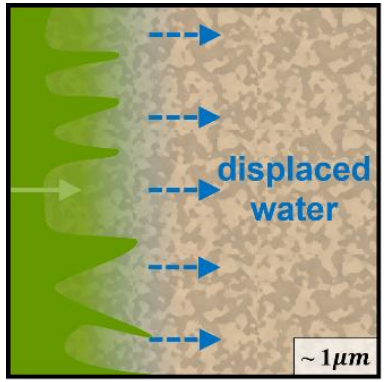

(ii) Visco-capillary two-phase flow

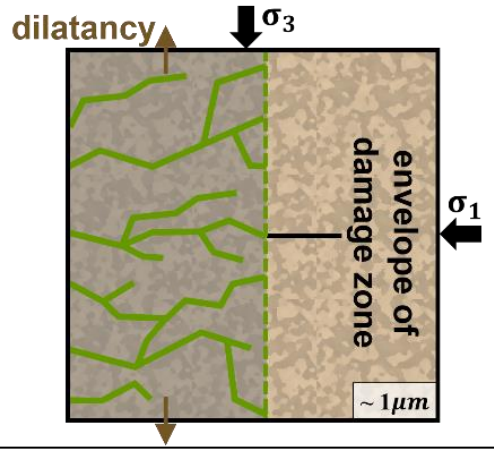

(iii) Gas flow in preferential pathways

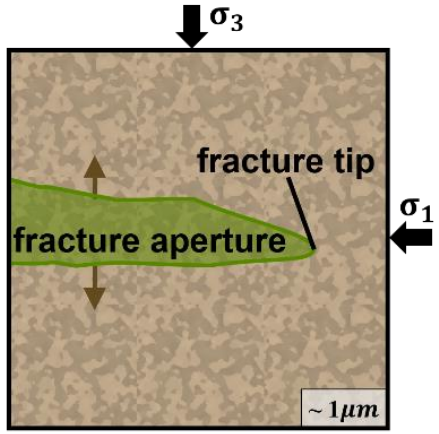

(iv) Gas flow in macroscopic fractures

[Marshall et al., 2005]

Gas pressure

Experimental insights for HM modelling

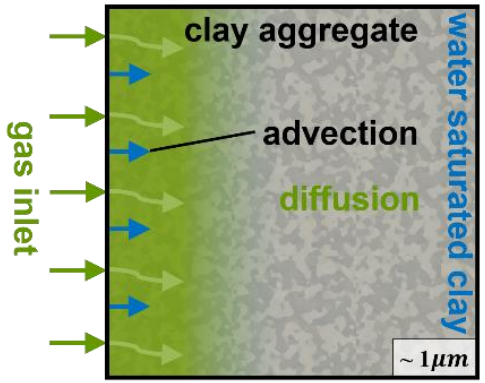

(i) Advection and diffusion of dissolved gas

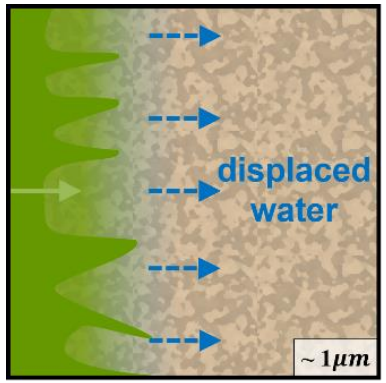

(ii) Visco-capillary two-phase flow

Liquid phase		Gas phase
Liquid water p_w	Equilibrium restriction $\propto \frac{m_m}{RT}$ *[Kelvin, 1871]*	*Water vapour* p_v
	Suction: $p_c = p_g - p_w$	
Dissolved gas p_{dg}	Solubility limit $\propto H_g$ *[Henry, 1803]*	*Dry gas* p_g

Diffusive transport mode

[Fick, 1855]

$$i \propto \bar{\tau} D_e \nabla \left(\frac{\rho_{dg}}{\rho_w} \right)$$

Advective transport mode

[Darcy, 1856]

$$q \propto \frac{k}{\mu} (\nabla p - \rho g)$$

Experimental insights for HM modelling

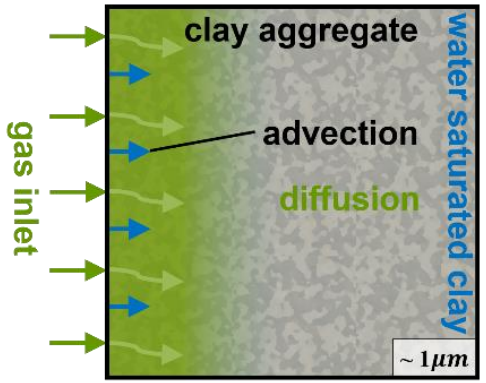

(i) Advection and diffusion of dissolved gas

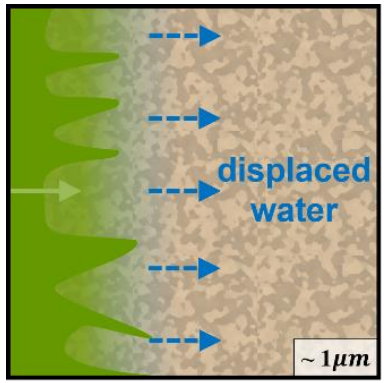

(ii) Visco-capillary two-phase flow

Liquid phase		Gas phase
Liquid water p_w	Equilibrium restriction $\propto \frac{m_m}{RT}$ *[Kelvin, 1871]*	*Water vapour* p_v
	Suction: $p_c = p_g - p_w$	
Dissolved gas p_{dg}	Solubility limit $\propto H_g$ *[Henry, 1803]*	*Dry gas* p_g

Diffusive transport mode
[Fick, 1855]

$$i \propto \bar{\tau} D_e \nabla \left(\frac{\rho_{dg}}{\rho_w} \right)$$

Retention curve
[van Genuchten, 1980]

$$S_{r,w} = f(p_c, P_e)$$

Advective transport mode
[Darcy, 1856]

$$q \propto \frac{k_{int} k_r}{\mu} (\nabla p - \rho g)$$

Relative permeability curves

$$k_r = f(S_{r,w})$$

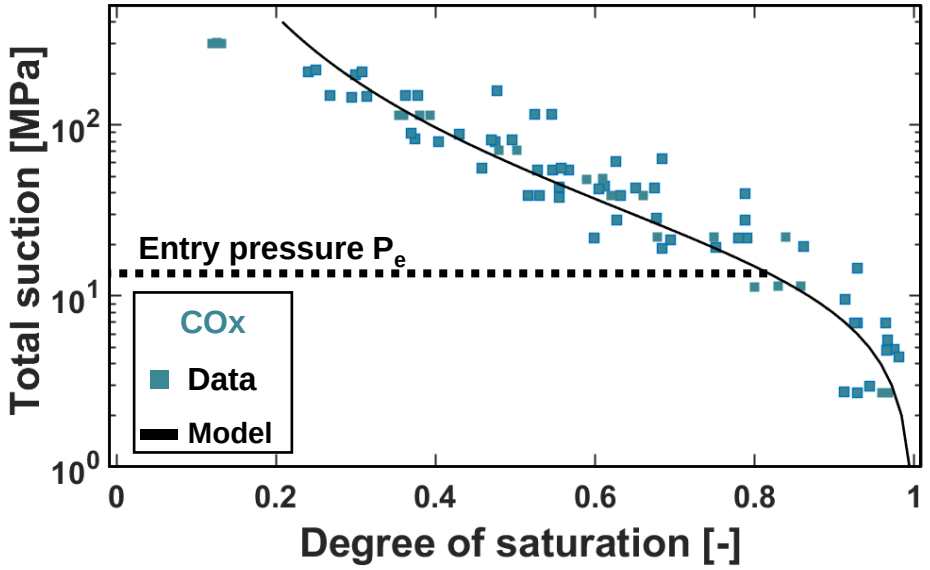

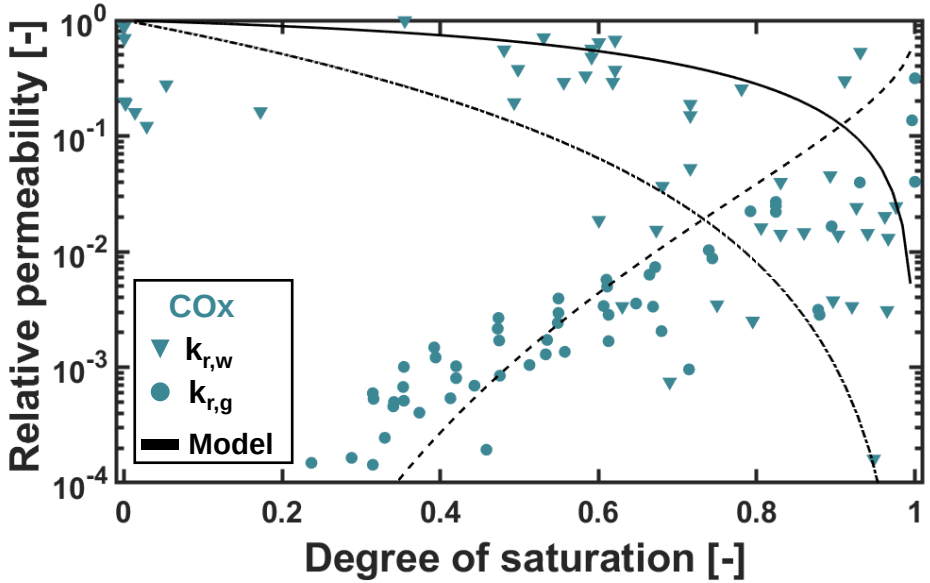

Experimental insights for HM modelling

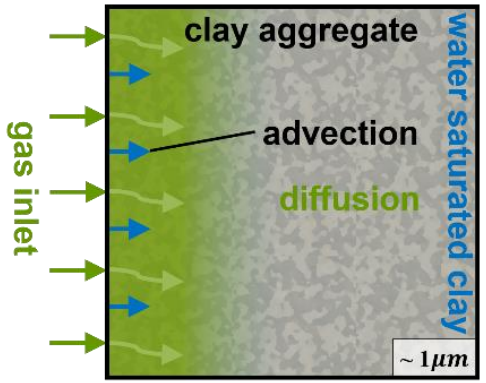

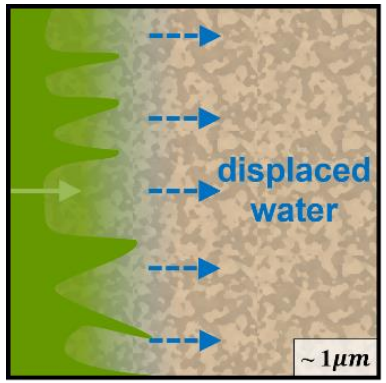

(i) Advection and diffusion of dissolved gas

(ii) Visco-capillary two-phase flow

Liquid phase		**Gas phase**
Liquid water p_w	Equilibrium restriction $\propto \frac{m_m}{RT}$ *[Kelvin, 1871]*	*Water vapour* p_v
	Suction: $p_c = p_g - p_w$	
Dissolved gas p_{dg}	Solubility limit $\propto H_g$ *[Henry, 1803]*	*Dry gas* p_g

Diffusive transport mode

[Fick, 1855]

$$i \propto \bar{\tau} D_e \nabla \left(\frac{\rho_{dg}}{\rho_w} \right)$$

Retention curve

[van Genuchten, 1980]

$$S_{r,w} = f(p_c, P_e)$$

Advective transport mode

[Darcy, 1856]

$$q \propto \frac{k_{int} k_r}{\mu} (\nabla p - \rho g)$$

Relative permeability curves

$$k_r = f(S_{r,w})$$

Classical two-phase flow HM models

Experimental insights for HM modelling

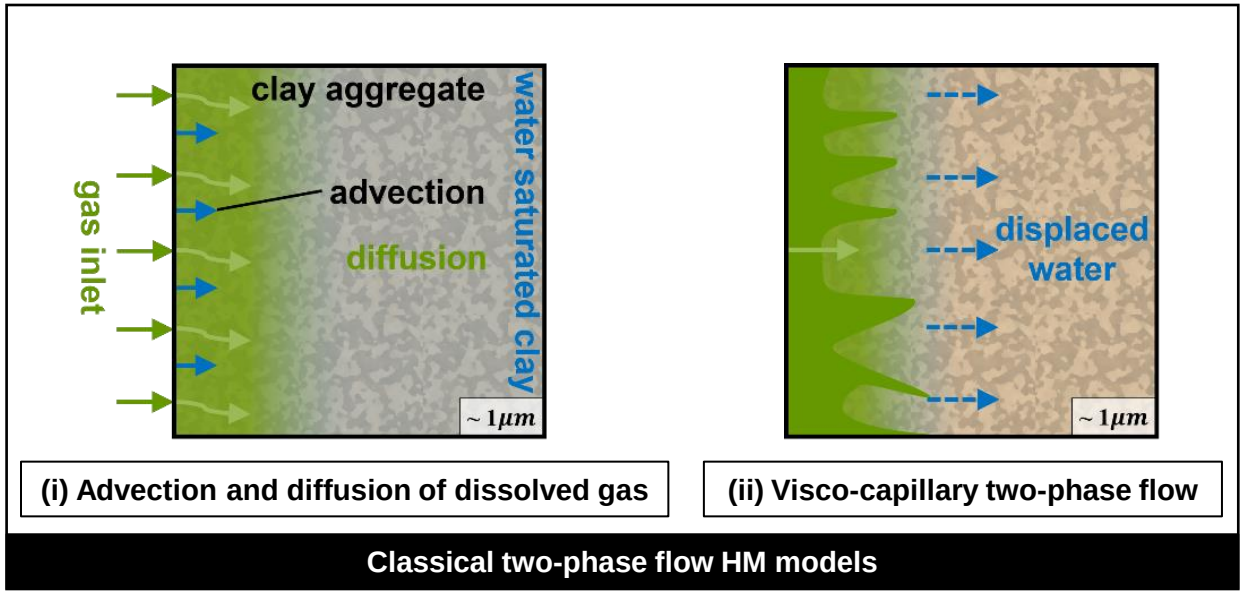

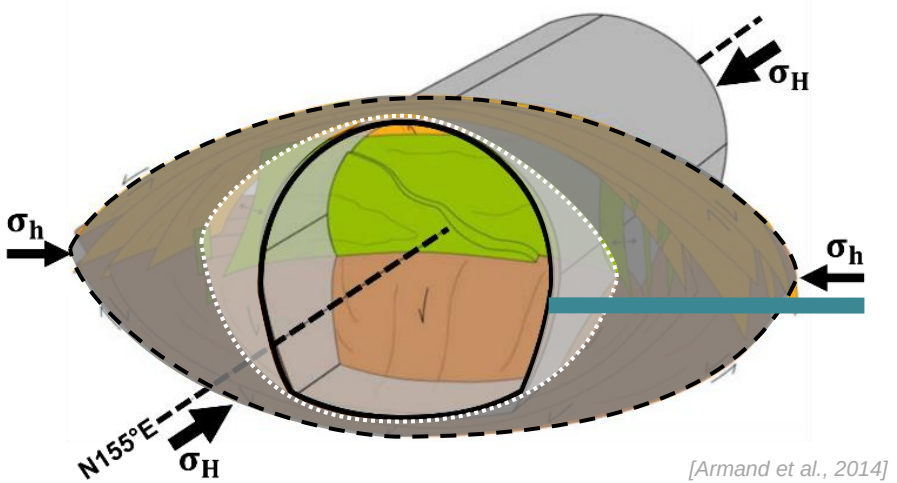

[Armand et al., 2014]

Excavation process in clay rocks creates an EDZ, characterised by:

+ Fracture geometry and patterns
+ Transport properties evolution

Modelling needs:

+ Fracture representation techniques
+ Advanced HM couplings ($k_w, P_r = f(\varepsilon)$)

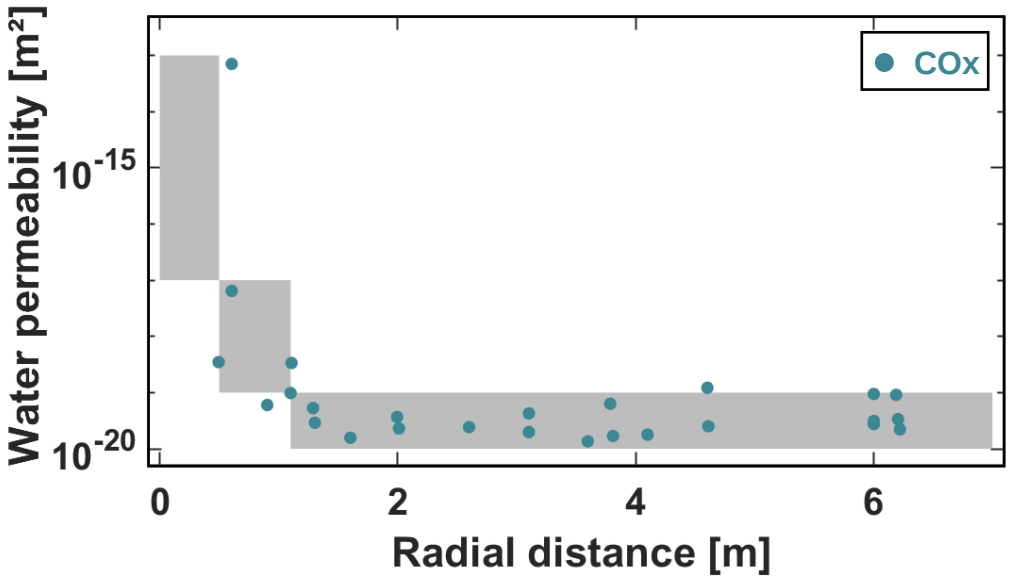

Experimental insights for HM modelling

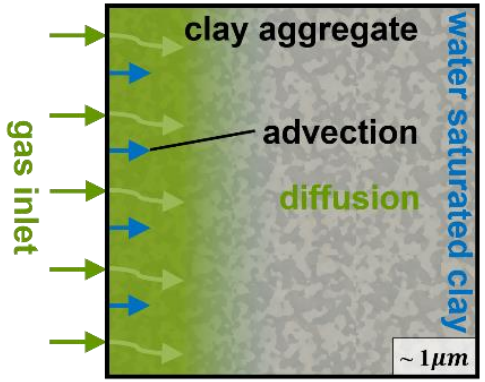

(i) Advection and diffusion of dissolved gas

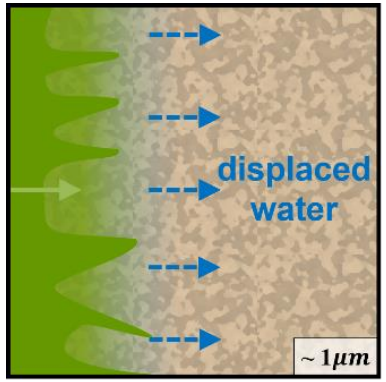

(ii) Visco-capillary two-phase flow

Classical two-phase flow HM models

+ Fracture representation techniques

+ Advanced HM couplings

Excavation Damaged Zone (EDZ)

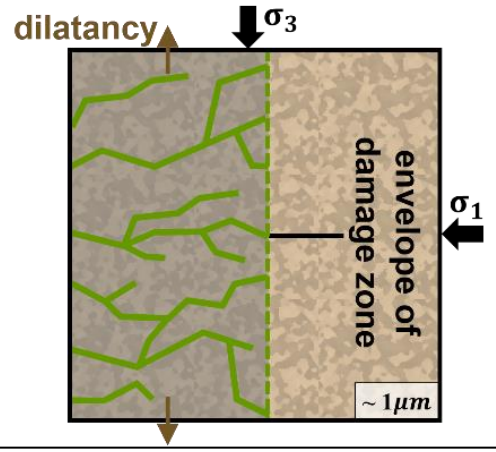

(iii) Gas flow in preferential pathways

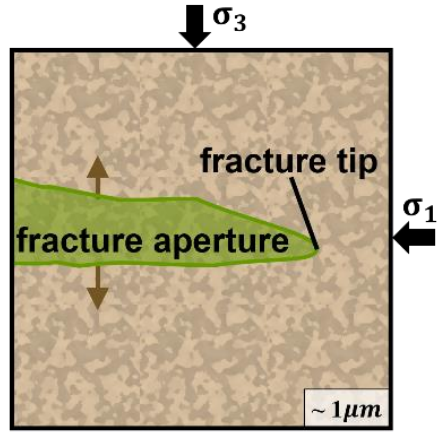

(iv) Gas flow in macroscopic fractures

Experimental insights for HM modelling

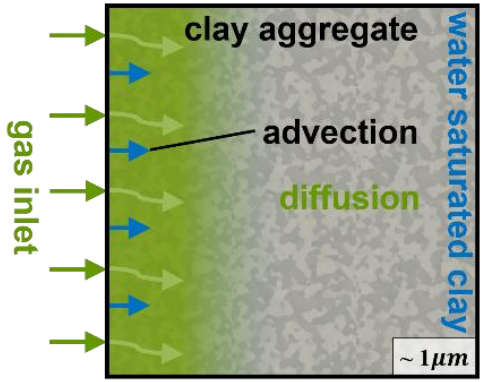

(i) Advection and diffusion of dissolved gas

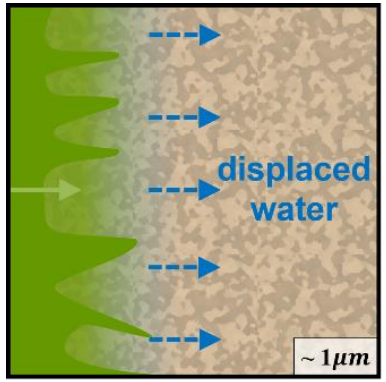

(ii) Visco-capillary two-phase flow

Classical two-phase flow HM models

+ Fracture representation techniques

+ Advanced HM couplings

Excavation Damaged Zone (EDZ)

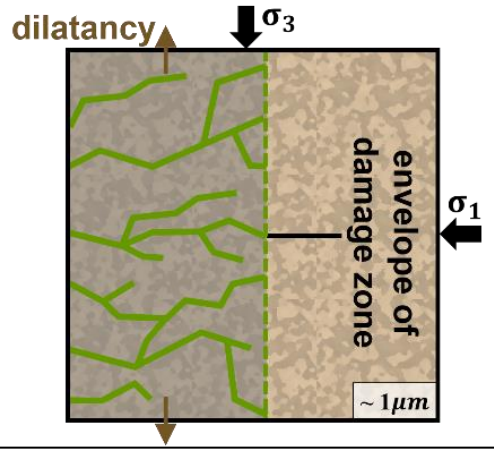

(iii) Gas flow in preferential pathways

(iv) Gas flow in macroscopic fractures

Experimental insights for HM modelling

Discrete gas-filled pathways
in sound rocks, driven by:

+ Natural heterogeneities & spatial variability of HM properties

+ Transport properties evolution

Modelling needs:

+ Microstructure-informed techniques

+ Advanced HM couplings ($k_w, P_r = f(\varepsilon)$)

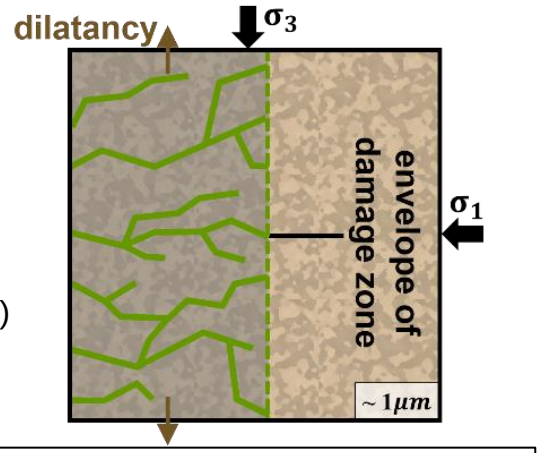

(iii) Gas flow in preferential pathways

Boom clay

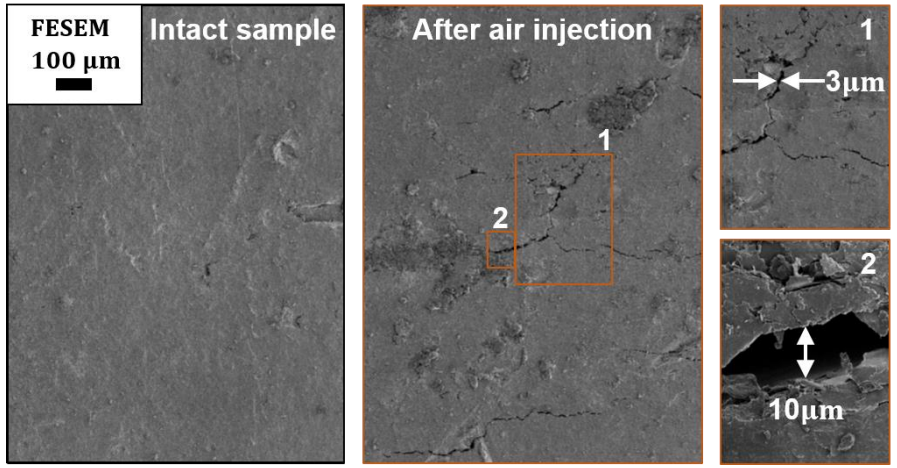

[Gonzalez-Blanco et al. 2022]

Callovo-Oxfordian claystone

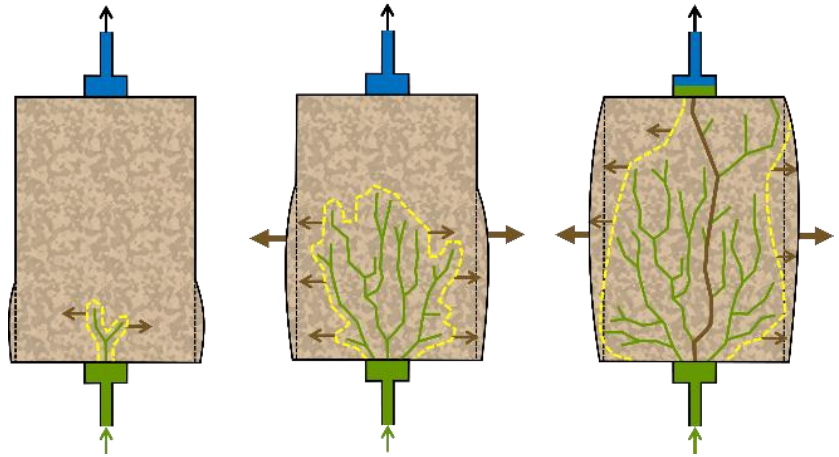

[Cuss et al. 2014]

Experimental insights for HM modelling

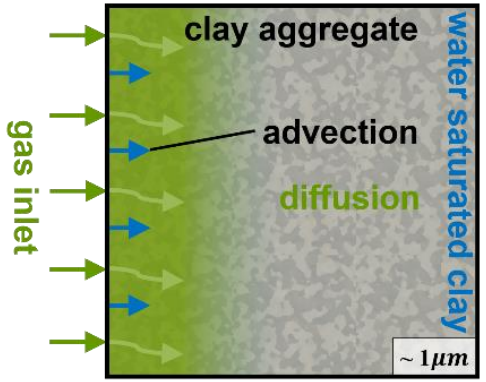

(i) Advection and diffusion of dissolved gas

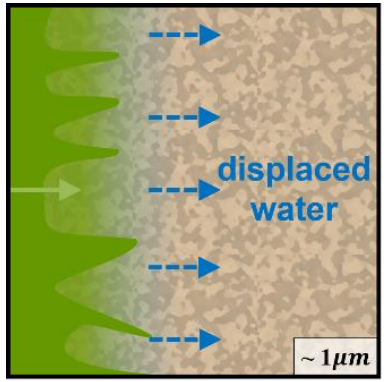

(ii) Visco-capillary two-phase flow

Classical two-phase flow HM models

+ Fracture representation techniques

+ Advanced HM couplings

Excavation Damaged Zone (EDZ)

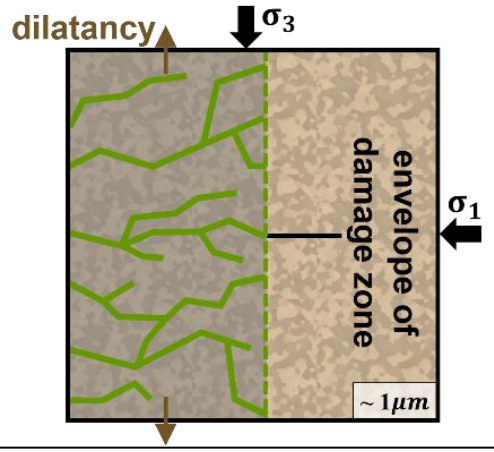

(iii) Gas flow in preferential pathways

Localised two-phase flow HM models

+ Microstructure-informed techniques

+ Advanced HM couplings

Sound rock

(iv) Gas flow in macroscopic fractures

Introduction

01 **Characterisation of gas transport processes**

02 **Modelling gas transport in the EDZ**

03 **Modelling gas transport in sound rocks**

Conclusion

Fracturing process

From geomaterials failure…

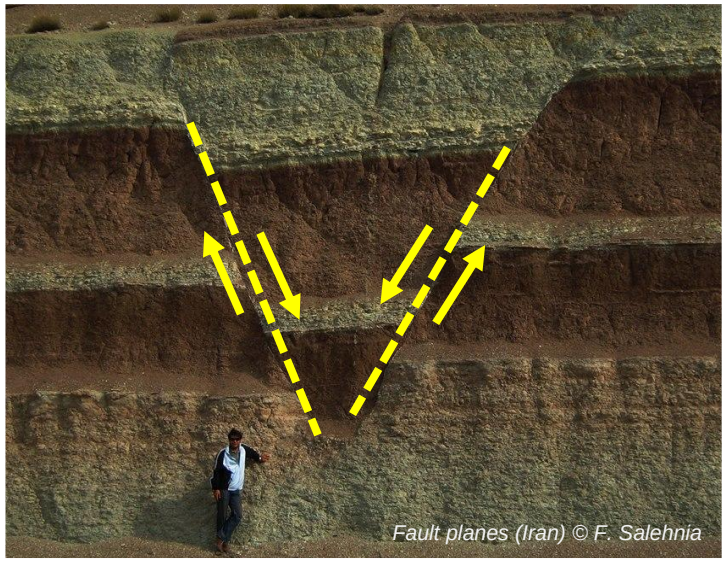

Fault planes (Iran) © F. Salehnia

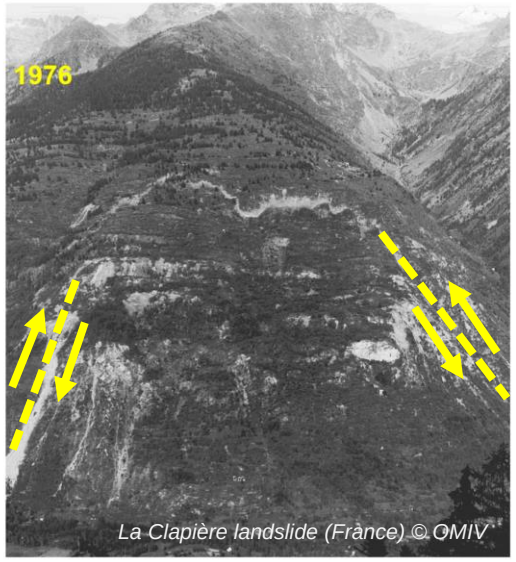

La Clapière landslide (France) © OMIV

Izmit earthquake (Turkey, 1999) © A. Barka

Fracturing process

From geomaterials failure to the drilling of underground galleries…

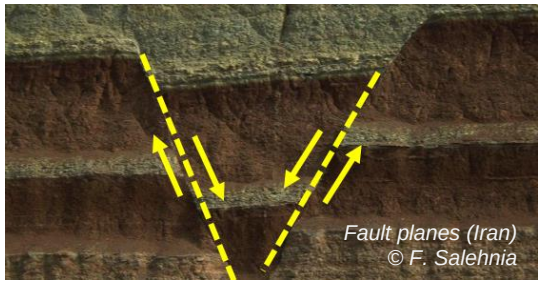

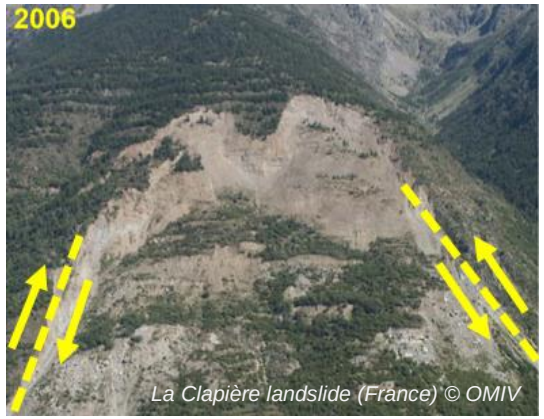

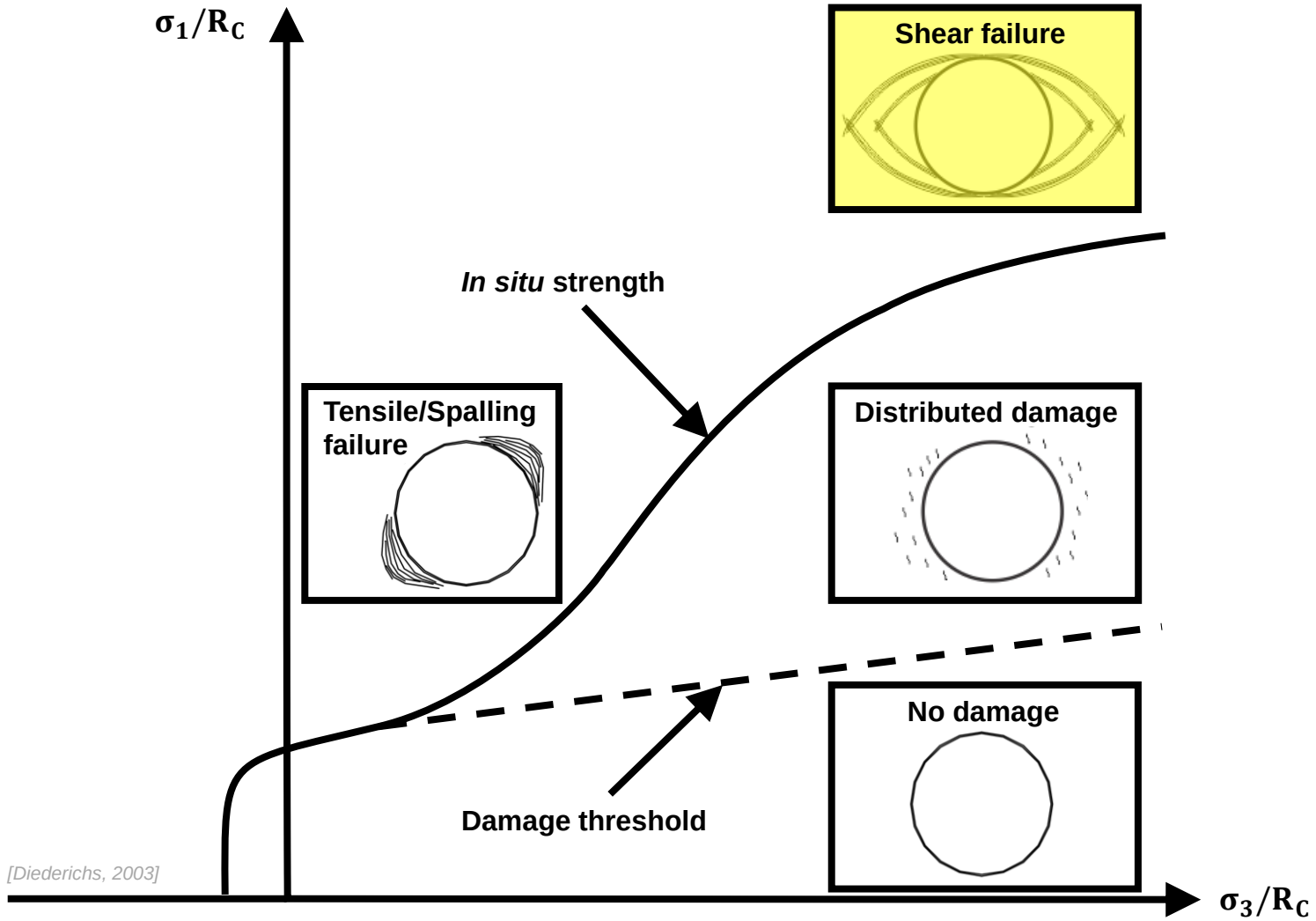

Fracturing process

From geomaterials failure to the drilling of underground galleries in clay host formations

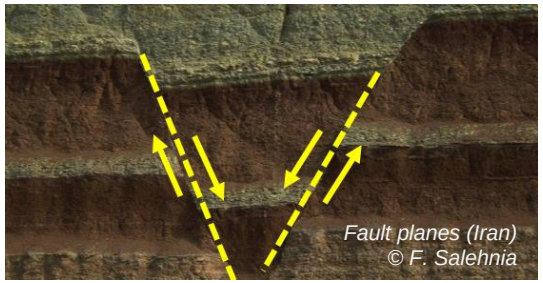

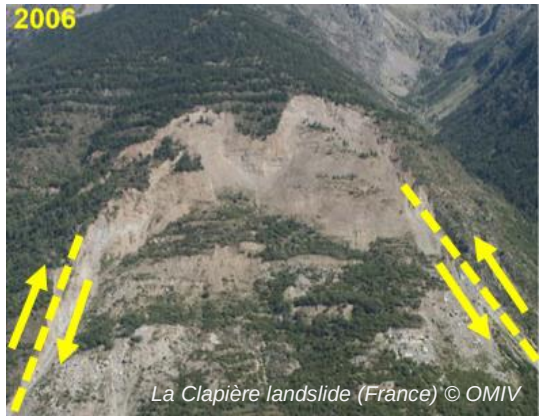

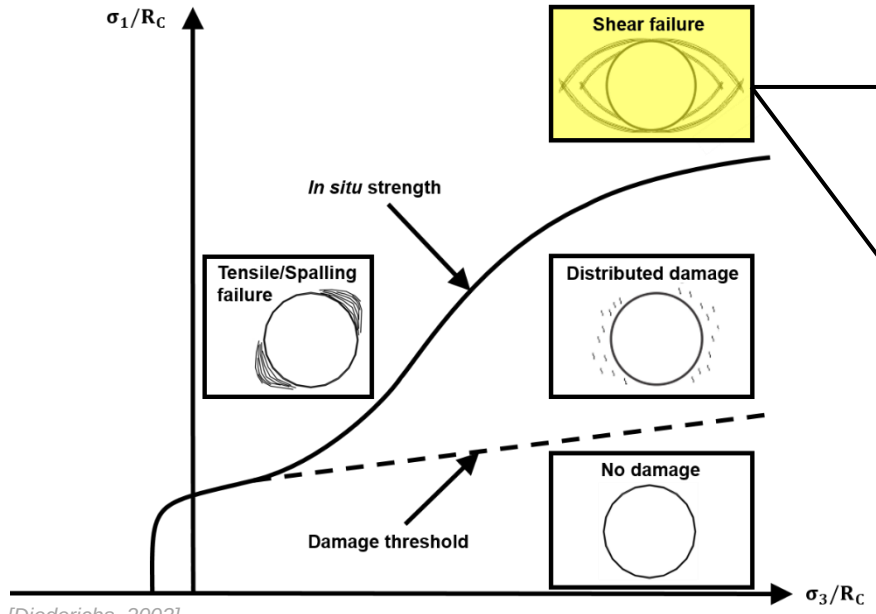

[Diederichs, 2003]

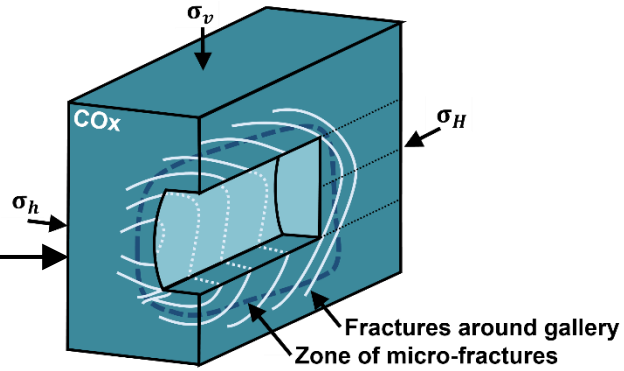

After [Bernier et al., 2008]

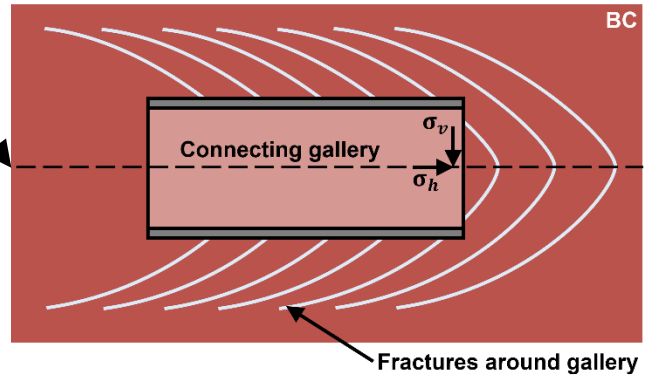

After [Bastiaens et al., 2003]

Second gradient H²M model

Shear strain localisation modelling

Axial displacement

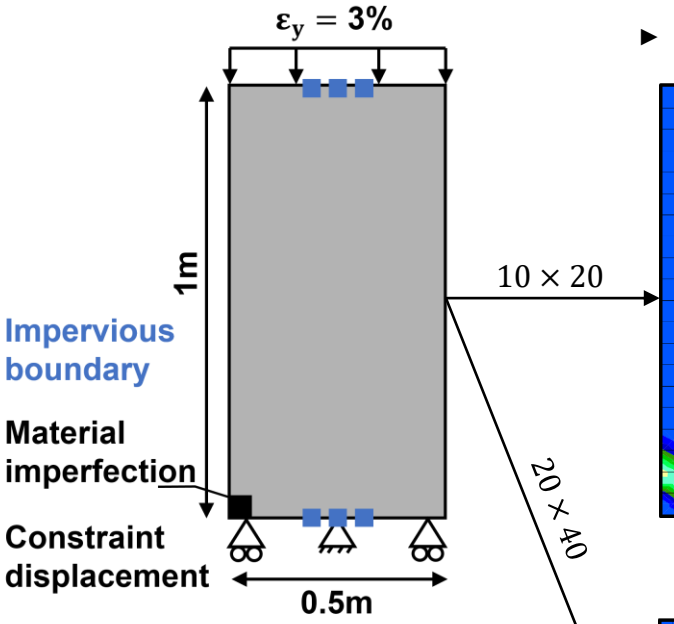

Classical FE methods

- Mesh size dependency

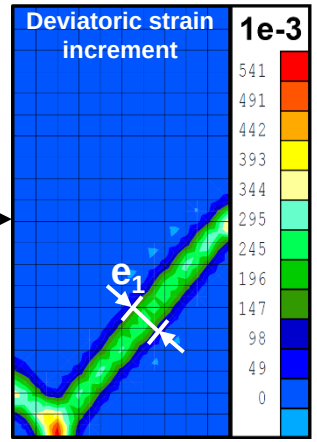

$e_1 \neq e_2$

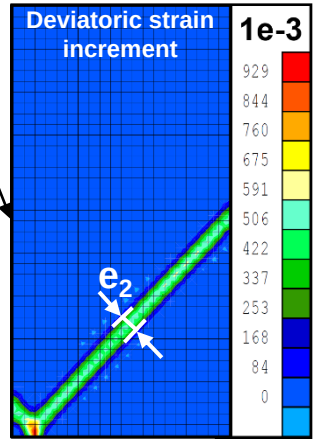

Regularisation technique

- Shear band width control

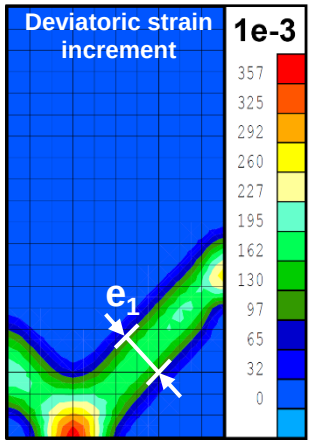

$e_1 = e_2$

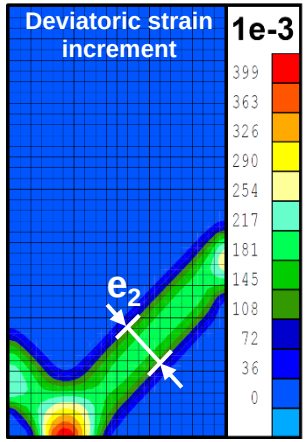

Numerical *vs* conceptual extension of the EDZ

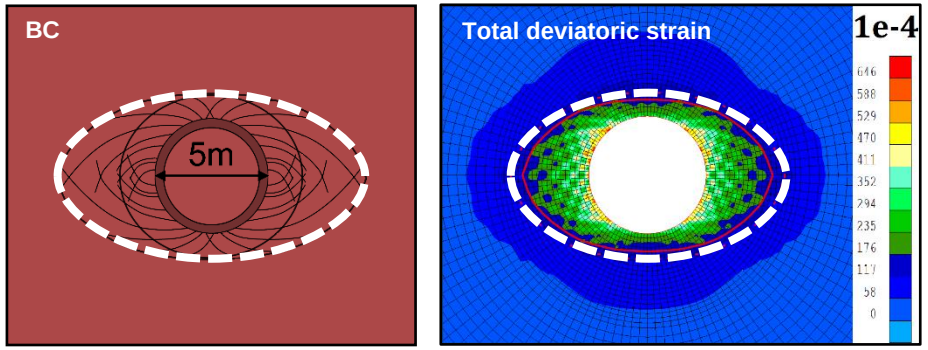

[Salehnia, 2015]

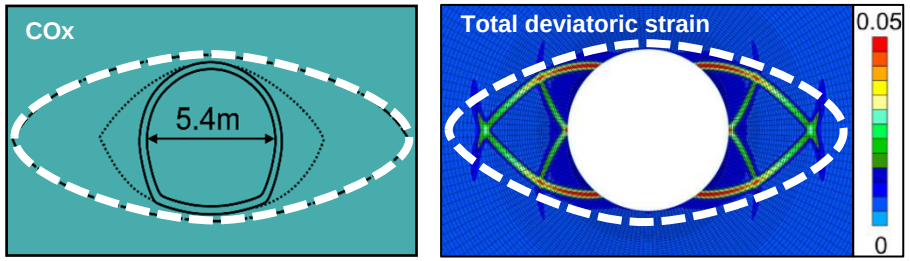

[Pardoen, 2015]

Second gradient H²M model

Advanced HM couplings

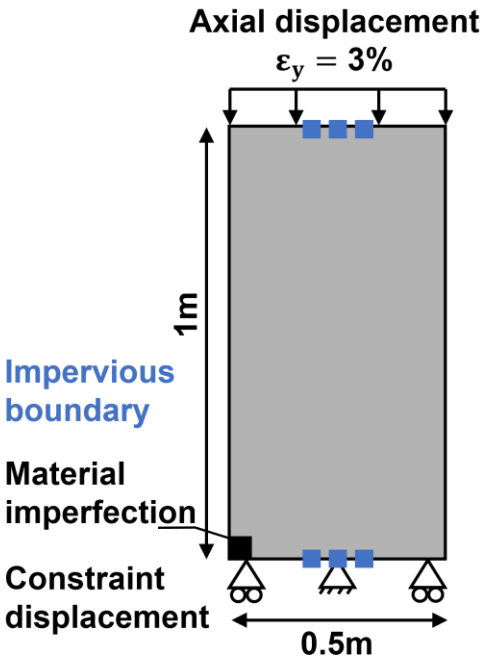

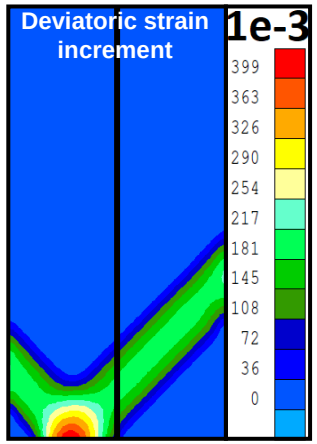

Intrinsic permeability

[Pardoen et al., 2014]

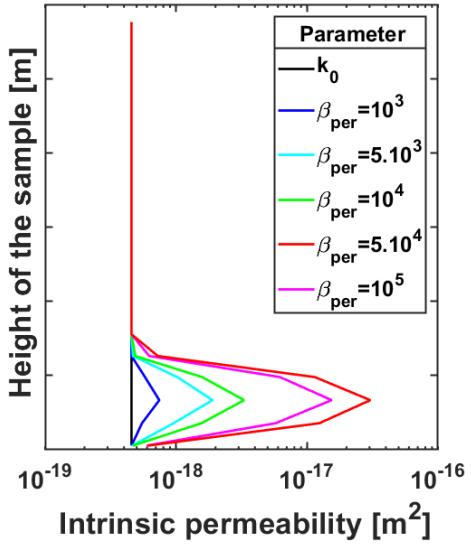

$$\mathbf{k_{ij}} = \mathbf{k_{ij,0}}\left(\mathbf{1} + \boldsymbol{\beta}_{\mathbf{per}}\left(\mathbf{YI} - \mathbf{YI^{thr}}\right)\hat{\boldsymbol{\varepsilon}}_{\mathbf{eq}}^{\mathbf{3}}\right)$$

$\hat{\varepsilon}_{eq}$: Von Mises' equivalent deviatoric plastic strain

β_{per}: evolution parameter

YI: yield index

Retention behaviour

[Olivella, 2008]

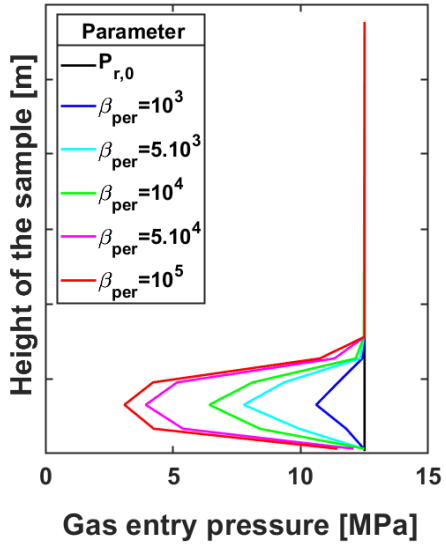

$$\mathbf{P_r} = \mathbf{P_{r,0}}\frac{\sqrt[3]{\mathbf{k_{ij,0}}}}{\sqrt[3]{\mathbf{k_{ij}}}}$$

P_r: van Genuchten's parameter identified as the entry pressure

Application

Problem statement

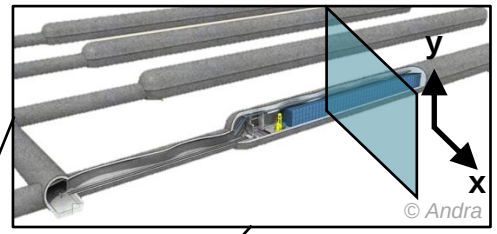

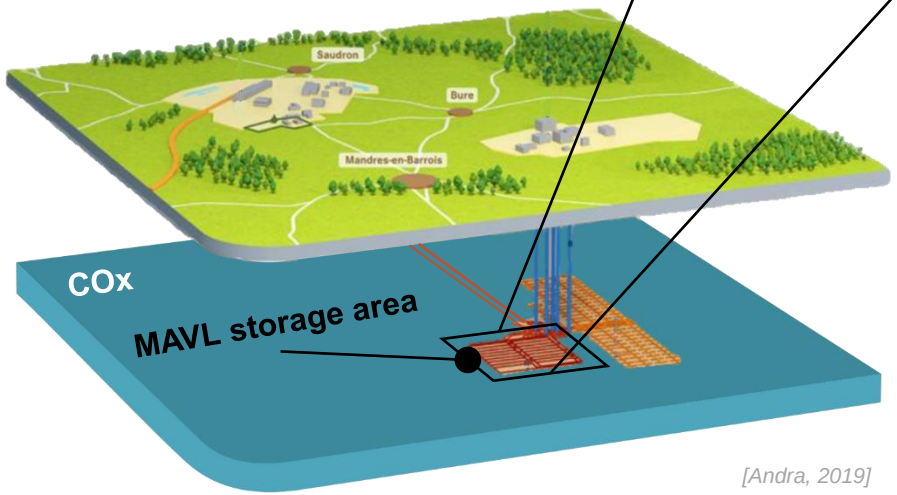

[Andra, 2019]

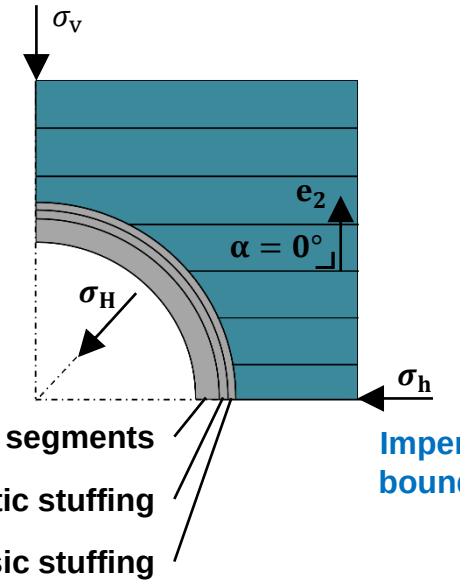

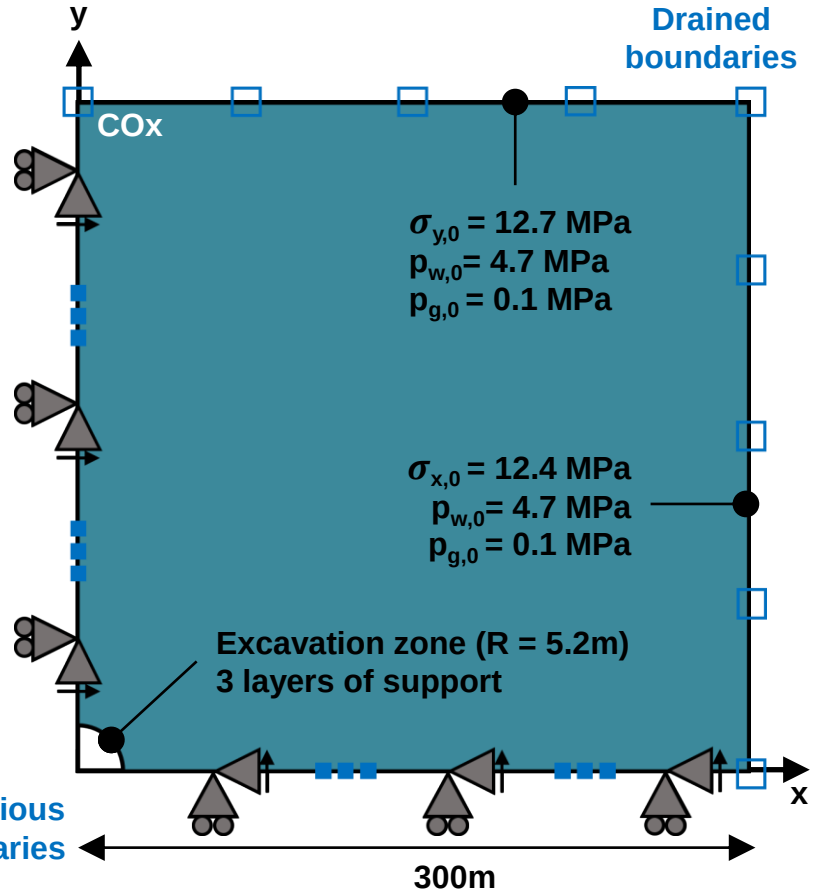

Three-step simulations

❶ Excavation phase

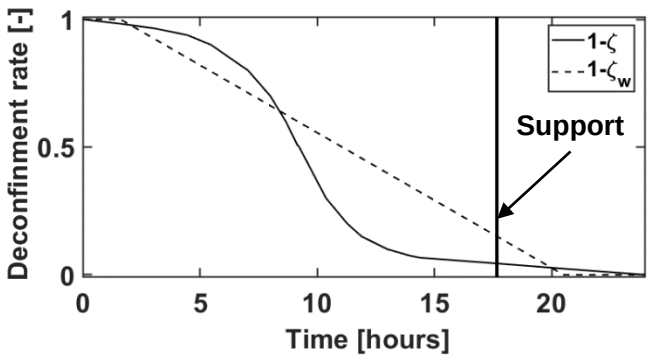

❷ Operation phase

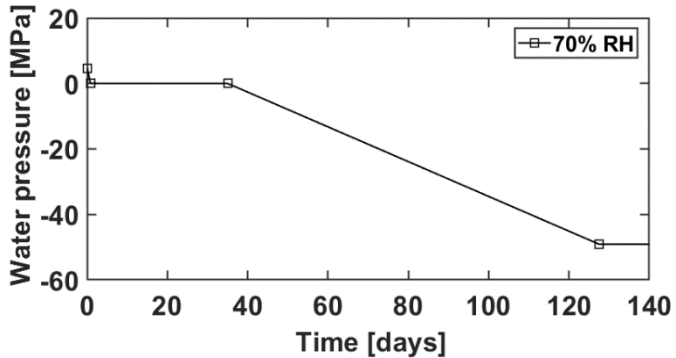

❸ Gas migration phase

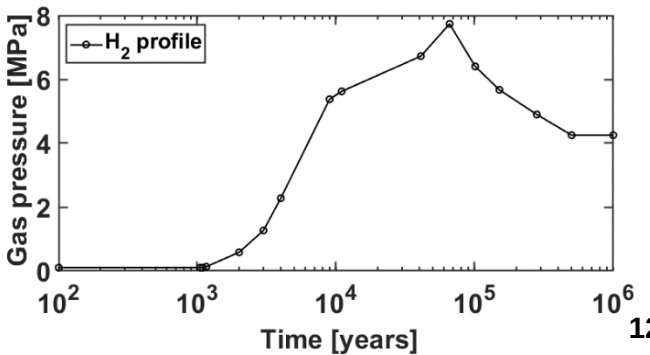

Application

Convergence of the rock mass

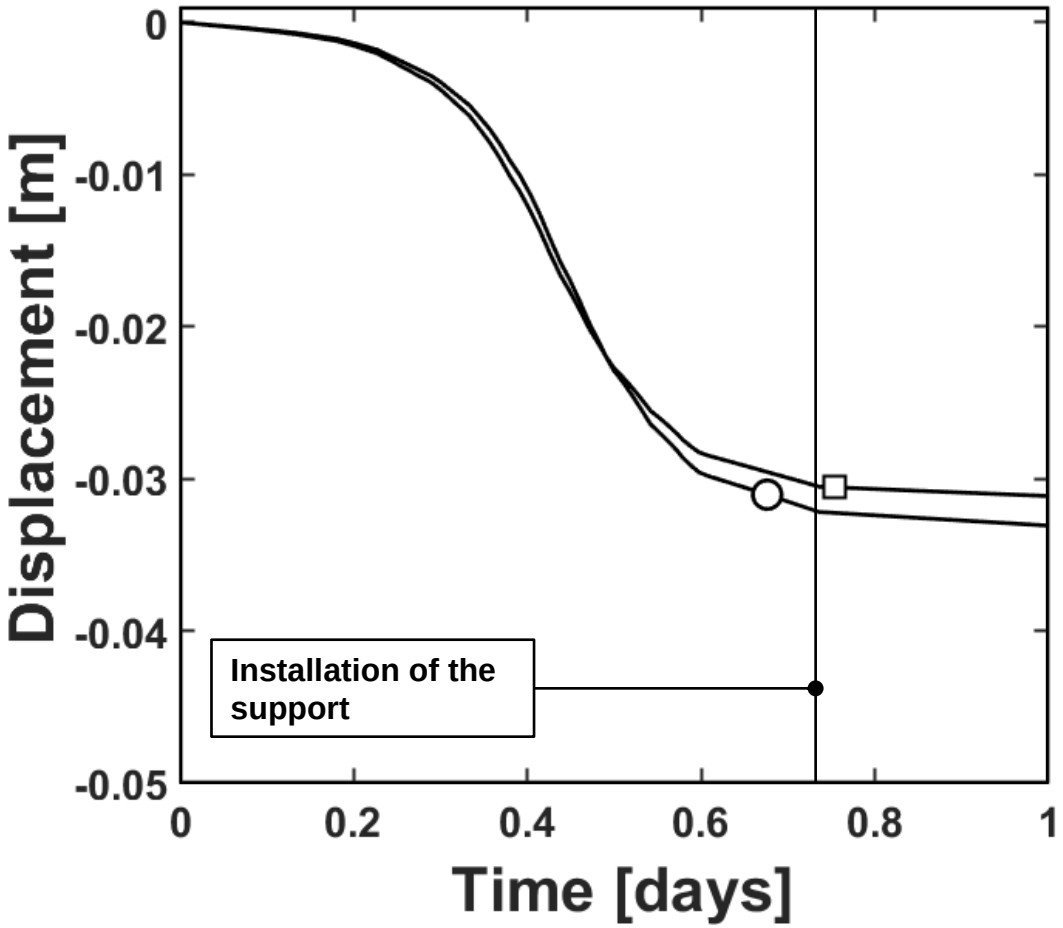

Application

Development of plasticity in the near field

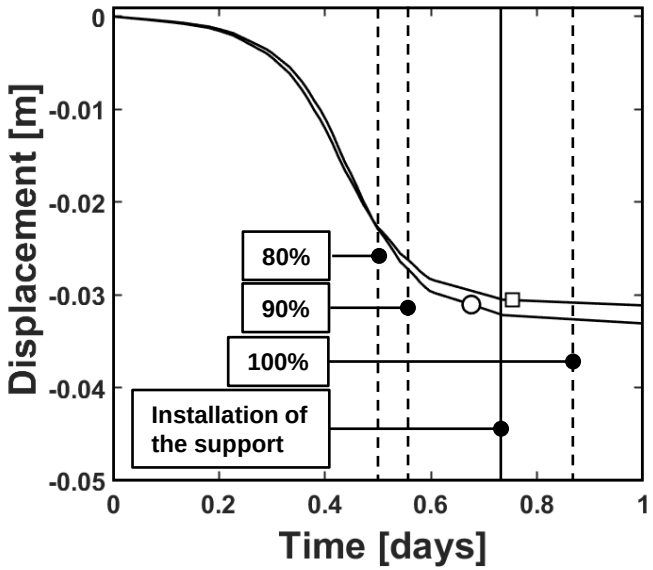

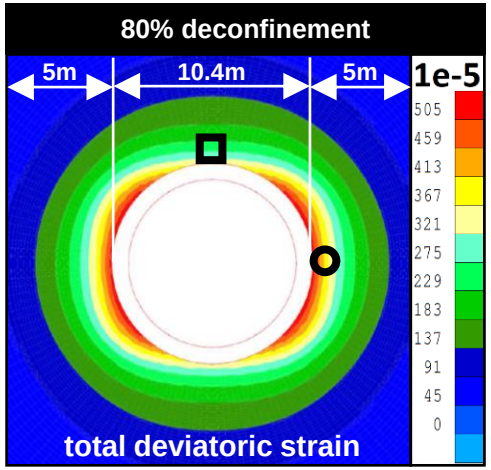

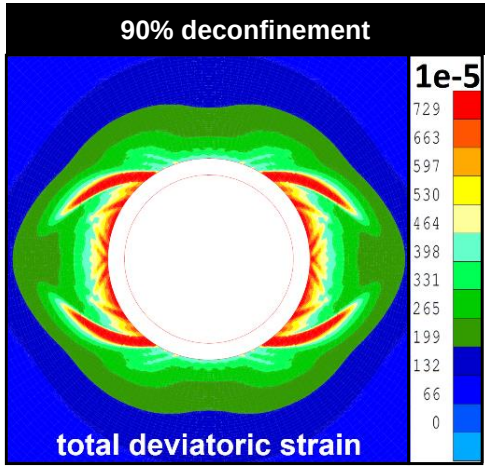

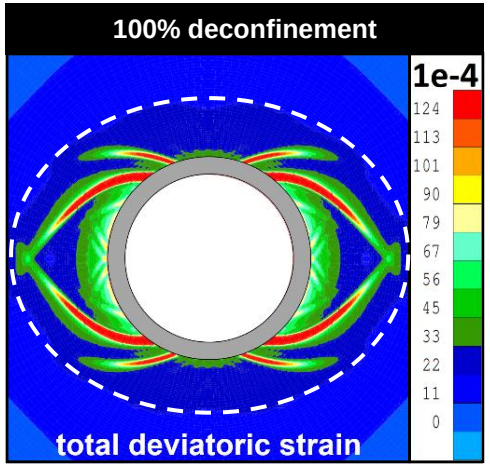

Application

Development of plasticity in the near field

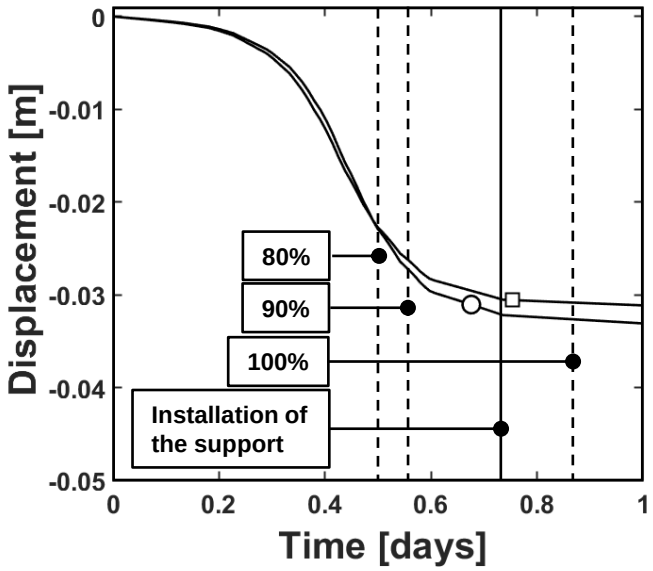

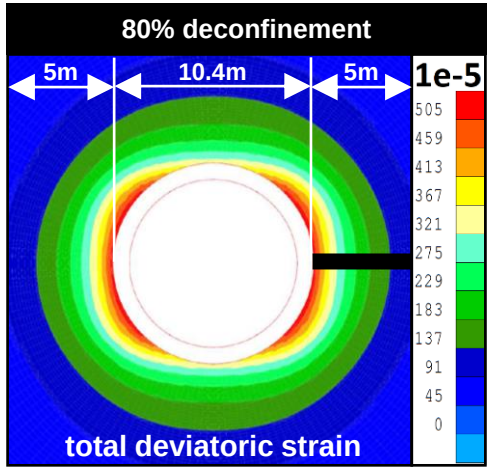

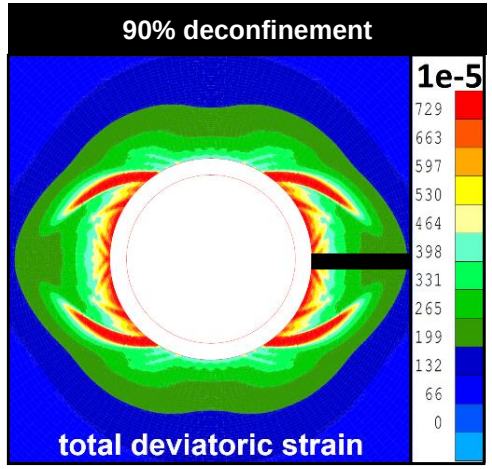

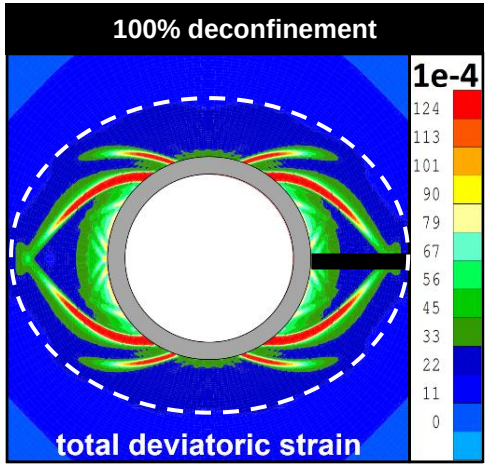

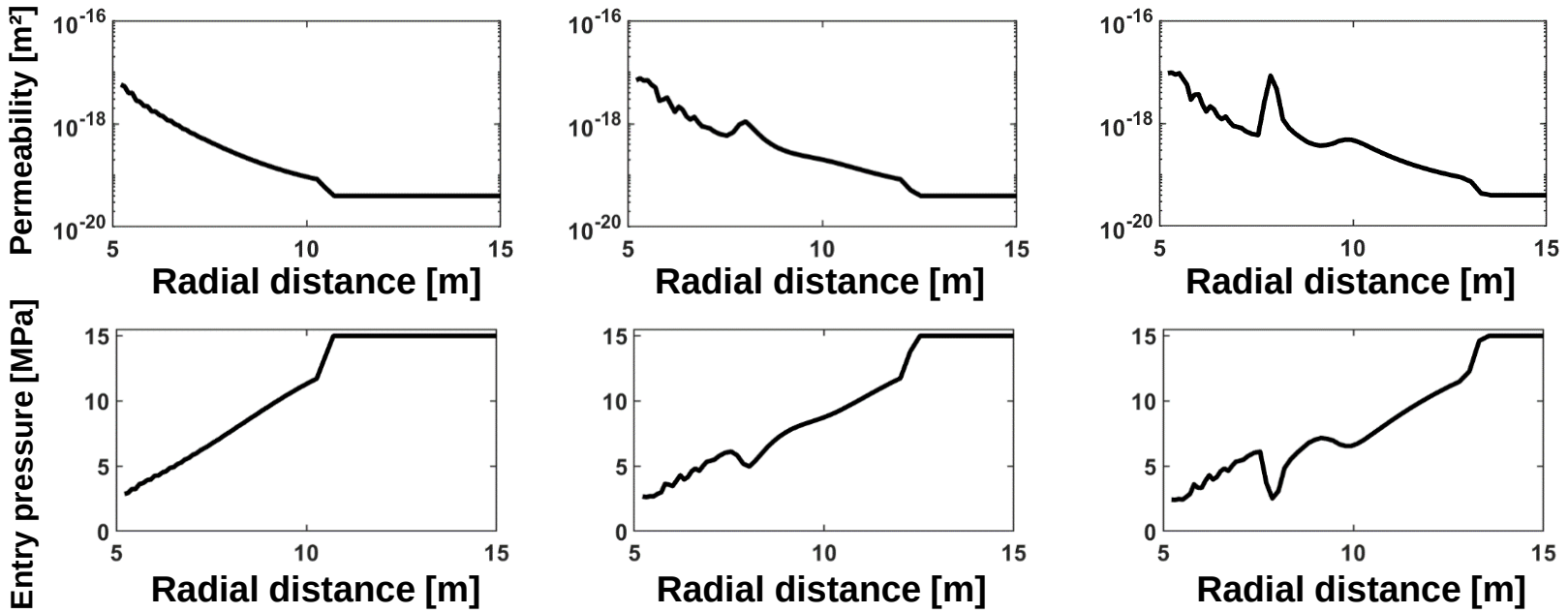

Application

Maps of gas (H^2) pressure evolution

No evolution of transfer properties

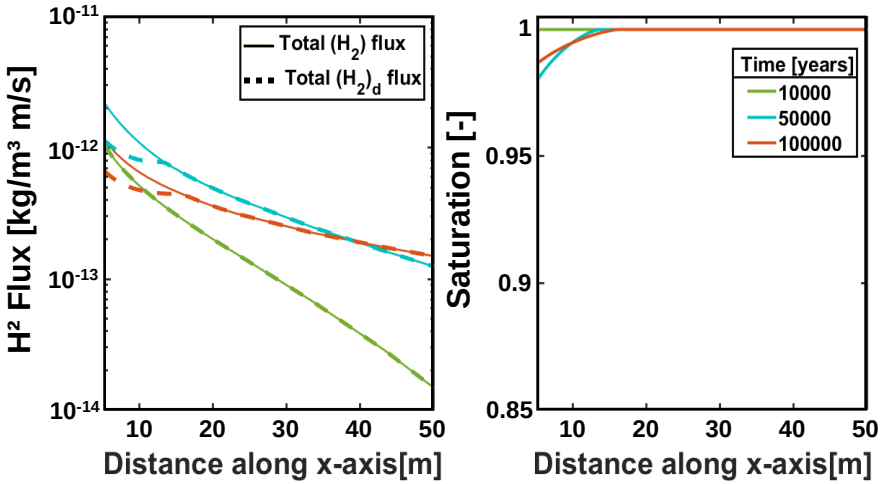

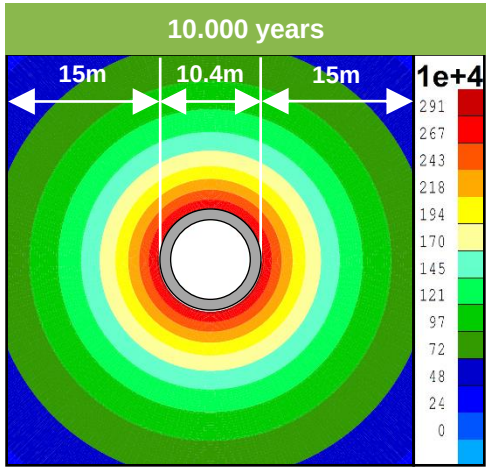

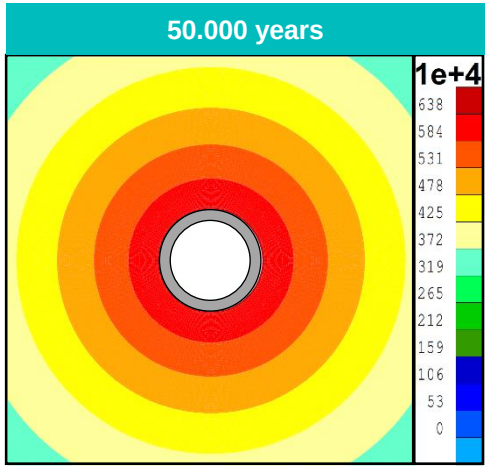

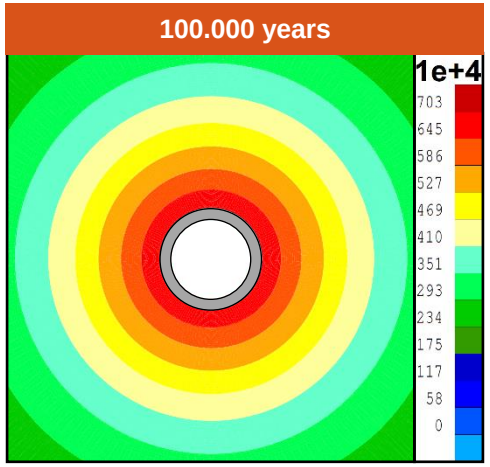

Application

Maps of gas (H^2) pressure evolution

No evolution of transfer properties

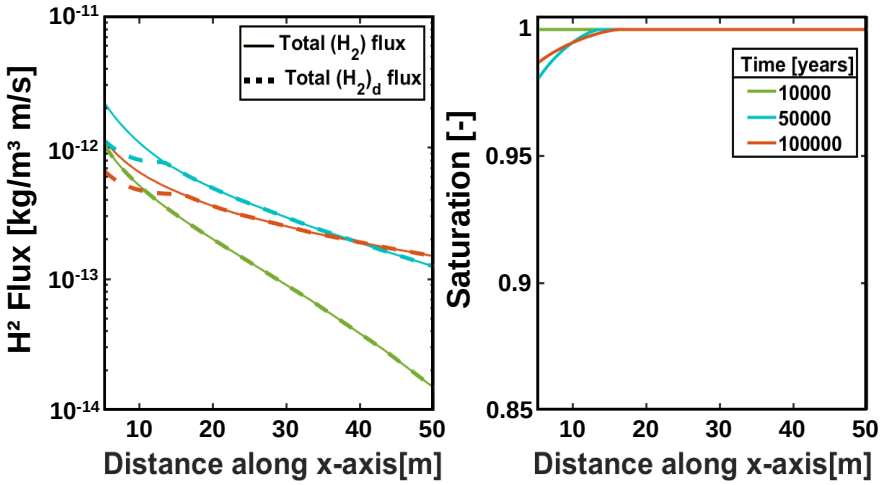

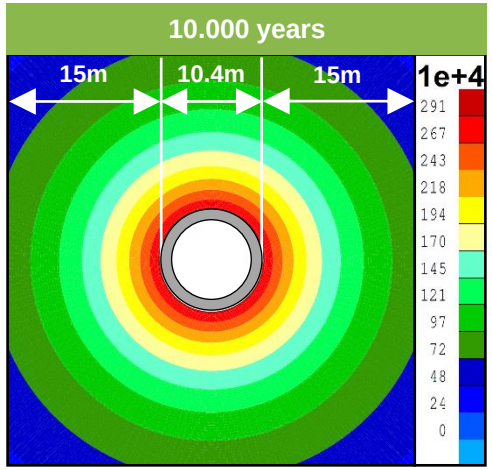

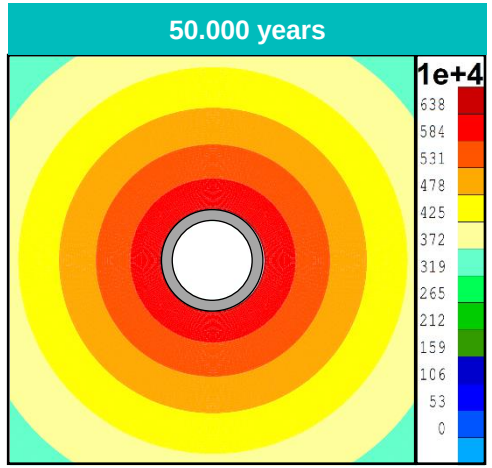

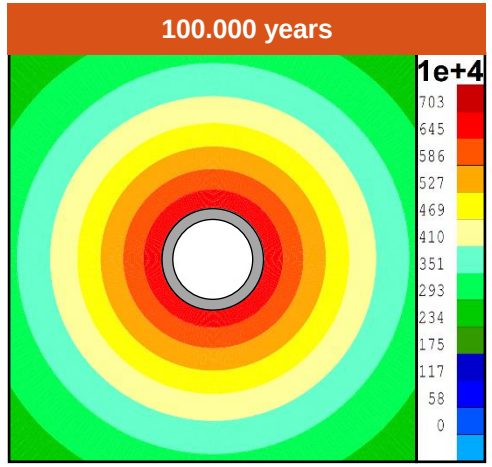

Evolution of transfer properties with strains

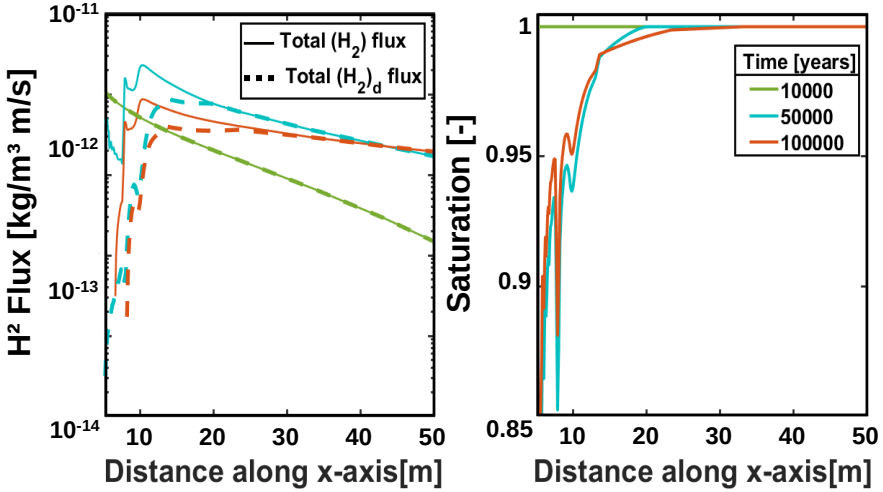

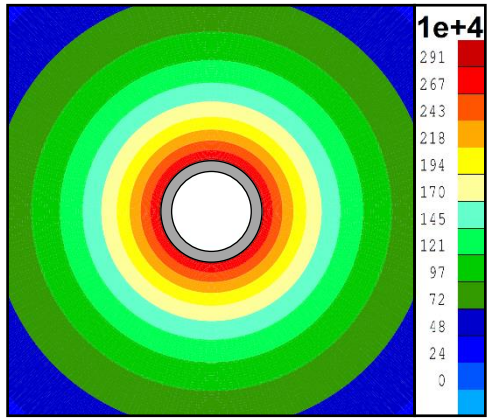

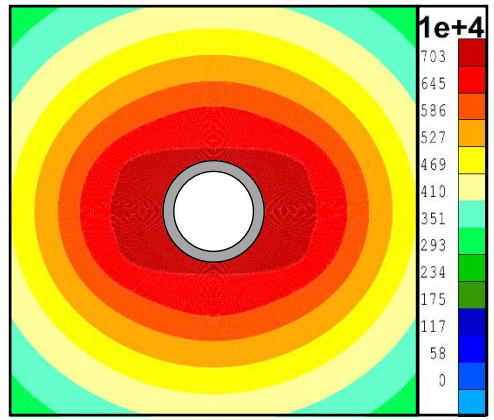

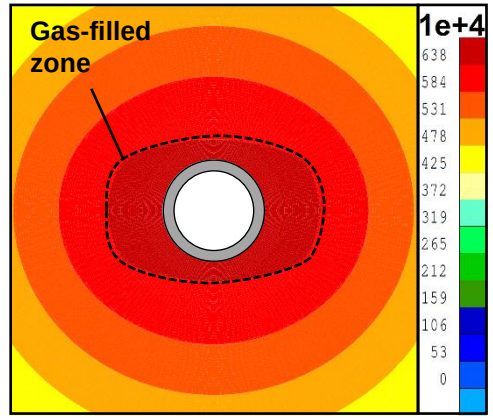

Introduction

01 **Characterisation of gas transport processes**

02 **Modelling gas transport in the EDZ**

03 **Modelling gas transport in sound rocks**

Conclusion

Hydro-mechanical multi-scale model

Macro-scale

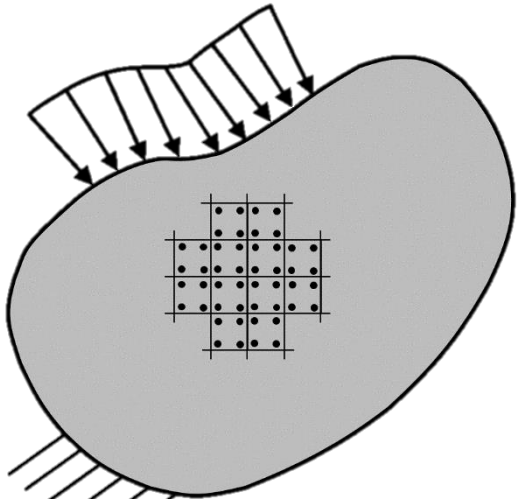

Micro-scale

Data-supported microstructure

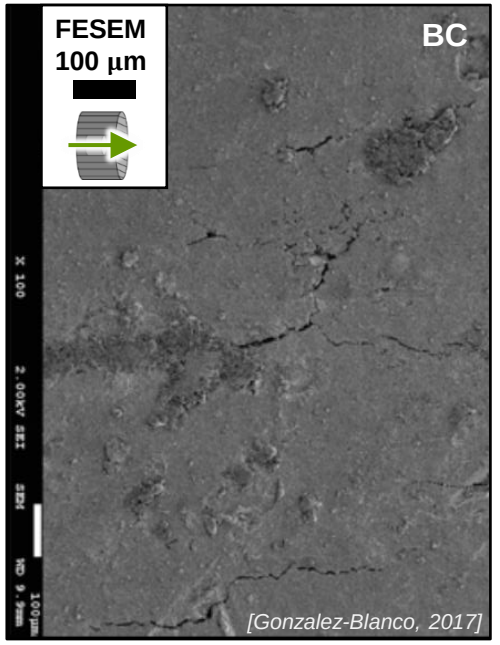

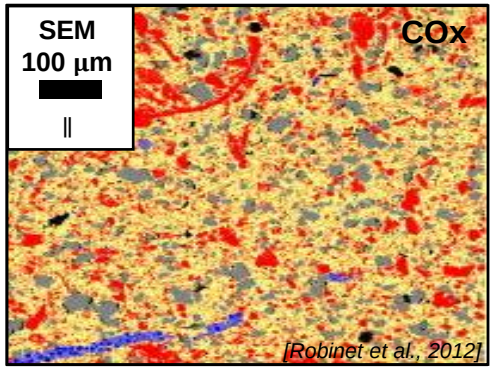

Hydro-mechanical multi-scale model

Macro-scale

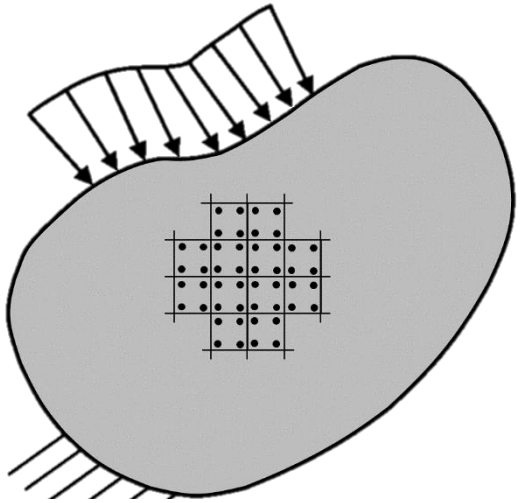

Micro-scale

Data-supported microstructure

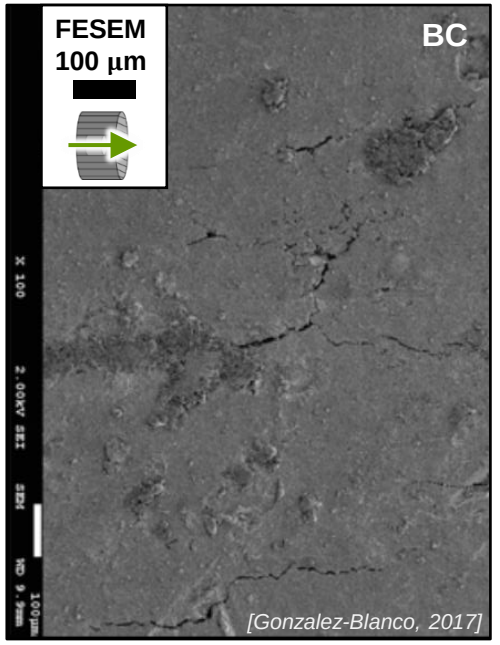

Physical idealisation

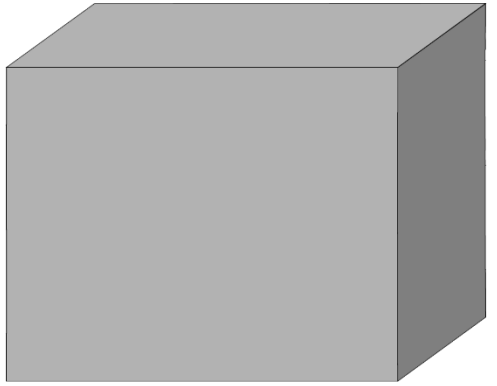

Hydro-mechanical multi-scale model

Macro-scale

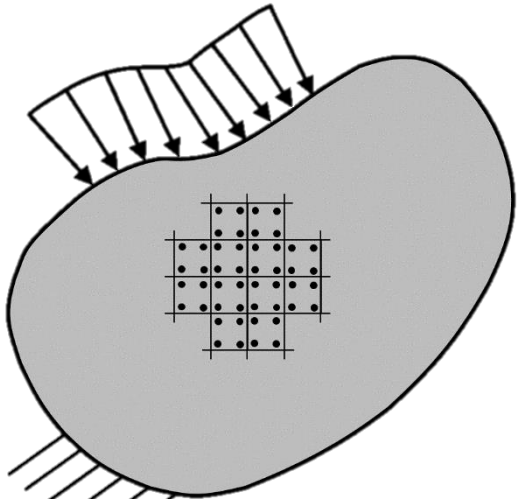

Micro-scale

Data-supported microstructure

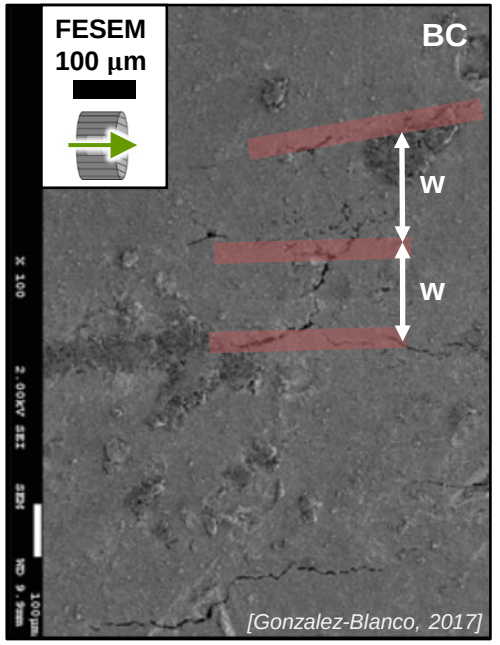

Physical idealisation

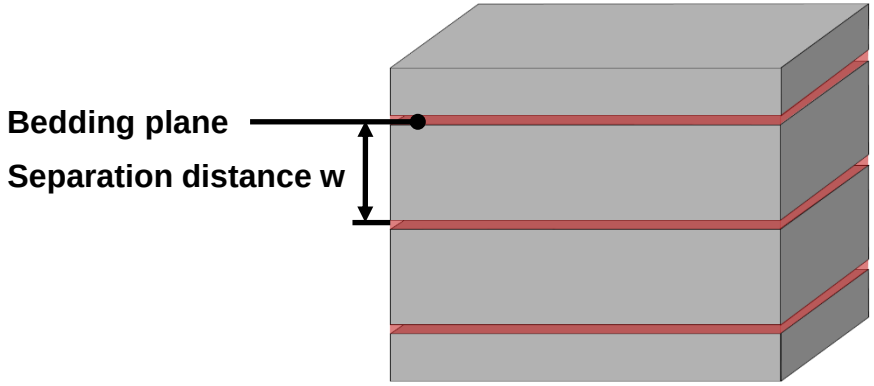

Hydro-mechanical multi-scale model

Macro-scale

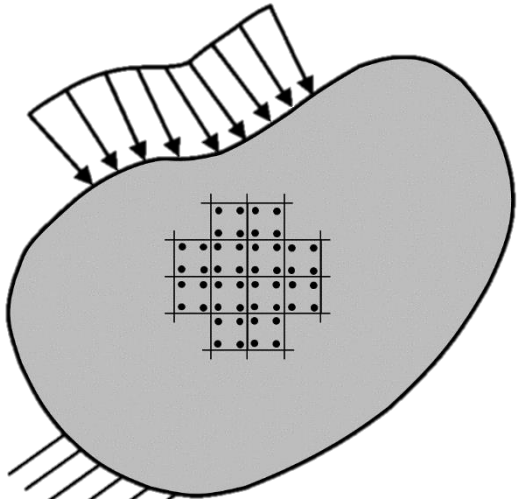

Micro-scale

Data-supported microstructure

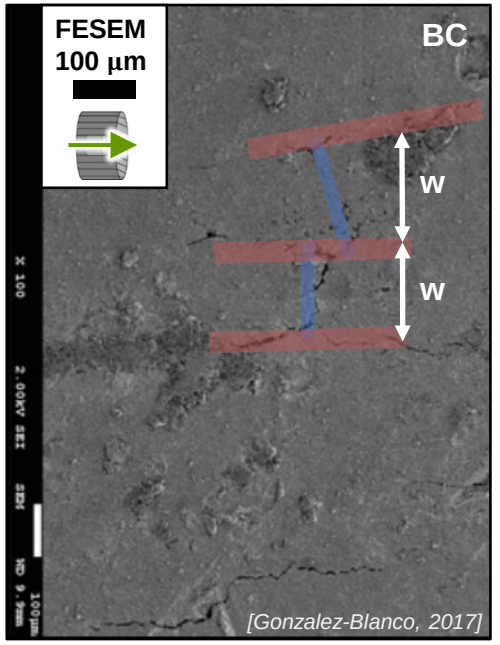

Physical idealisation

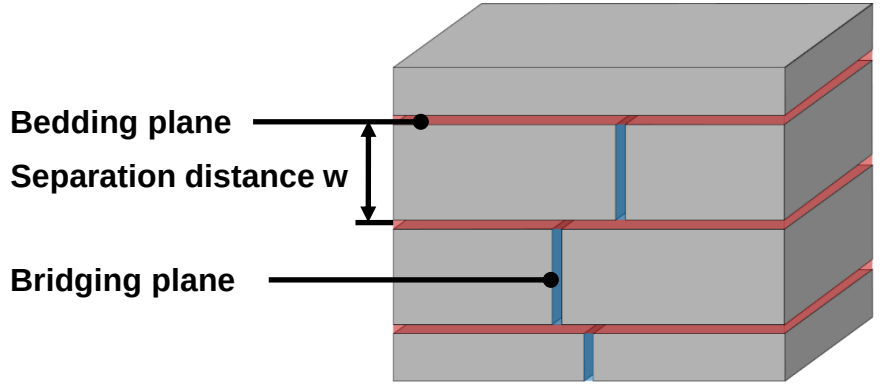

Hydro-mechanical multi-scale model

Macro-scale

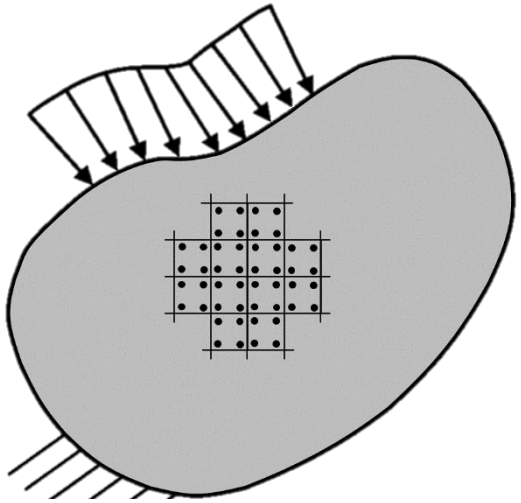

Micro-scale

Data-supported microstructure

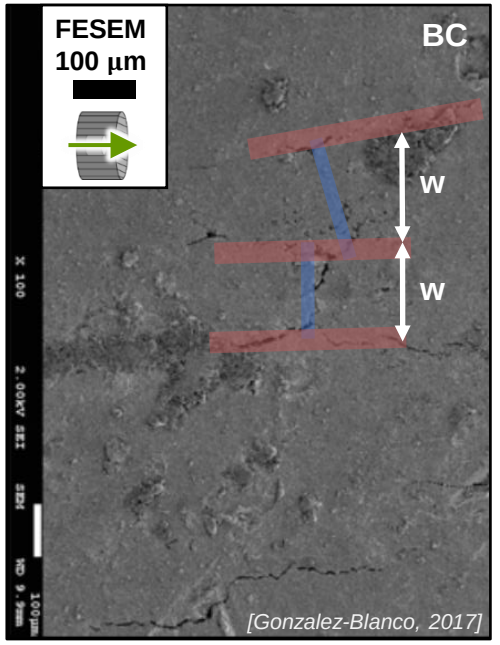

Physical idealisation

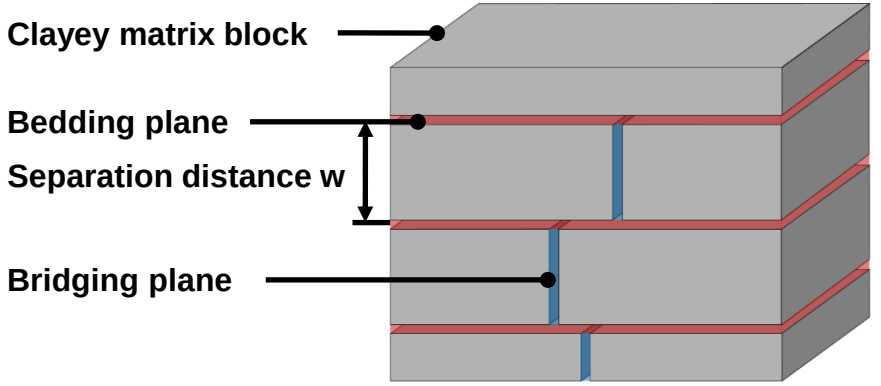

Hydro-mechanical multi-scale model

Macro-scale

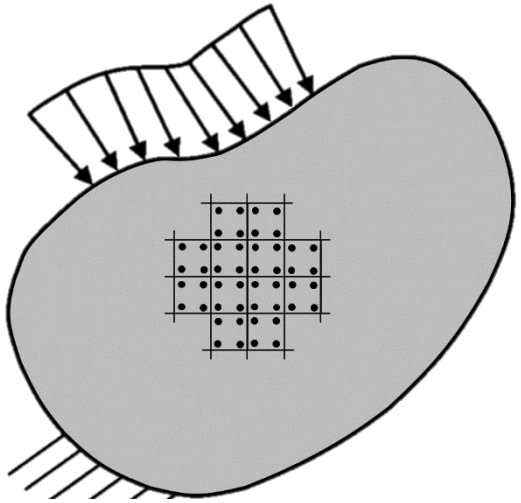

Micro-scale (REV)

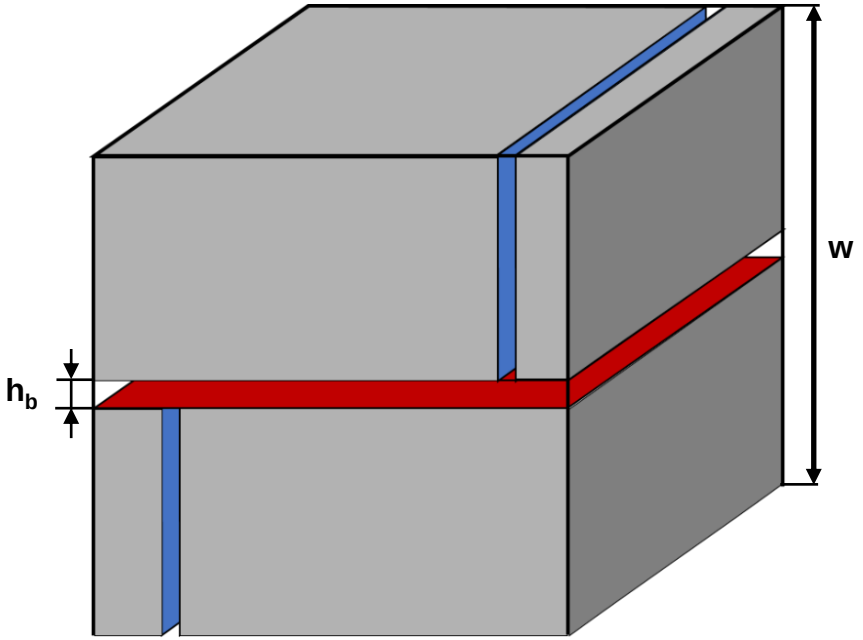

Data-supported microstructure

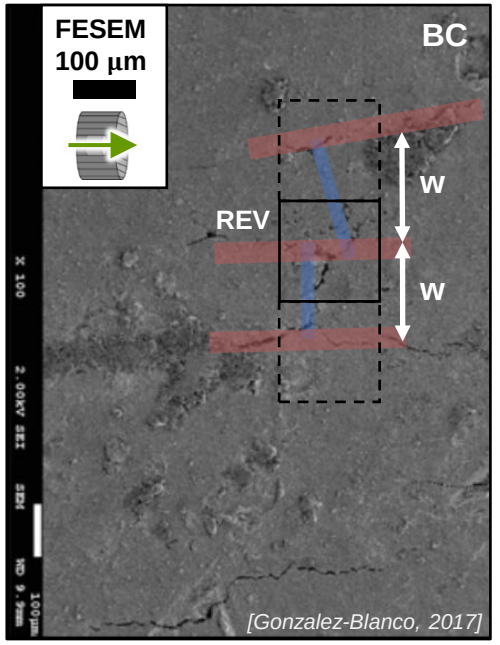

Physical idealisation

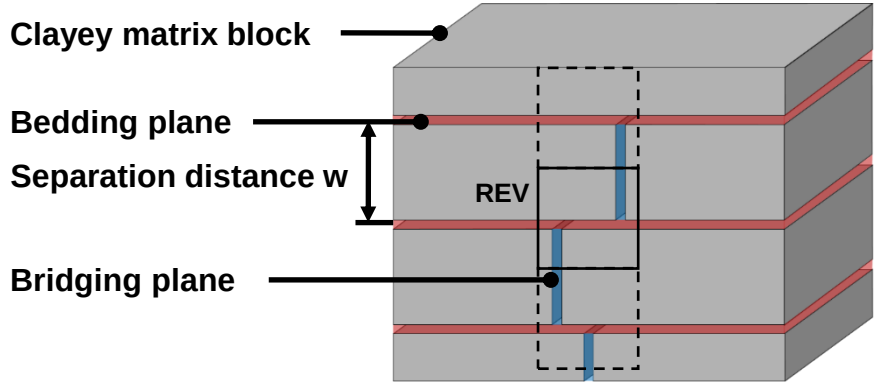

Hydro-mechanical multi-scale model

Macro-scale

Mechanics

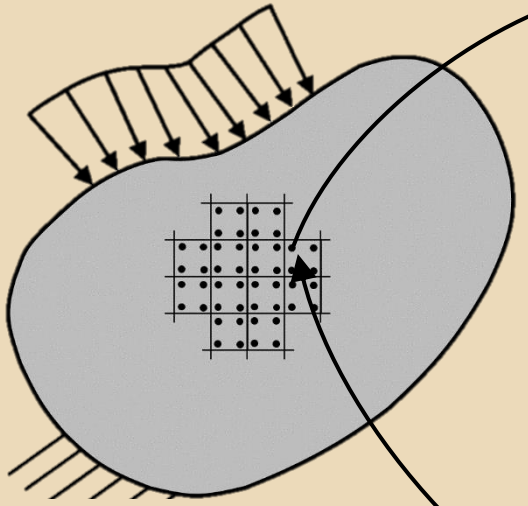

4. Macro-scale FE computations

1. Localisation

HM couplings

2. Resolution of the hydraulic system

3. Homogenisation

Micro-scale (REV)

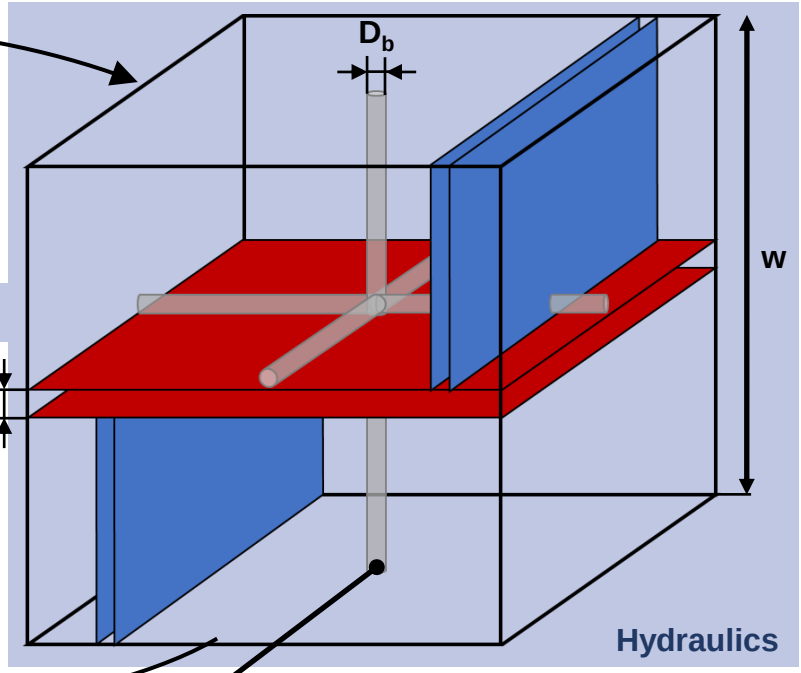

Equivalent bundle of tubes

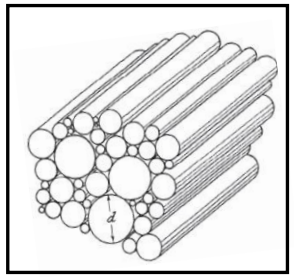

Data-supported microstructure

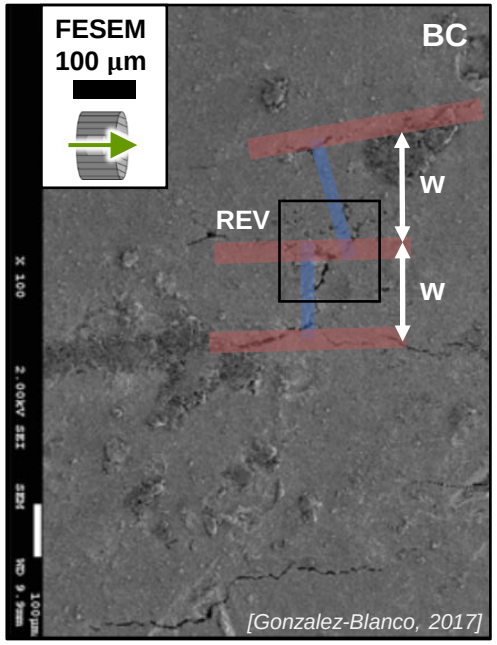

Physical idealisation

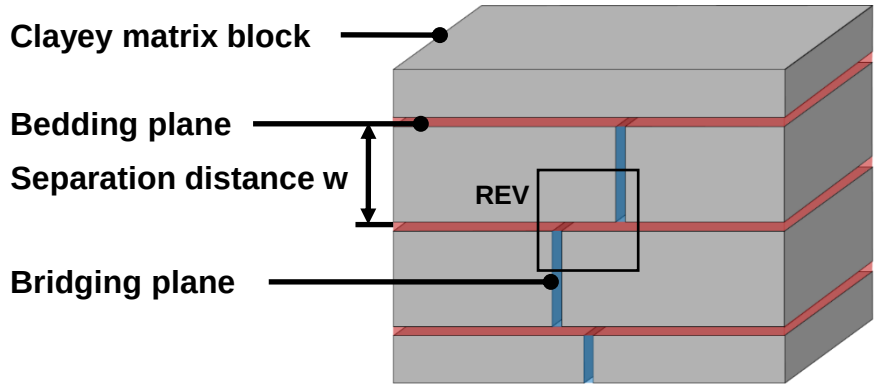

Gas injection test modelling

Problem statement

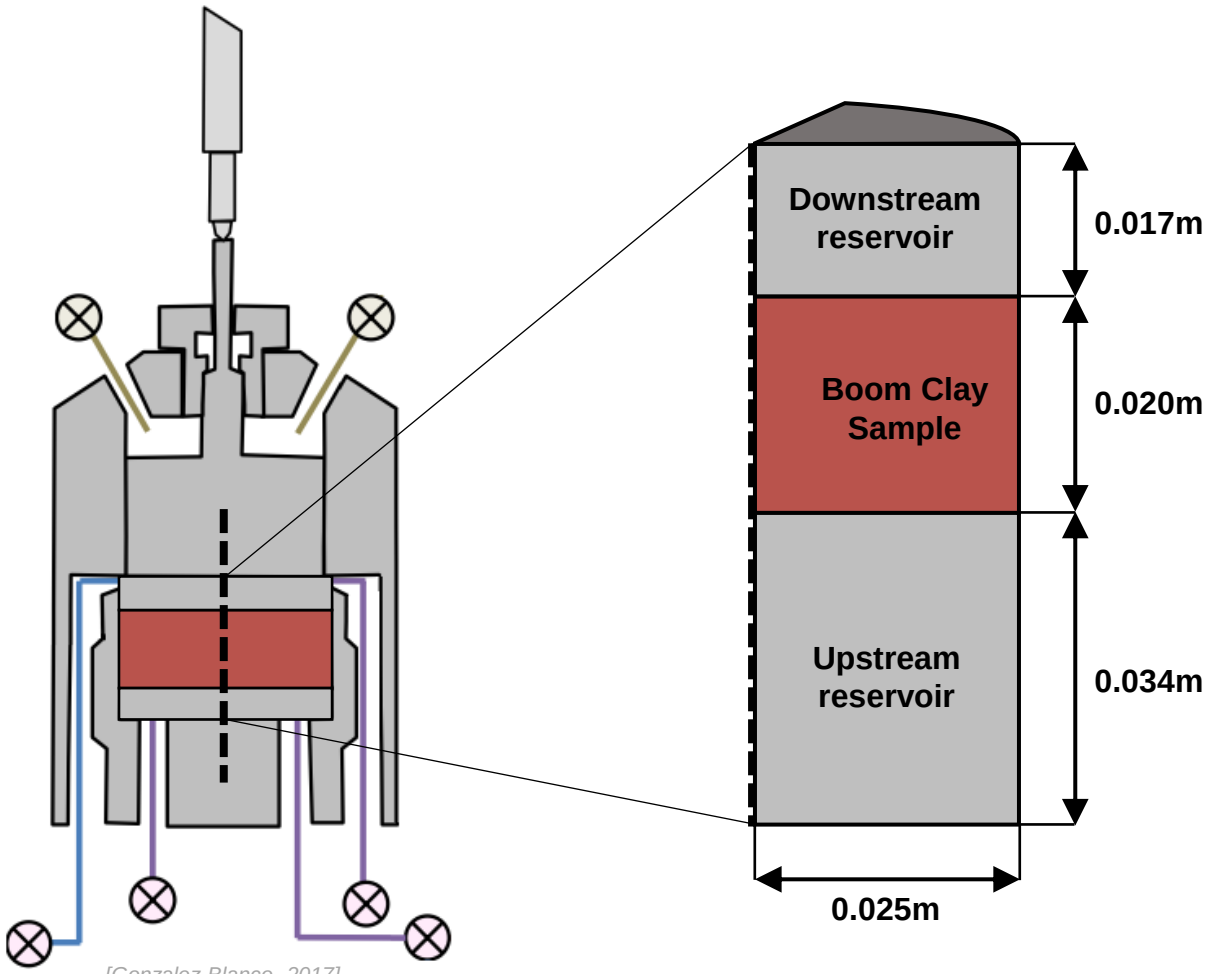

[Gonzalez-Blanco, 2017]

Gas injection test modelling

Problem statement

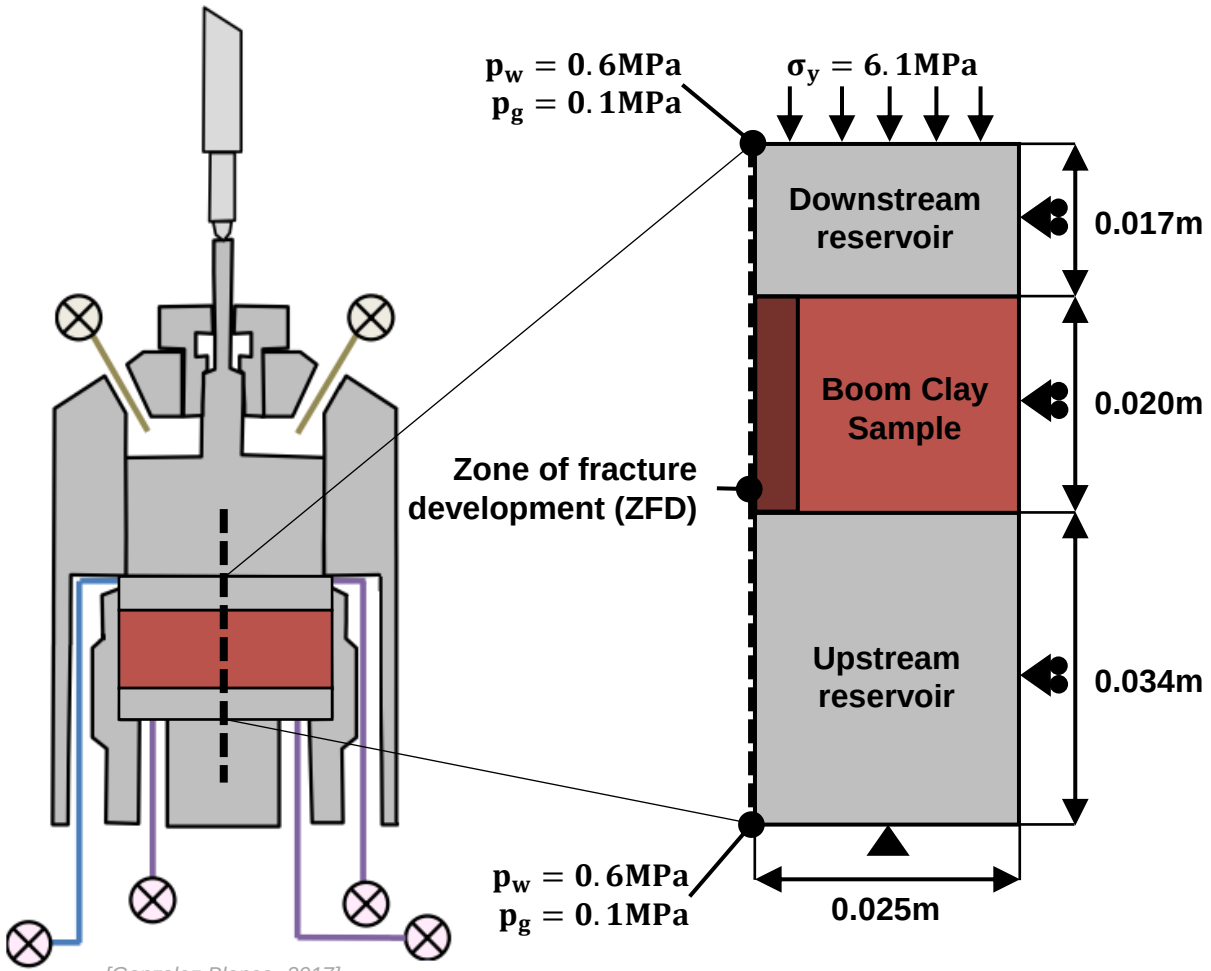

[Gonzalez-Blanco, 2017]

Gas injection test modelling

Problem statement

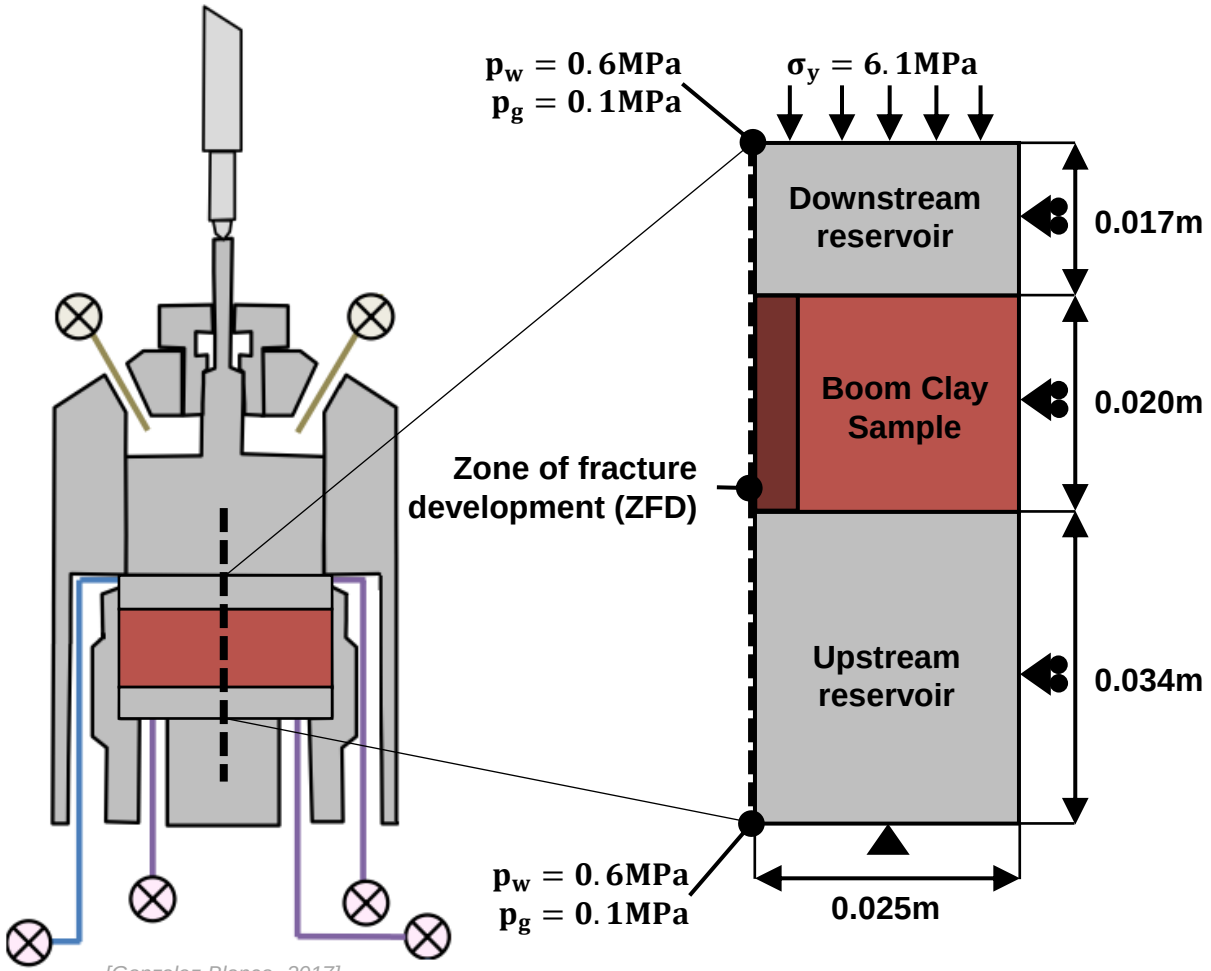

[Gonzalez-Blanco, 2017]

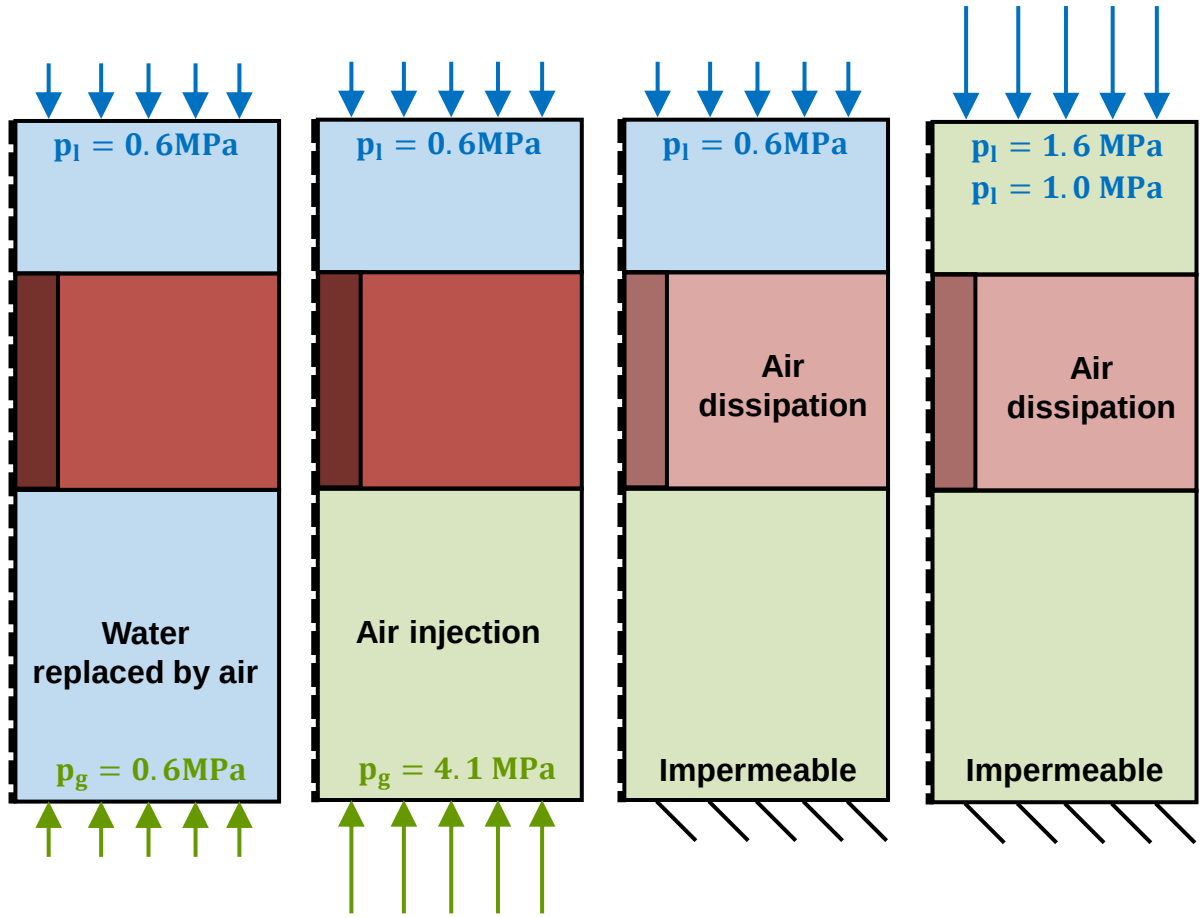

Gas injection test modelling

Average axial strain

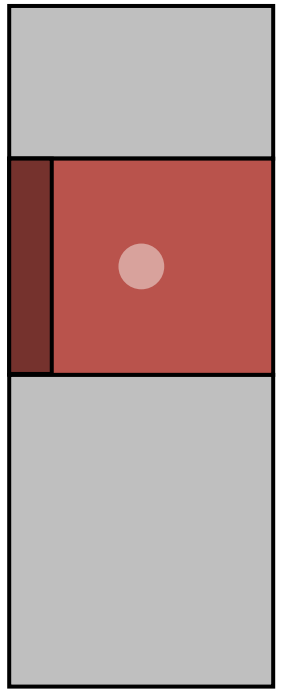

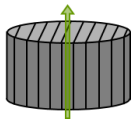

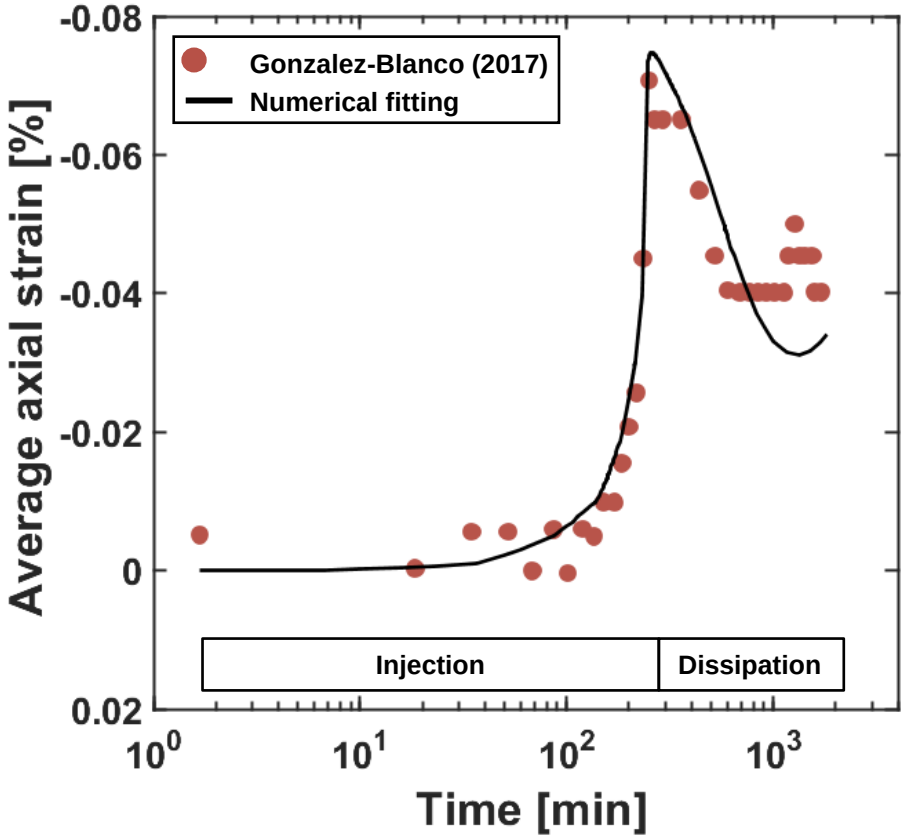

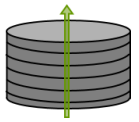

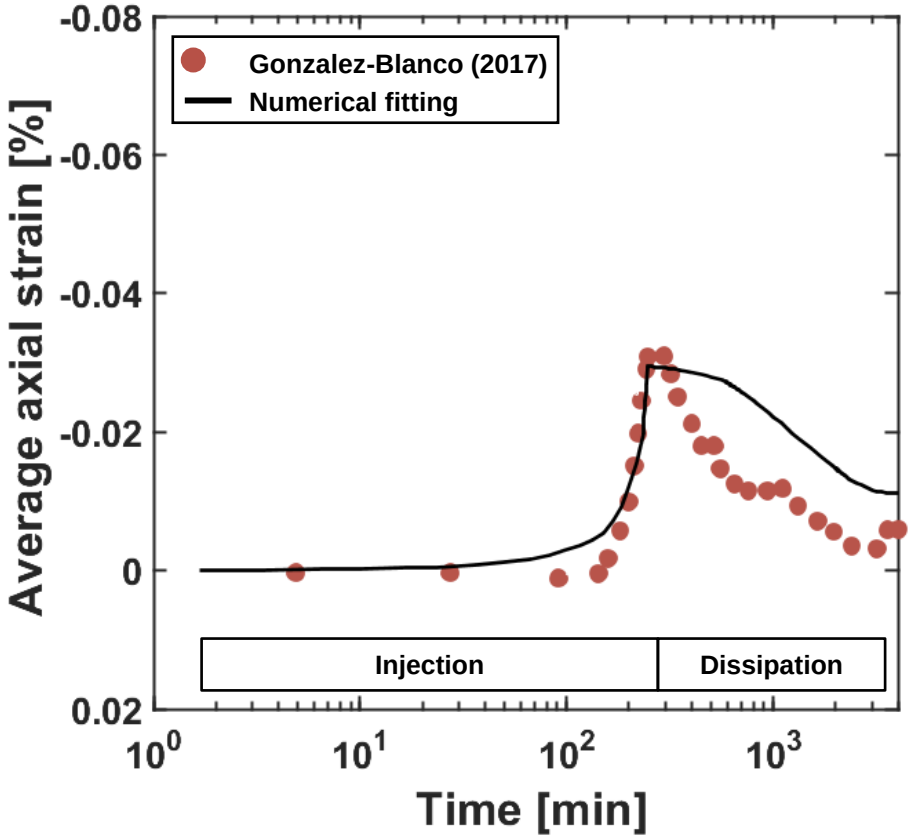

Gas injection test modelling

Injection and recovery pressure

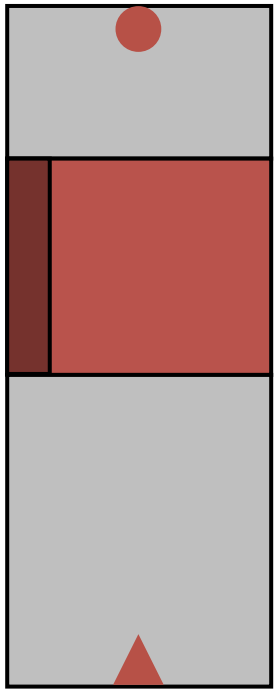

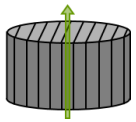

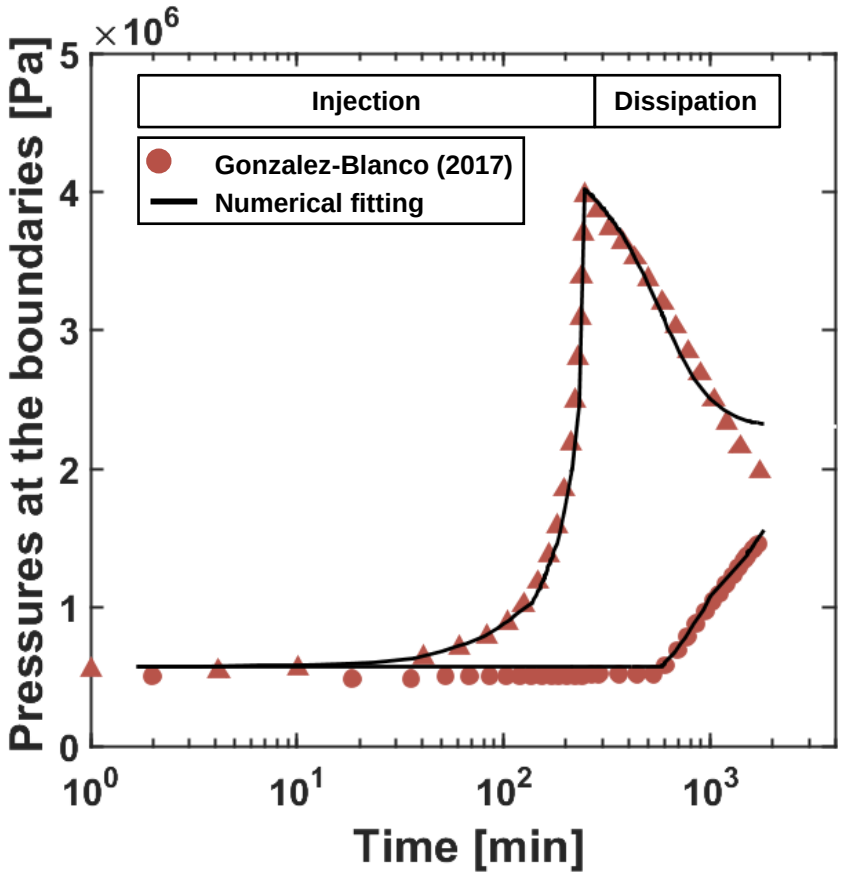

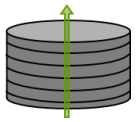

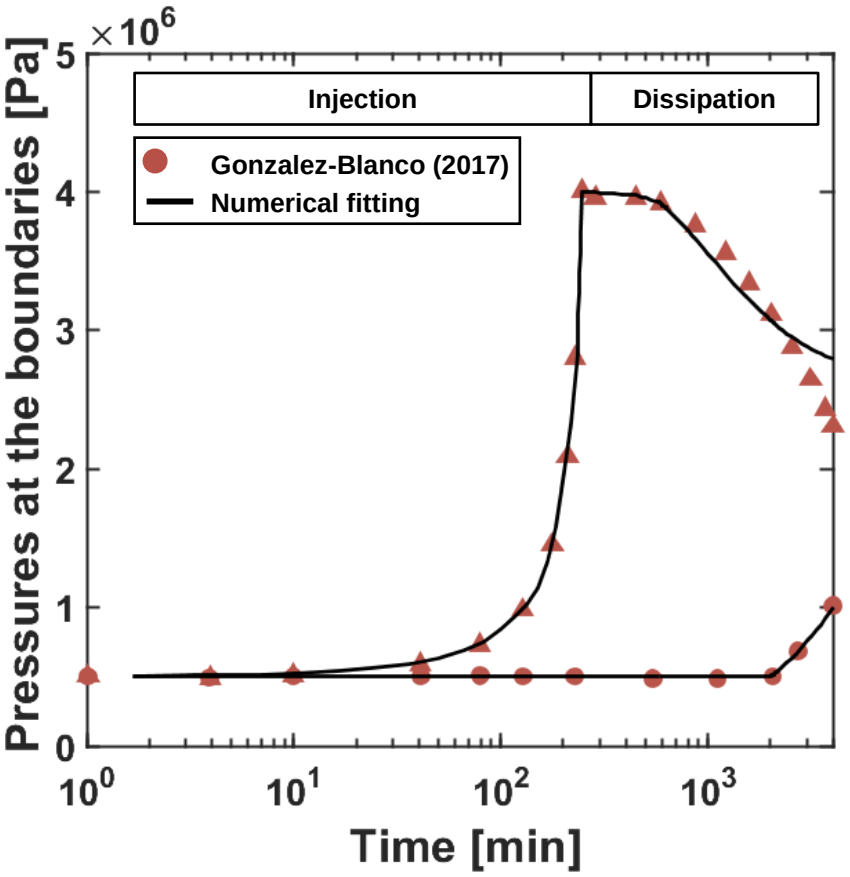

Gas injection test modelling

Maps of gas pressure

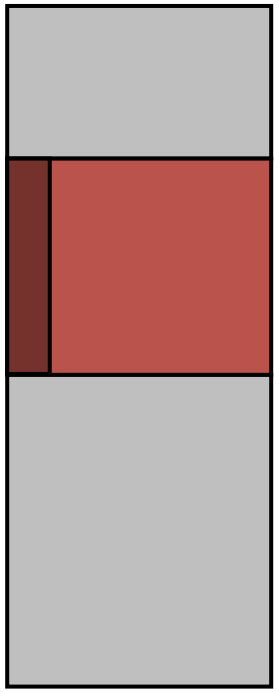

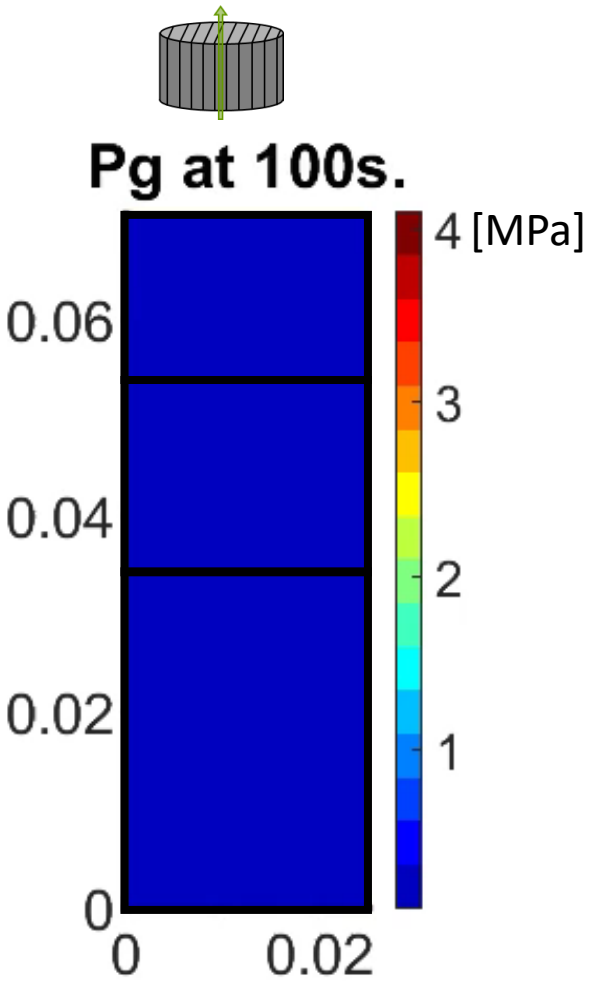

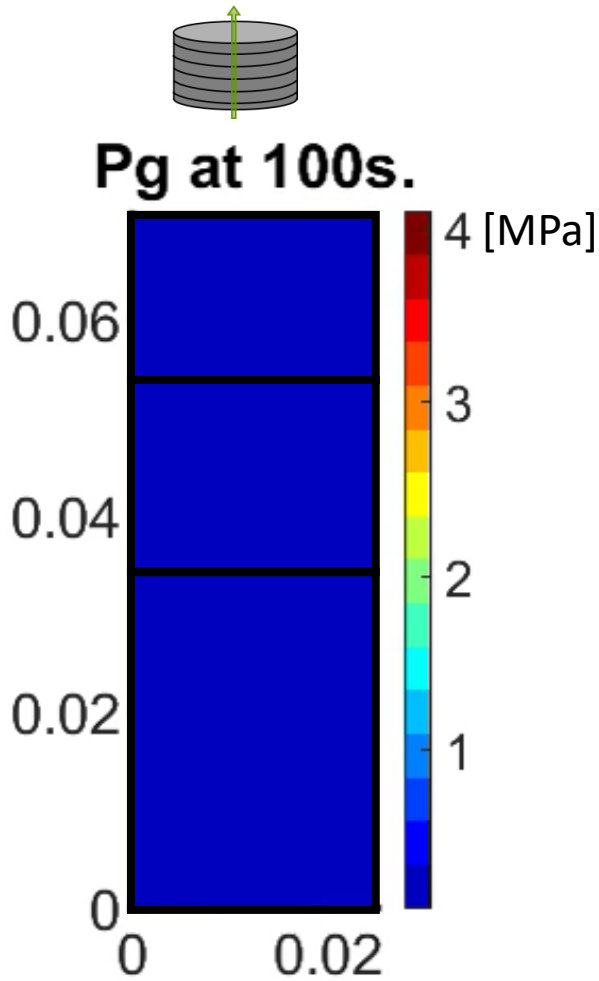

Gas injection test modelling

Maps of gas pressure

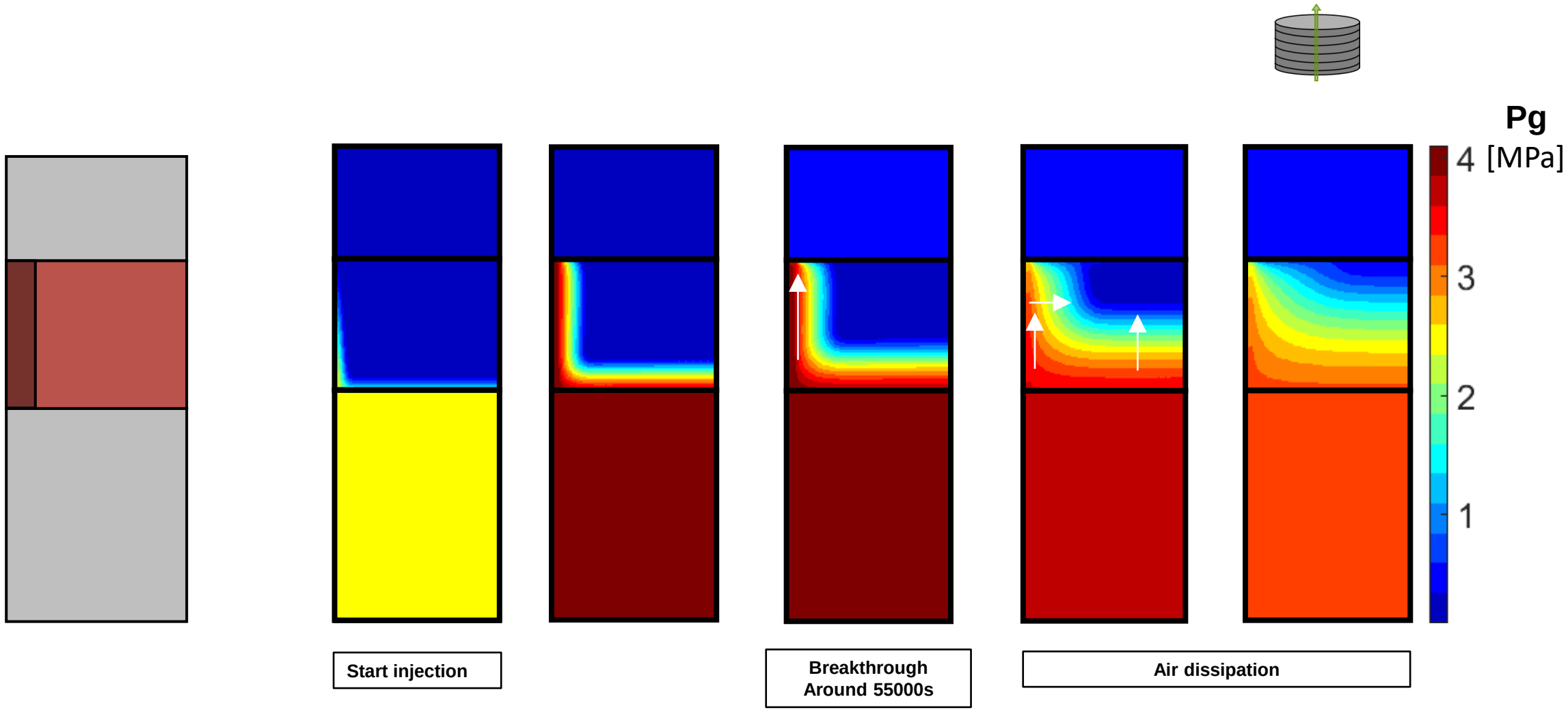

Up-scaled configuration modelling

Problem statement

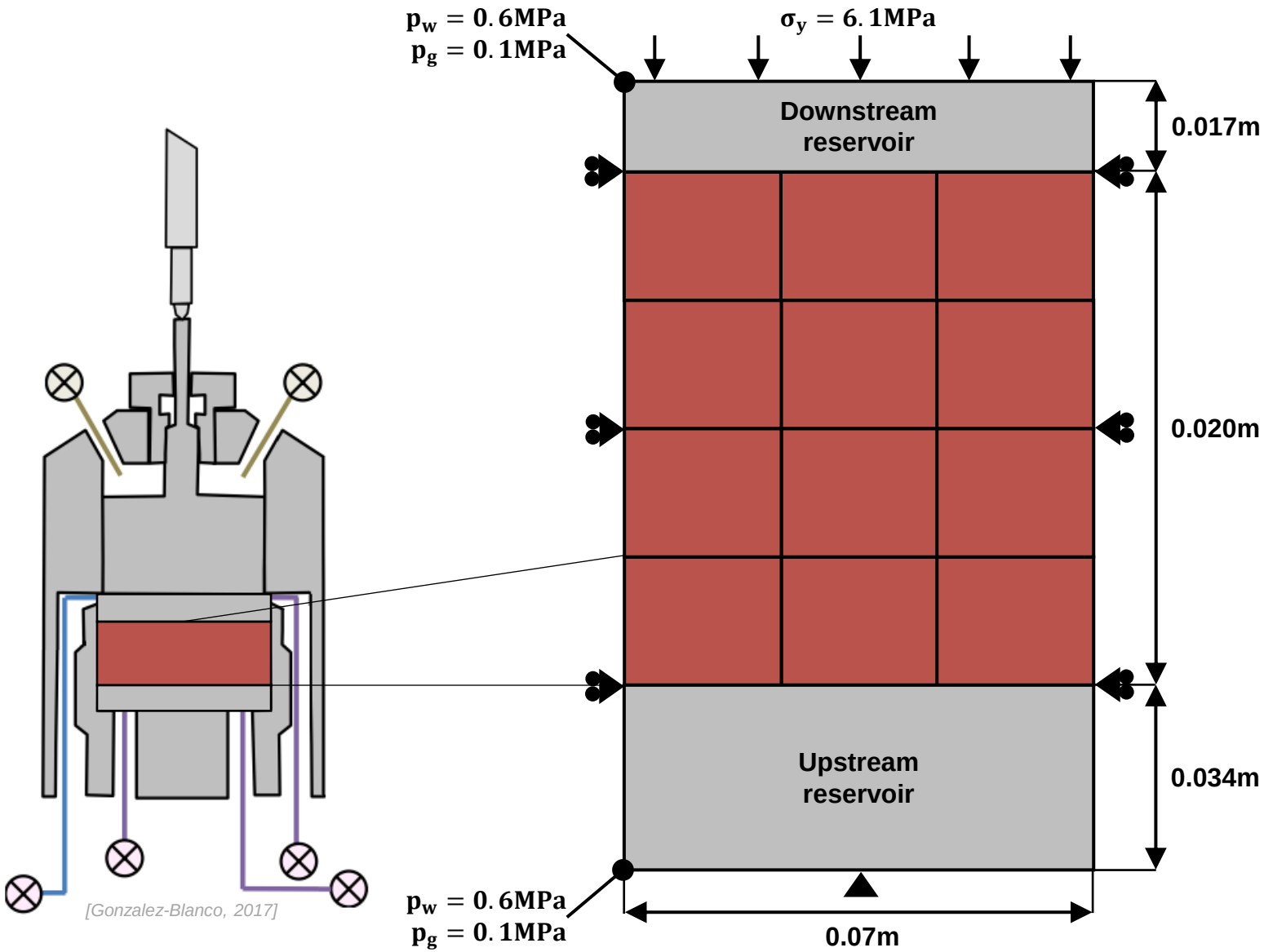

[Gonzalez-Blanco, 2017]

Up-scaled configuration modelling

Problem statement

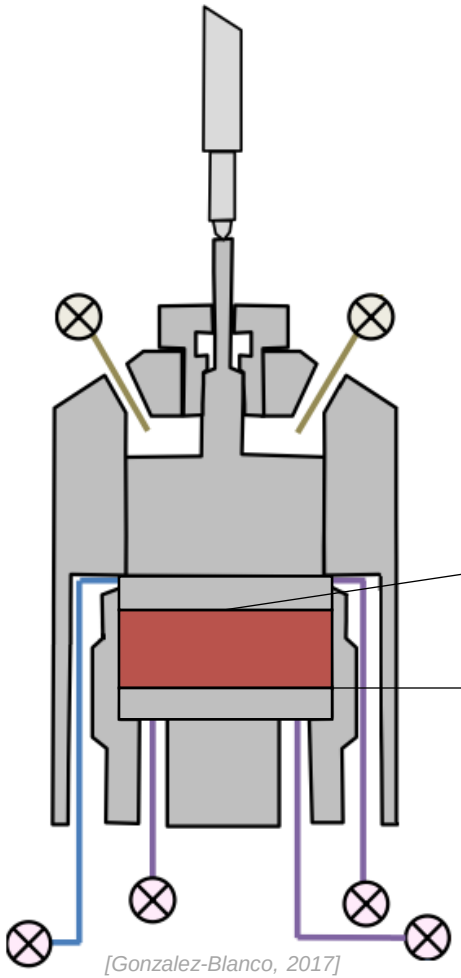

[Gonzalez-Blanco, 2017]

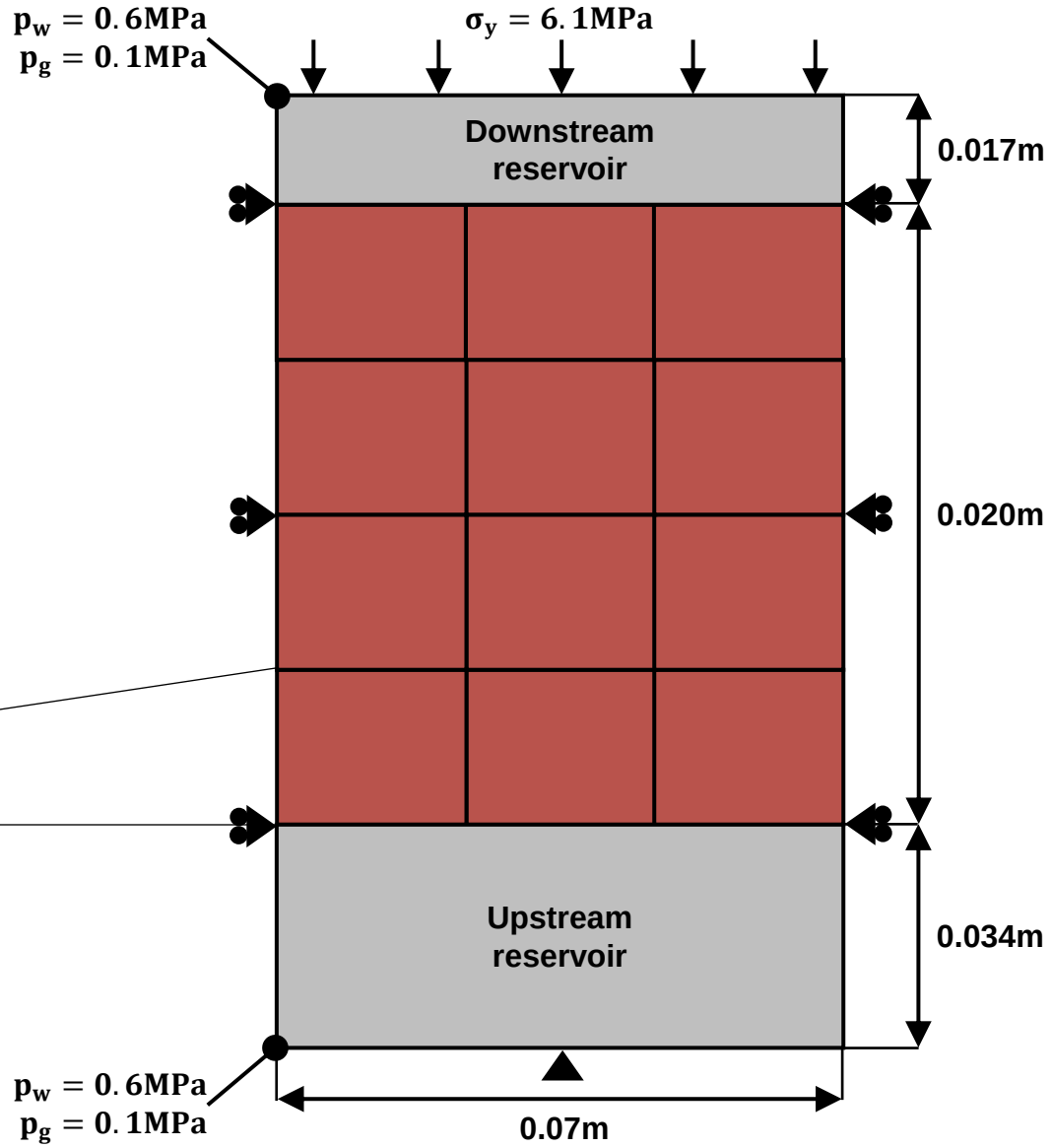

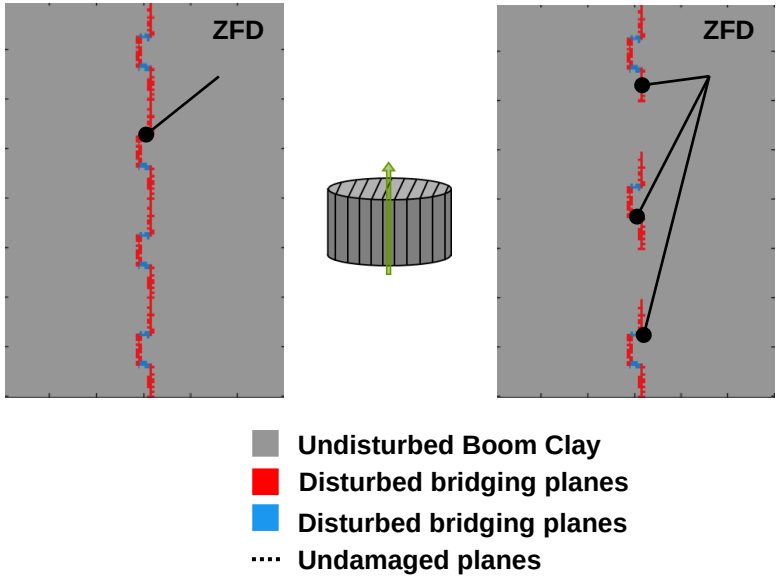

Conceptualisation

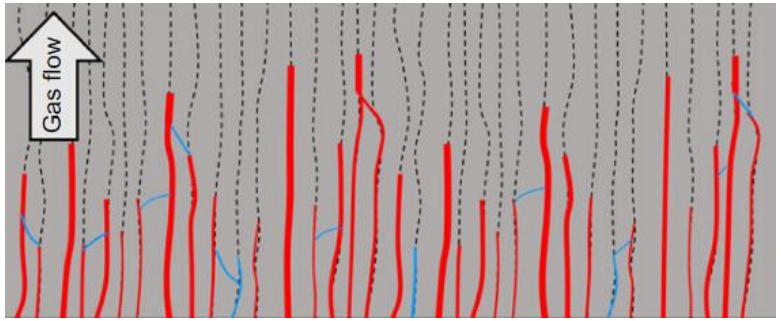

[Gonzalez-Blanco, 2017]

Up-scaled configuration modelling

Maps of gas pressure

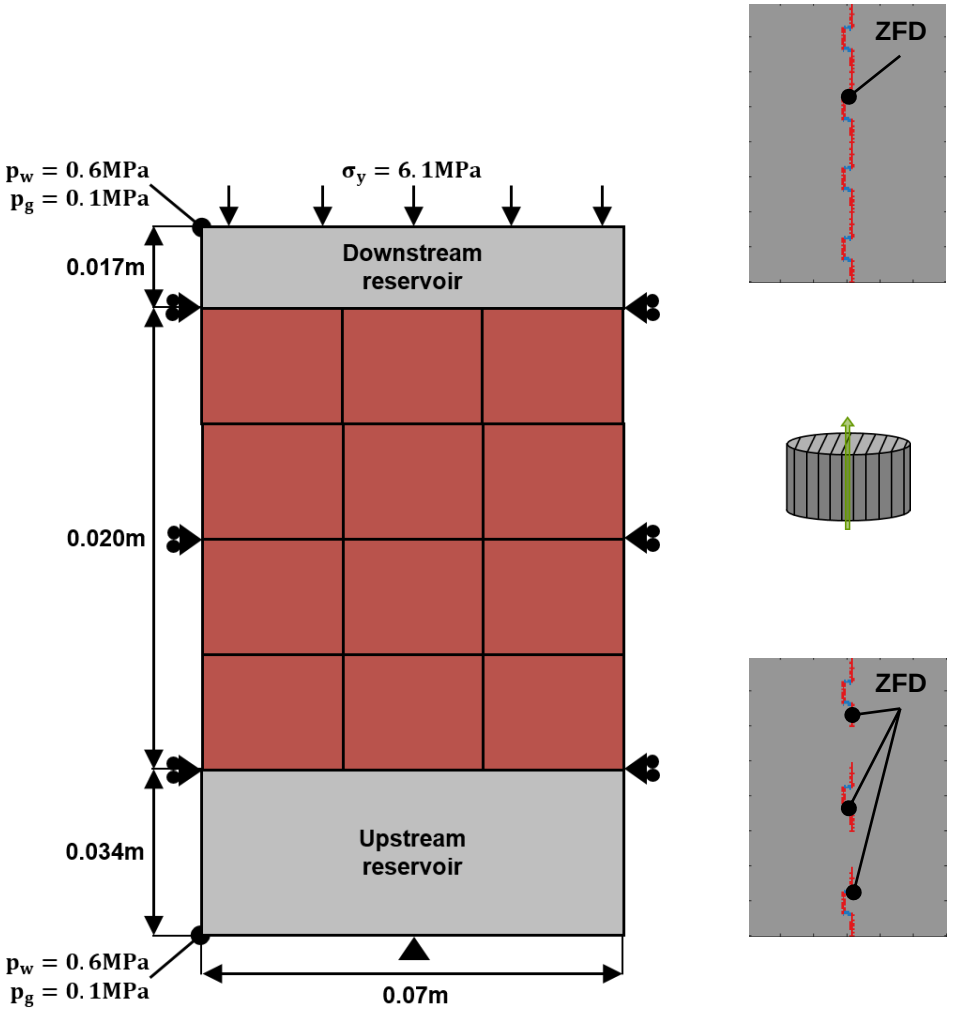

Undisturbed Boom Clay
Disturbed bridging planes
Disturbed bridging planes

Up-scaled configuration modelling

Maps of gas pressure

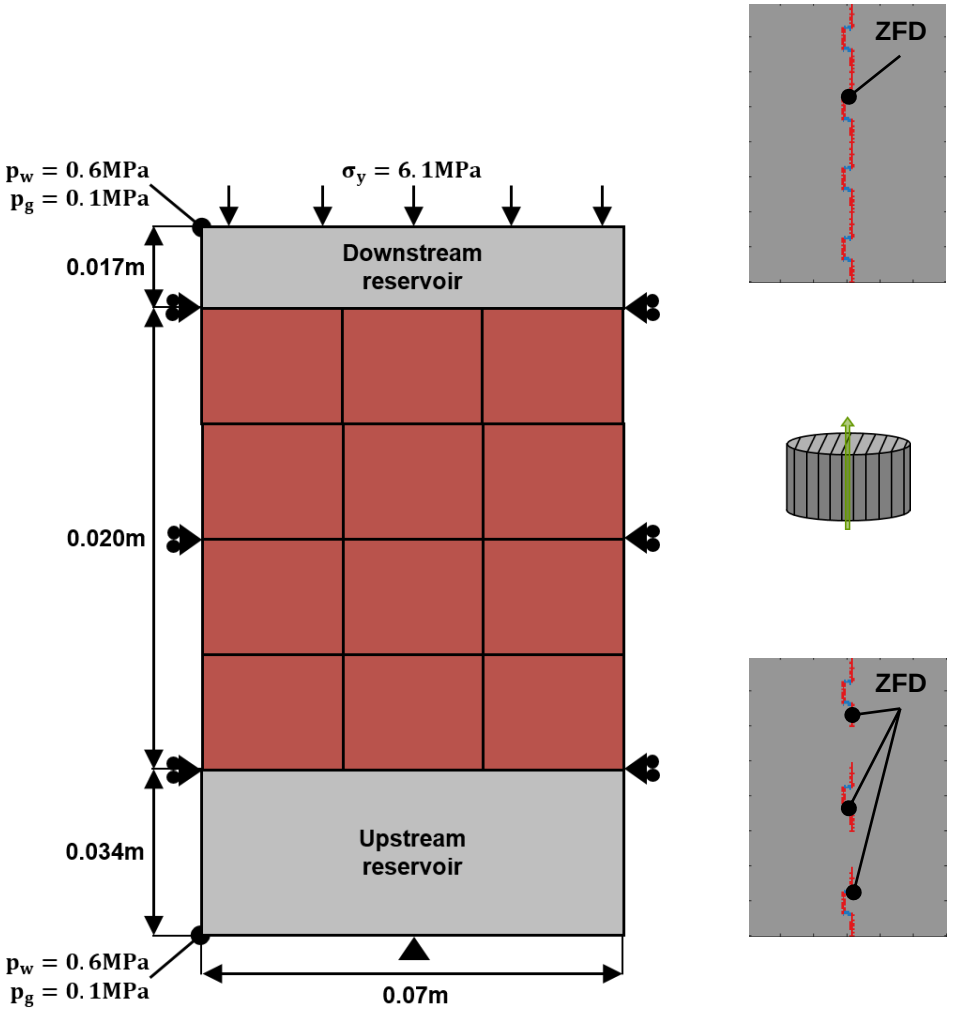

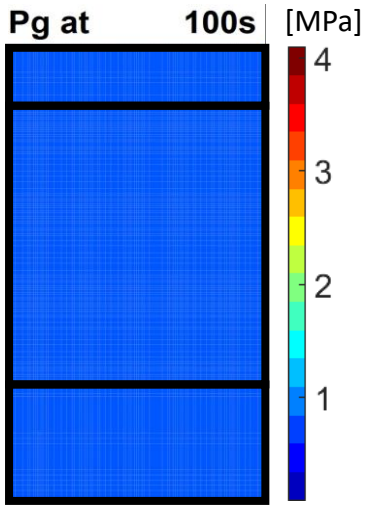

Undisturbed Boom Clay
Disturbed bridging planes
Disturbed bridging planes

Up-scaled configuration modelling

Maps of gas pressure

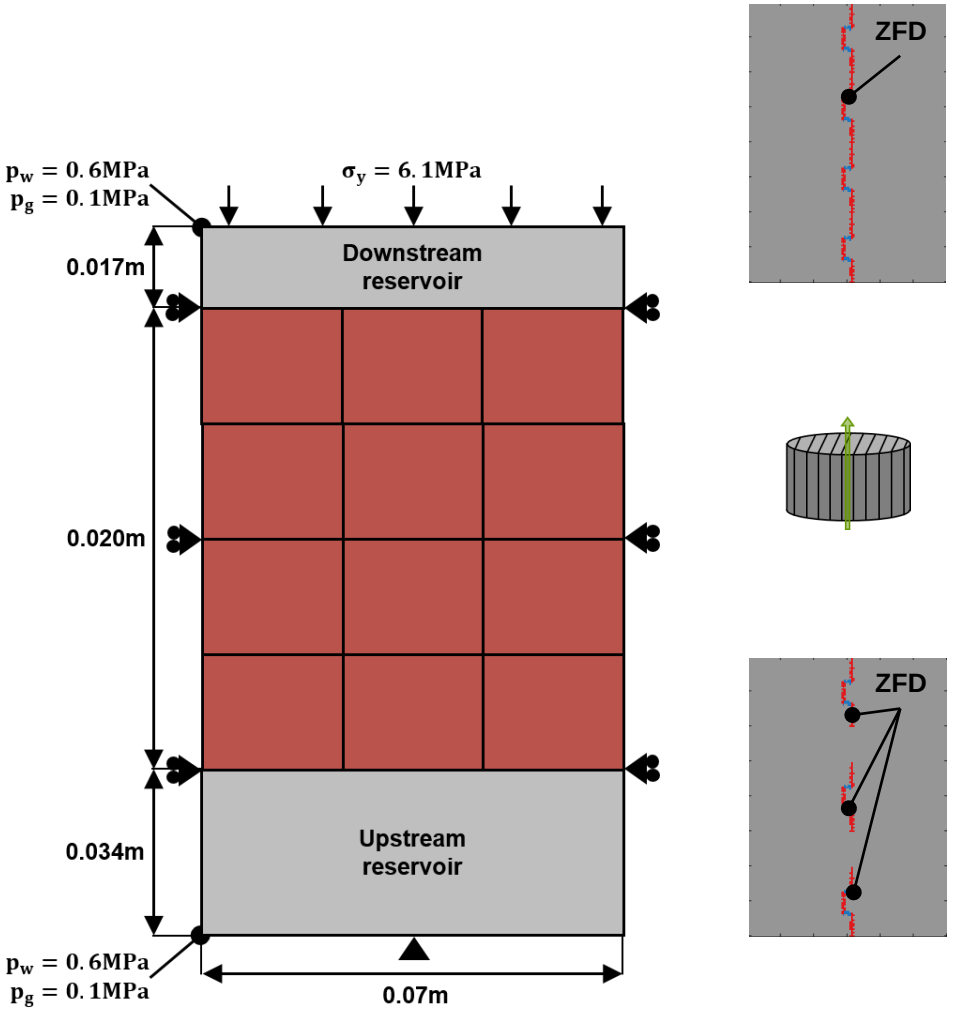

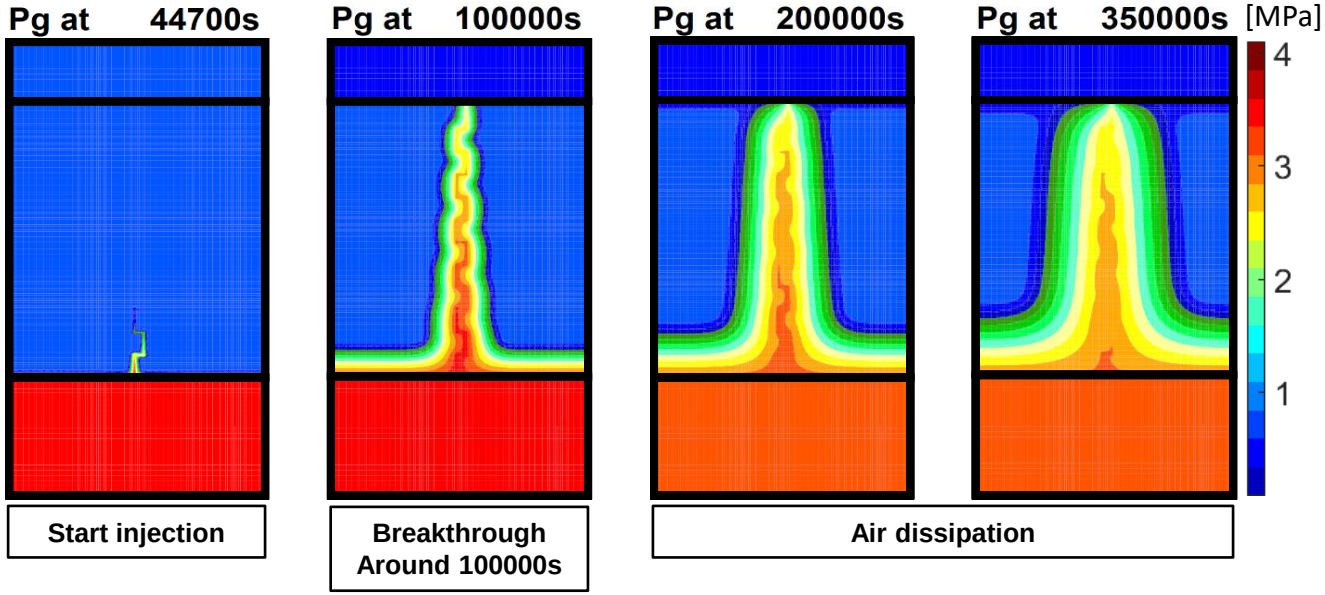

Undisturbed Boom Clay
Disturbed bridging planes
Disturbed bridging planes

Up-scaled configuration modelling

Maps of gas pressure

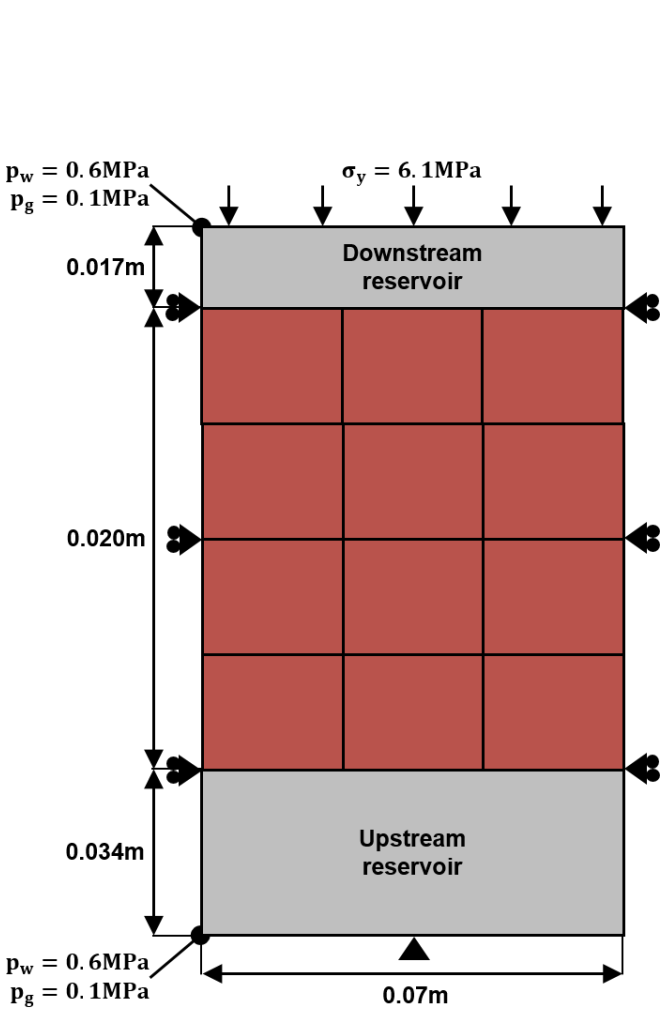

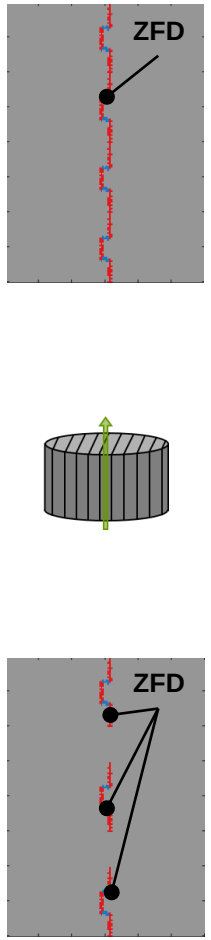

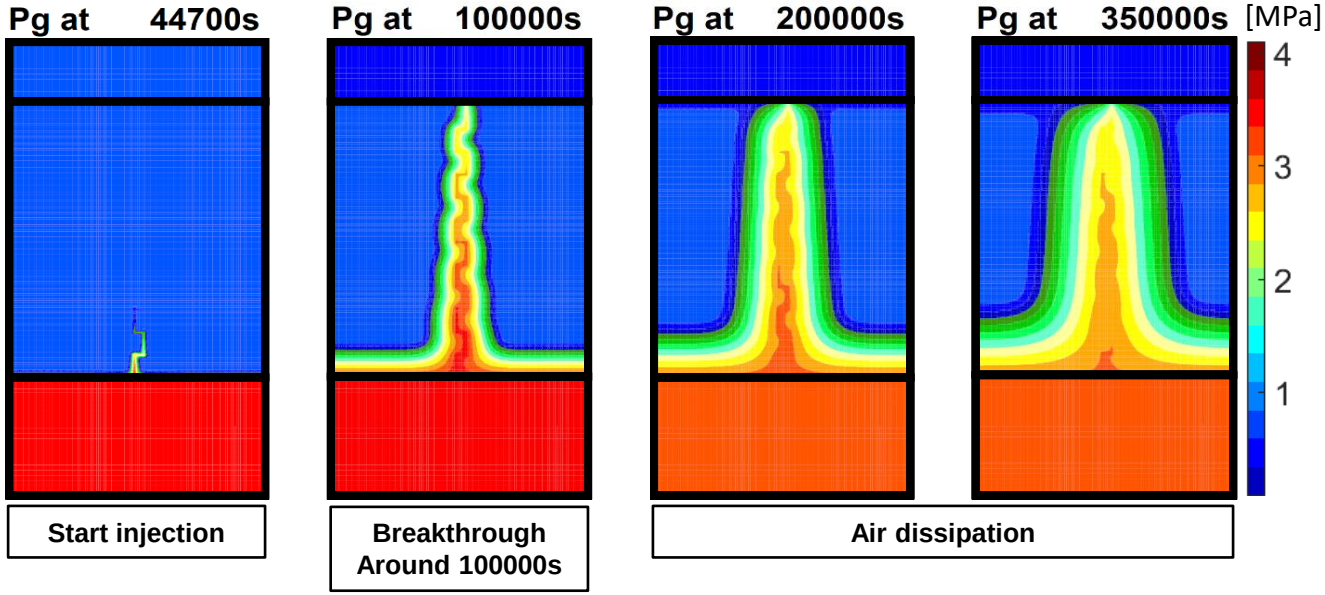

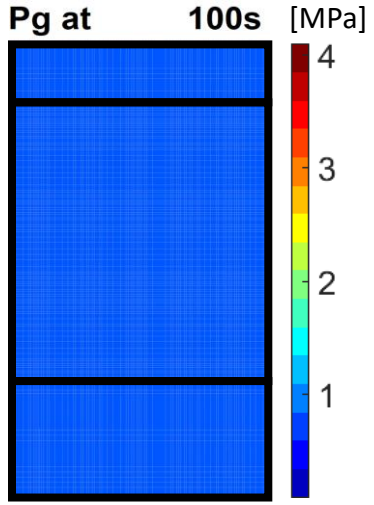

Undisturbed Boom Clay
Disturbed bridging planes
Disturbed bridging planes

Up-scaled configuration modelling

Maps of gas pressure

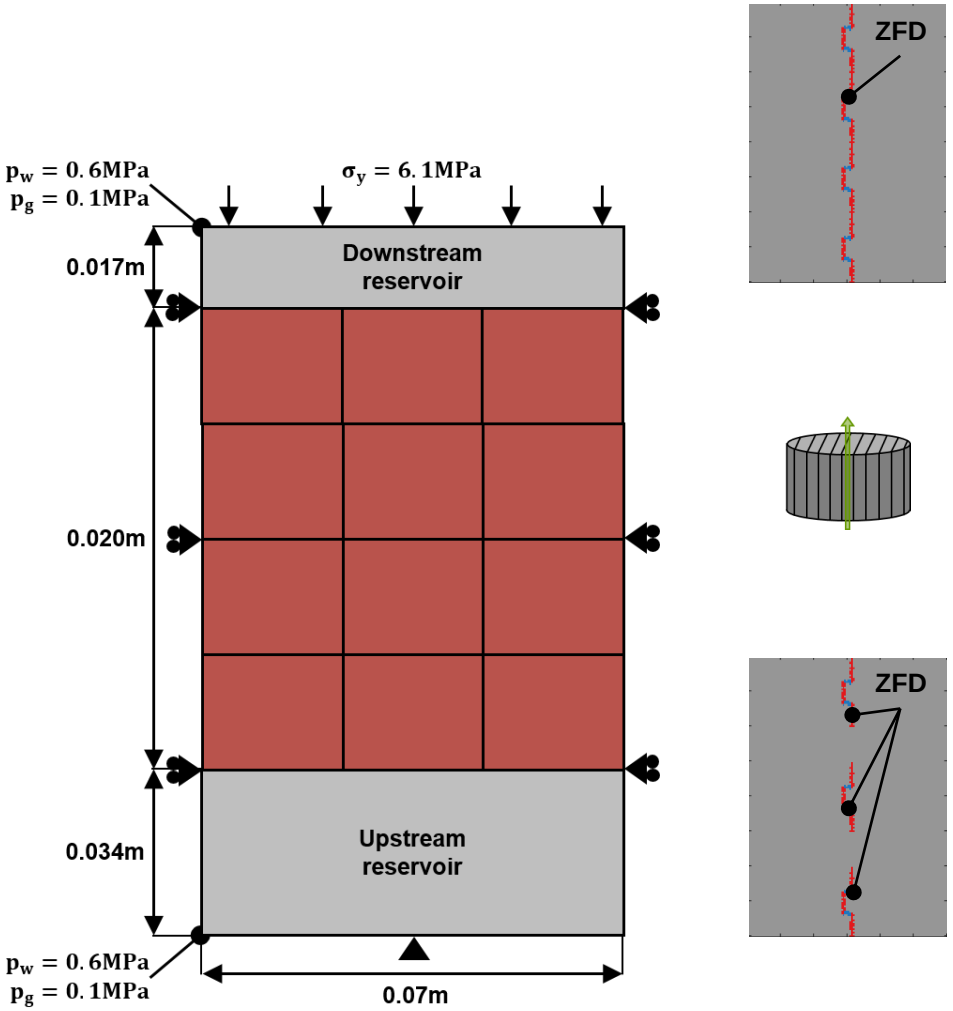

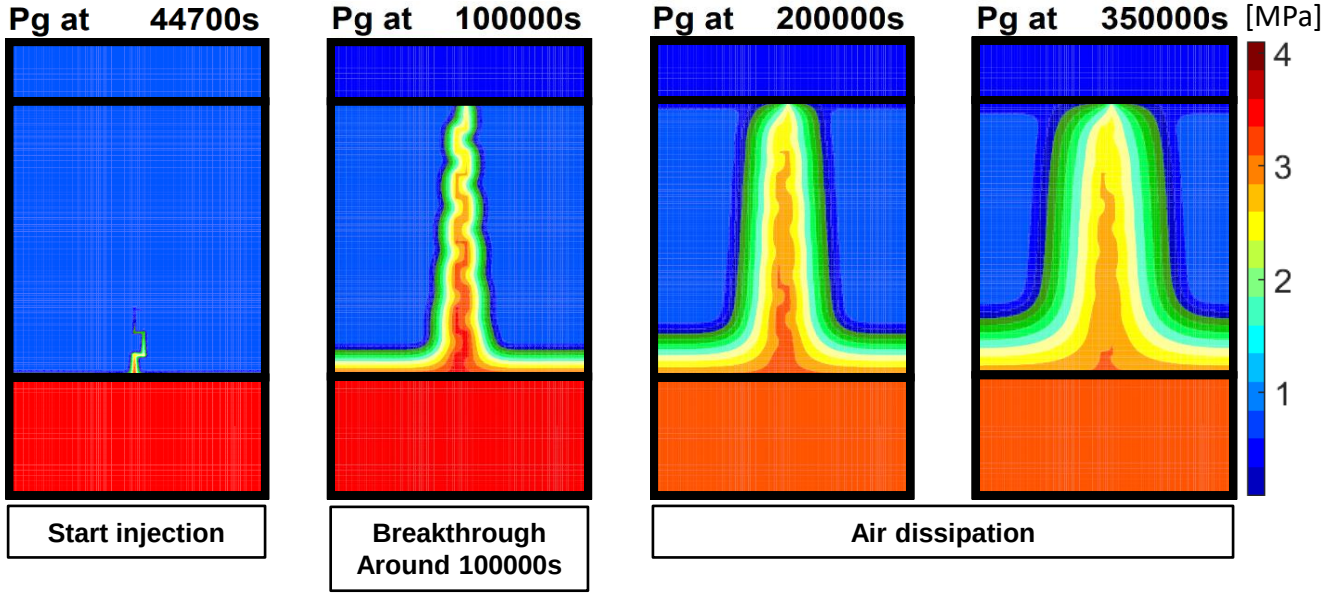

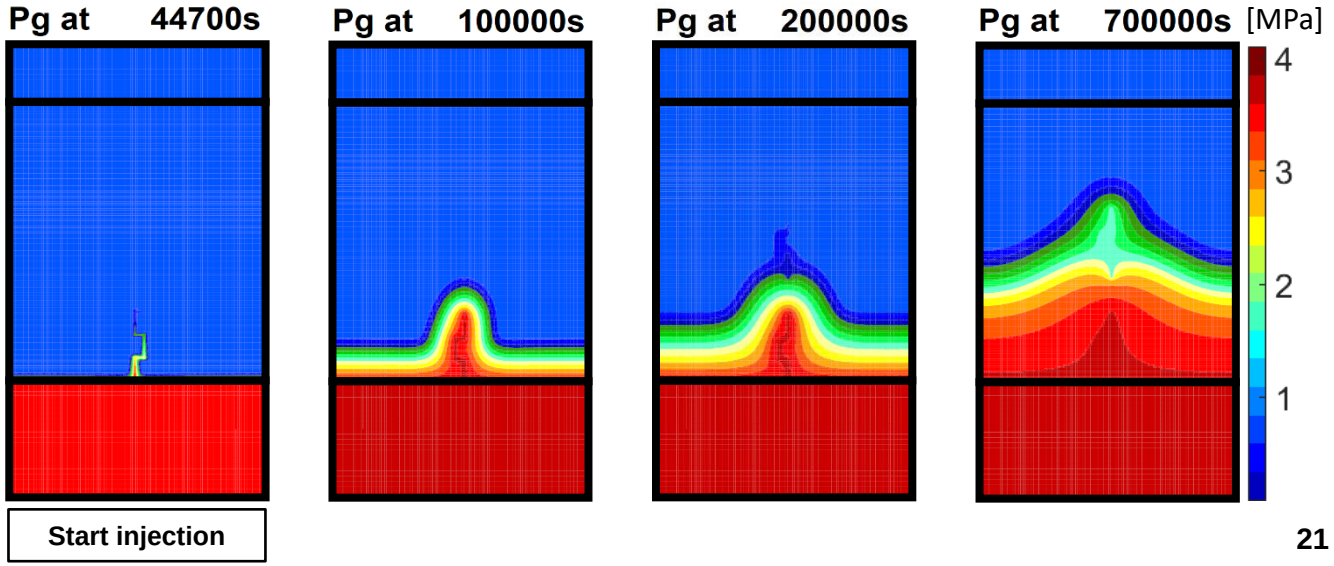

Conclusion

When gas builds up, do clay-rich rocks (re)fracture?

Phenomenological description

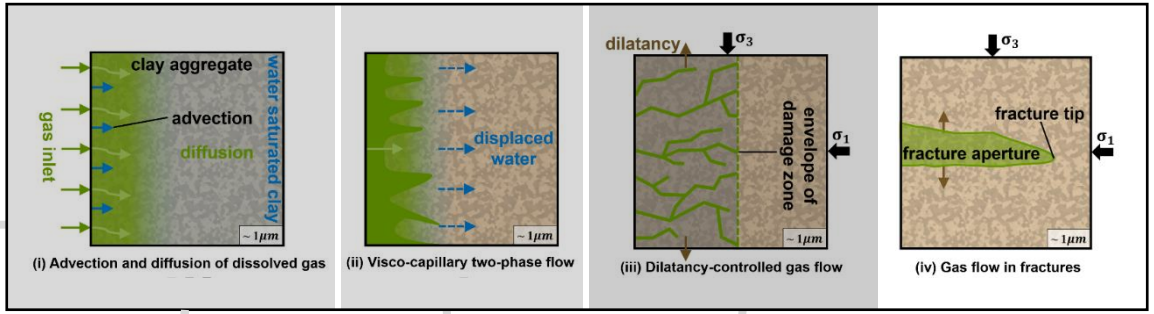

Numerical implementation

Second gradient H²M model

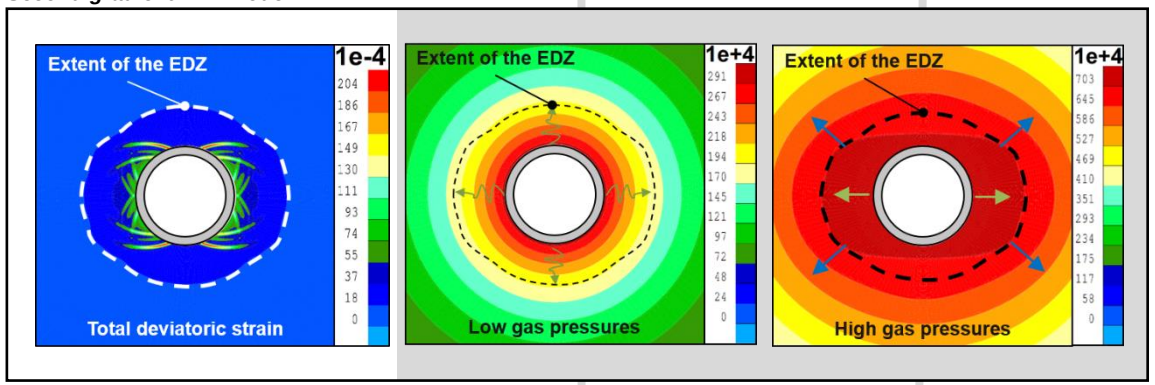

Multi-scale HM model

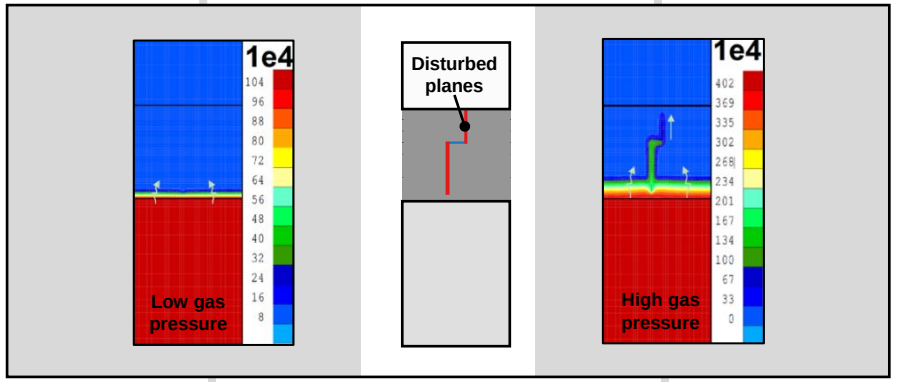

Repository-scale conceptualisation

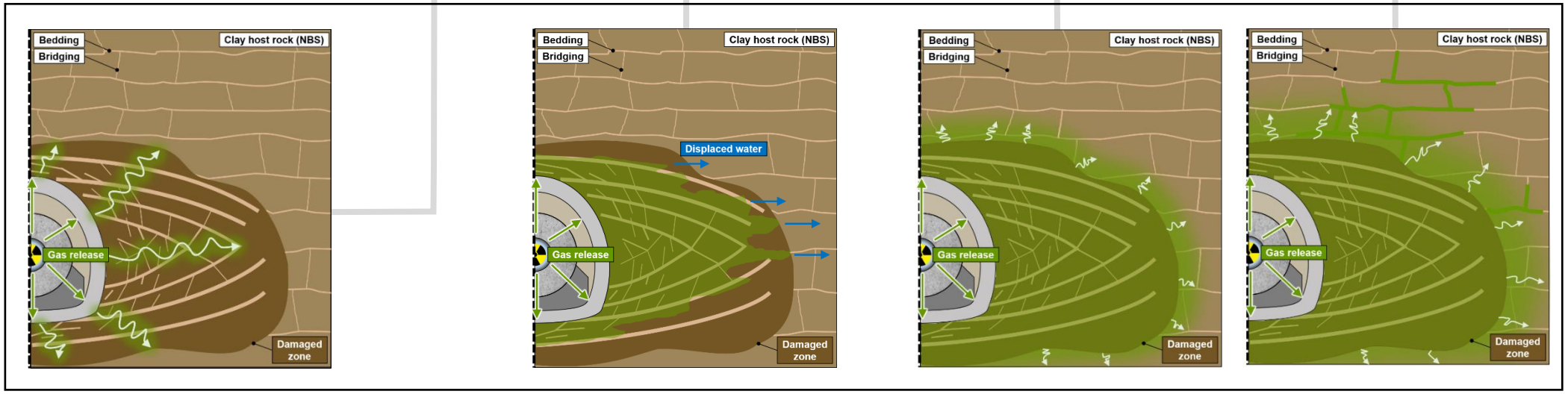

CFMR
COMITÉ FRANÇAIS DE MÉCANIQUE DES ROCHES

Thank you for your attention

**When gas builds up,
do clay-rich rocks (re)fracture?**

Gilles CORMAN & Frédéric COLLIN
gilles.corman@uliege.be

May 28, 2026 • Mines Paris (France)

This project has received funding from the European Union's Horizon 2020 research and innovation programme under grant agreement n° 847593.

eurad
European Joint Programme on Radioactive Waste Management

LIÈGE université

References I

- [BP, 2022] BP (2022). BP Statistical Review of World Energy 2022. Technical report, BP, London, The United Kingdom.
- [Smil, 2016] Smil, V. (2016). Energy Transitions: Global and National Perspectives, 2nd Edition. Online, Praeger Edition.
- [IAEA, 2021] IAEA (2021). Energy, Electricity and Nuclear Power Estimates for the Period up to 2050. Reference data series No. 1, 2021 Edition. Technical report, International Atomic Energy Agency, Vienna, Austria.
- [IPCC, 2022] IPCC (2022). Mitigation pathways compatible with long-term goals. In *IPCC, 2022: Climate Change 2022: Mitigation of Climate Change. Contribution of Working Group III to the Sixth Assessment Report of the Intergovernmental Panel on Climate Change.* Cambridge University Press.
- [IAEA, 2023] PRIS – The Database on Nuclear Power Reactors, Online, Accessed 18 December 2023.
- [IAEA, 2009] IAEA (2009). Classification of Radioactive Waste. General Safety Guide No. GSG-1. Technical report, International Atomic Energy Agency, Vienna, Austria.
- [KASAM, 1998] KASAM (1998). Nuclear Waste. State-of-the-art reports 1998. Technical report, Report from the Swedish National Council for Nuclear Waste, Stockholm, Sweden.
- [ENSI/IFSN, 2021] ENSI/IFSN (2021). Geologische Tiefenlager – Radioaktive Abfälle Sicher Entsorgen. Informationsbroschüre from the Swiss Federal Nuclear Safety Inspectorate, Brugg, Switzerland.
- [Sillen, 2012] Sillen, X. (2012). Keynote on repository-induced perturbations of the host rock, in the context of the safety case for the geological disposal of VHLW and SF in clay formations. In *Proceedings of the European Commission TIMODAZ-THERESA International Conference*, pages 159–171, Brussels, Belgium.
- [Marschall et al., 2005] Marschall, P., Horseman, S., and Gimmi, T. (2005). Characterisation of Gas Transport Properties of the Opalinus Clay, a Potential Host Rock Formation for Radioactive Waste Disposal. *Oil & Gas Science and Technology – Rev. IFP*, 60(1):121–139.
- [Henry, 1803] Henry, W. (1803). Experiments on the quantity of gases absorbed by water, at different temperatures, and under different pressures. *Society*, 93:29–274.
- [Fick, 1855] Fick, A. (1855). Über Diffusion [Translated: On liquid diffusion]. *Poggendorff's Annalen der Physik und Chemie*, 170(1):59–86.

References II

- [Jacops et al., 2013] Jacops, E., Volckaert, G., Maes, N., Weetjens, E., and Govaerts, J. (2013). Applied Clay Science Determination of gas diffusion coef fi cients in saturated porous media : He and CH4 diffusion in Boom Clay. *Applied Clay Science*, 83-84:217–223.
- [Jacops et al., 2015] Jacops, E.,Wouters, K., Volckaert, G., Moors, H., Maes, N., Bruggeman, C., Swennen, R., and Littke, R. (2015). Measuring the effective diffusion coefficient of dissolved hydrogen in saturated Boom Clay. *Applied Geochemistry*, 61:175–184.
- [Jacops et al., 2016] Jacops, E., Maes, N., Bruggeman, C., and Grade, A. (2016). Measuring diffusion coefficients of dissolved He and Ar in three potential clay host formations: Boom Clay, Callovo-Oxfordian Clay and Opalinus Clay. *Geological Society Special Publication*, 443(1):349–360.
- [Darcy, 1856] Darcy, H. (1856). *Les fontaines publiques de la ville de Dijon*. Librairie des Corps Impériaux des Ponts et Chaussées et des Mines, Paris, France.
- [Kelvin, 1871] Thomson, W. (1871). On the equilibrium of vapour at a curved surface of liquid. *Philosophical Magazine, series 4, 42 (282) : 448-452.*
- [Clapeyron, 1834] Clapeyron, E. (1834). Mémoire sur la Puissance Motrice de la Chaleur. *Journal de l'École polytechnique*, 23:153–191.
- [van Genuchten, 1980] van Genuchten, M. (1980). Predicting the hydraulic conductivity of unsaturated soils. *Soil. Sci. Soc. Am. J*, 44(5):892–898.
- [Brooks and Corey, 1964] Brooks, R. H. and Corey, A. (1964). Hydraulic properties of porous media and their relation to drainage design. *Transactions of the ASAE*, 7(1):26–28.
- [Armand et al., 2014] Armand, G., Leveau, F., Nussbaum, C., de La Vaissiere, R., Noiret, A., Jaeggi, D., Landrein, P., and Righini, C. (2014). Geometry and properties of the excavation-induced fractures at the Meuse/Haute-Marne URL drifts. *Rock Mechanics and Rock Engineering*, 47(1):21–41.
- [Mertens et al., 2004] Mertens, J., Bastiaens, W., and Dehandschutter, B. (2004). Characterisation of induced discontinuities in the Boom Clay around the underground excavations (URF, Mol, Belgium). *Applied Clay Science*, 26:413–428.
- [Wiseall et al., 2015] Wiseall, A. C., Cuss, R. J., Graham, C. C., and Harrington, J. F. (2015b). The visualization of flow paths in experimental studies of clay-rich materials. *Mineralogical Magazine*, 79(6):1335–1342.
- [Cuss et al., 2014a] Cuss, R., Harrington, J., Giot, R., and Auvray, C. (2014a). Experimental observations of mechanical dilation at the onset of gas flow in Callovo-Oxfordian claystone. *Geological Society Special Publication*, 400(1):507–519.

References III

- [Gonzalez-Blanco et al., 2022] Gonzalez-Blanco, L., Romero, E., Marschall, P., and Levasseur, S. (2022). Hydro - mechanical Response to Gas Transfer of Deep Argillaceous Host Rocks for Radioactive Waste Disposal. *Rock Mechanics and Rock Engineering*, 55(3):1159–1177.
- [Corman et al., 2022] Corman, G., Vu, M., and Collin, F. (2022). Numerical investigation of the couplings between strain localisation processes and gas migrations in clay materials*. International Journal of Solids and Structures*, 256(June):111974.
- [Diederichs, 2003] Diederichs, M. S. (2003). Rock Fracture and Collapse Under Low Confinement Conditions. *Rock Mechanics and Rock Engineering*, 36(5):339–381.
- [Wileveau and Bernier, 2008] Wileveau, Y. and Bernier, F. (2008). Similarities in the hydromechanical response of Callovo-Oxfordian clay and Boom Clay during gallery excavation. *Physics and Chemistry of the Earth*, 33(SUPPL. 1):343–349.
- [Bastiaens et al., 2003] Bastiaens, W., Bernier, F., Buyens, M., Demarche, M., Li, X. L., Linotte, J. M., and Verstricht, J. (2003). The connecting gallery-the extension of the HADES underground research facility at Mol, Belgium. Technical report, European Underground Research Infrastructure for Disposal of nuclear waste in Clay Environment (EURIDICE), Mol, Belgium.
- [Chambon et al., 1998] Chambon, R., Caillerie, D., and El Hassan, N. (1998). One-dimensional localisation studied with a second grade model. *European Journal of Mechanics, A/Solids*, 17(4):637–656.
- [Pardoen, 2015] Pardoen, B. (2015). Hydro-mechanical analysis of the fracturing induced by the excavation of nuclear waste repository galleries using shear banding. PhD thesis, University of Liège.
- [Salehnia, 2015] Salehnia, F. (2015). From some obscurity to clarity in Boom Clay behavior : Analysis of its coupled hydro-mechanical response in the presence of strain localization. PhD thesis, University of Liège.
- [Pardoen et al., 2014] Pardoen, B., Levasseur, S., and Collin, F. (2014). Excavation damaged zone modelling including hydraulic permeability evolution in unsaturated argilaceous rock. *Unsaturated Soils: Research and Applications - Proceedings of the 6th International Conference on Unsaturated Soils, UNSAT 2014*, (Desrues):1387–1393.
- [Olivella and Alonso, 2008] Olivella, S. and Alonso, E. E. (2008). Gas flow through clay barriers. *Géotechnique*, 58(3):157–176.

References IV

- [Volckaert et al., 1995] Volckaert, G., Ortiz, L., Canniere, P. D., Put, M., Horseman, S. T., Harrington, J. F., Fioravante, V., and Impey, M. (1995). MEGAS: modelling and experiments on GAS migration in repository host rocks. Final report phase 1. Technical report, Eur. Comm., [Rep.] EUR 16235 EN.

- [Corman et al., 2024] Corman, G., Gonzalez-Blanco, L., Levasseur, S. and Collin, F. (2024, under review). Hydro-mechanical modelling of gas transport processes in clay materials using a multi-scale approach*. Computers and Geotechnics*.

- [Gonzalez-Blanco, 2017] Gonzalez-Blanco, L. (2017). Gas migration in deep argillaceous formations : Boom Clay and indurated clays. PhD thesis, Universitat Politècnica de Catalunya (UPC).

- [Bertrand et al., 2019] Bertrand, F., Buzzi, O., Collin, F. (2019). Cleat-scale modelling of the coal permeability evolution due to sorption-induced strain. *International Journal of Coal Geology*, 216, 103320.

- [Jing et al., 2016] Jing, Y., Armstrong, R. T., Ramandi, H. L., and Mostaghimi, P. (2016). Coal cleat reconstruction using micro-computed tomography imaging. *Fuel*, 181:286–299.
- [Gerard et al., 2014] Gerard, P., Harrington, J., Charlier, R., and Collin, F. (2014). Modelling of localised gas preferential pathways in claystone. *International Journal of Rock Mechanics and Mining Sciences*, 67:104–114.

- [van den Eijnden et al., 2016] van den Eijnden, A. P., Bésuelle, P., Chambon, R., and Collin, F. (2016). A FE2 modelling approach to hydromechanical coupling in cracking-induced localization problems*. International Journal of Solids and Structures*, 97-98:475–488.

- [Robinet et al., 2012] Robinet, J. C., Sardini, P., Coelho, D., Parneix, J. C., Prt, D., Sammartino, S., Boller, E., and Altmann, S. (2012). Effects of mineral distribution at mesoscopic scale on solute diffusion in a clay-rich rock: Example of the Callovo-Oxfordian mudstone (Bure, France). *Water Resources Research*, 48(5):1–17.

- [Bishop, 1959] Bishop, A. W. (1959). The principle of effective stress. *Teknisk Ukeblad*, 39:859–863.

- [Yuster, 1951] Yuster, S. (1951). Theoretical considerations of multiphase flow in idealized capillary systems.pdf. *Proceedings of the 3rd World Petroleum Congress, Section II*,The Hague, 2:437–445.

- [Goodman, 1976] Goodman, R. (1976). *Methods of geological engineering in Discontinuous Rocks*. West Publishing Co.

References V

- [Bandis et al., 1983] Bandis, S. C., Lumsden, A. C., and Barton, N. R. (1983). Fundamentals of rock joint deformation. *International Journal of Rock Mechanics and Mining Sciences & Geomechanics Abstracts*, 20(6):249–268.
- [Hill, 1965] Hill, R. (1965). A self-consistent mechanics of composite materials. *Journal of the Mechanics and Physics of Solids*, 13(4):213–222.
- [Mandel, 1966] Mandel, J. (1966). Conditions de Stabilite et Postulat de Drucker. In Kravtchenko, J. and Sirieys, P., editors, *Rheology and Soil Mechanics / Rhéologie et Mécanique des Sols*, pages 58–68. International Union of Theoretical and Applied Mechanics. Springer, Berlin, Germany.
- [Bésuelle et al., 2014] Bésuelle, P., Viggiani, G., Desrues, J., Coll, C., and Charrier, P. (2014). A laboratory experimental study of the hydromechanical behavior of boom clay. *Rock Mechanics and Rock Engineering*, 47(1):143–155.

Appendices
Model 1

Representation of fracturing

Shear strain localisation conceptualisation

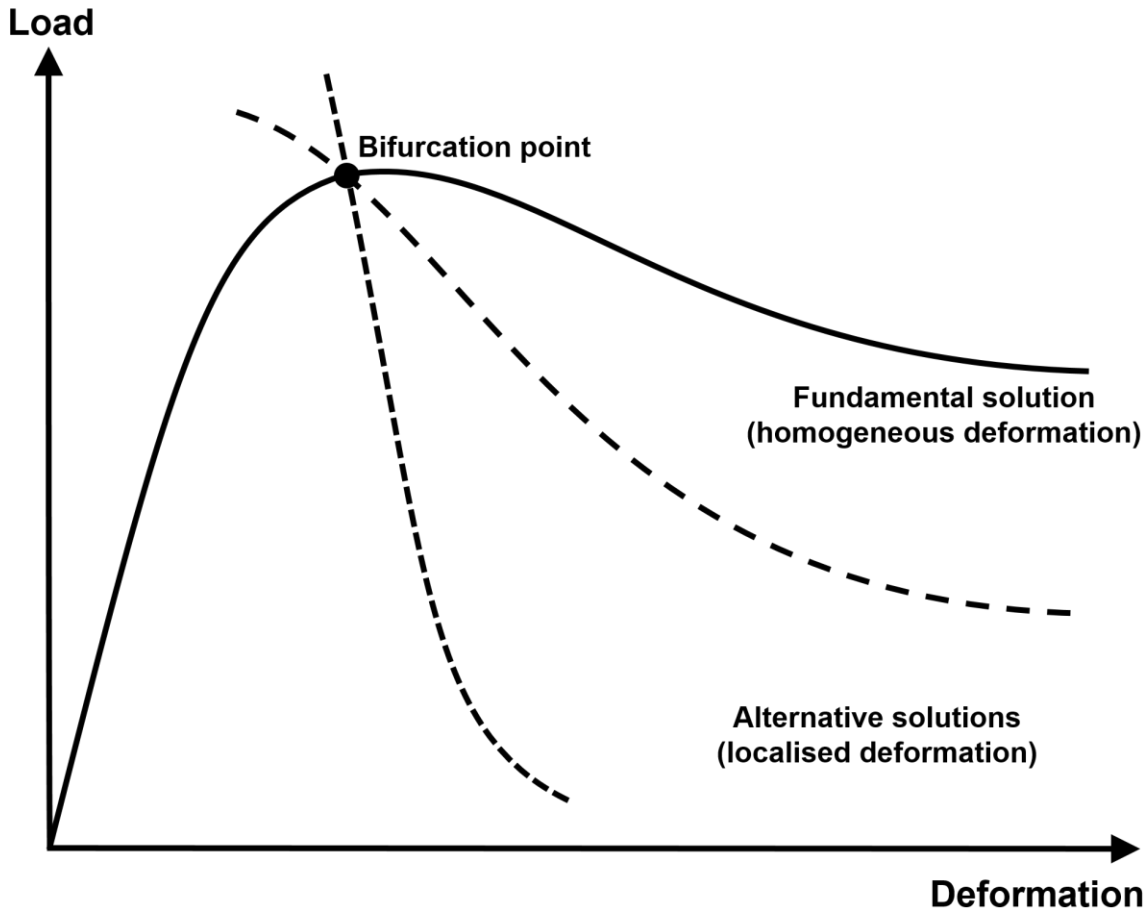

Representation of fracturing

Shear strain localisation conceptualisation

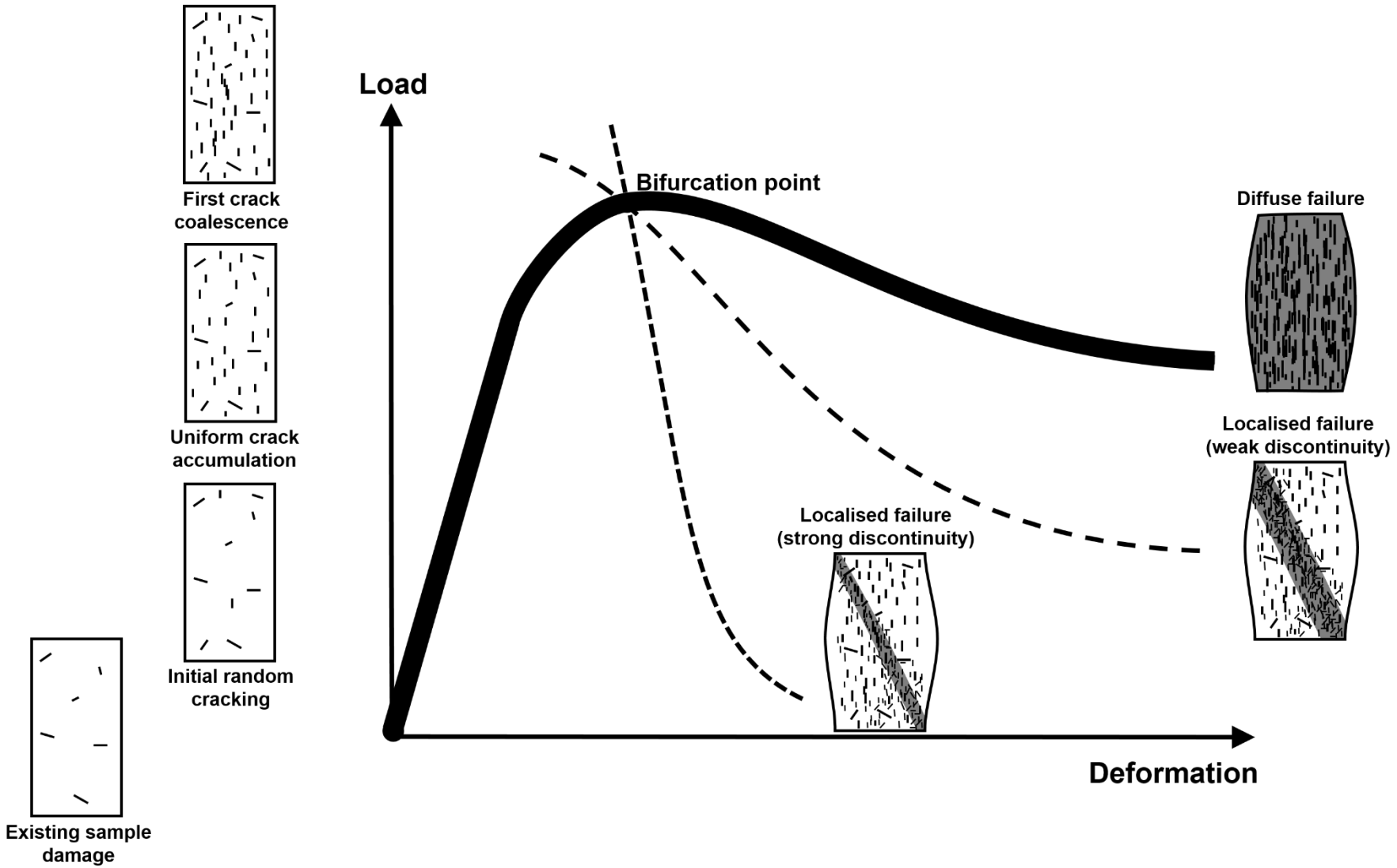

Representation of fracturing

Shear strain localisation modelling

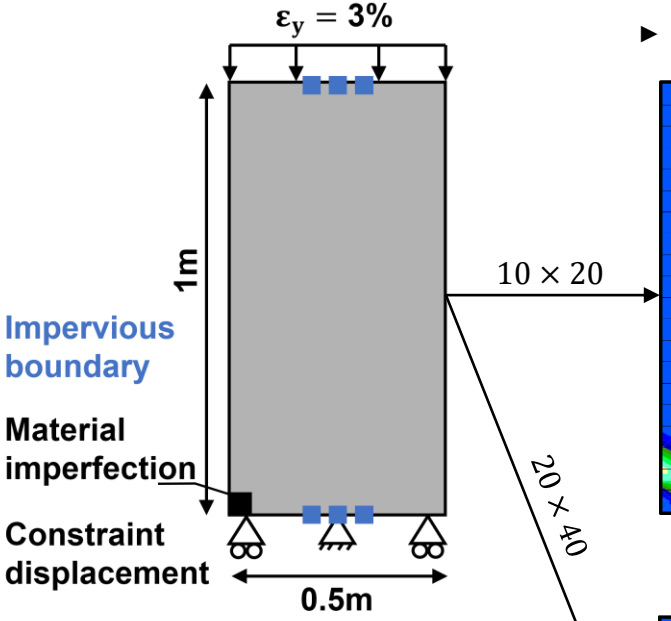

Classical FE methods

- Mesh size dependency

Regularisation technique

- Shear band width control

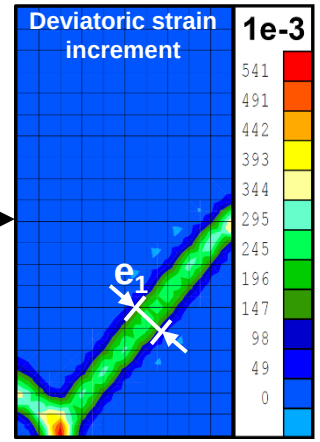

10×20

20×40

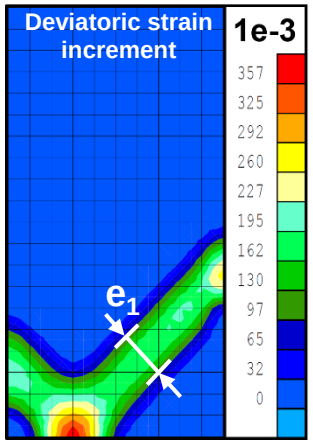

$e_1 \neq e_2$

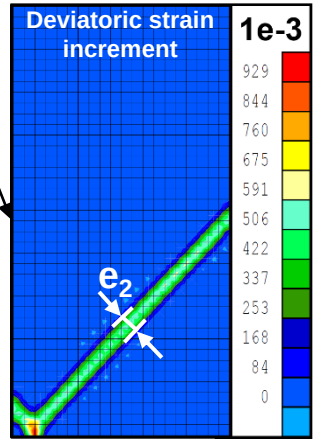

$e_1 = e_2$

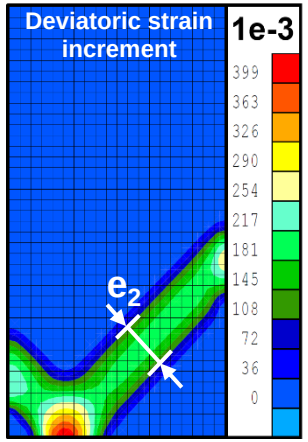

Enrichment of the kinematics with microstructure effects

2nd gradient type [Chambon et al., 1998]

	Macro-kinematics	+	Micro-kinematics
Volume	Ω		Ω^m
Displacement	u_i		u_i^m
Deformation	$F_{ij} = \frac{\partial u_i}{\partial x_j}$		$\nu_{ij} = \frac{\partial u_i^m}{\partial x_j}$

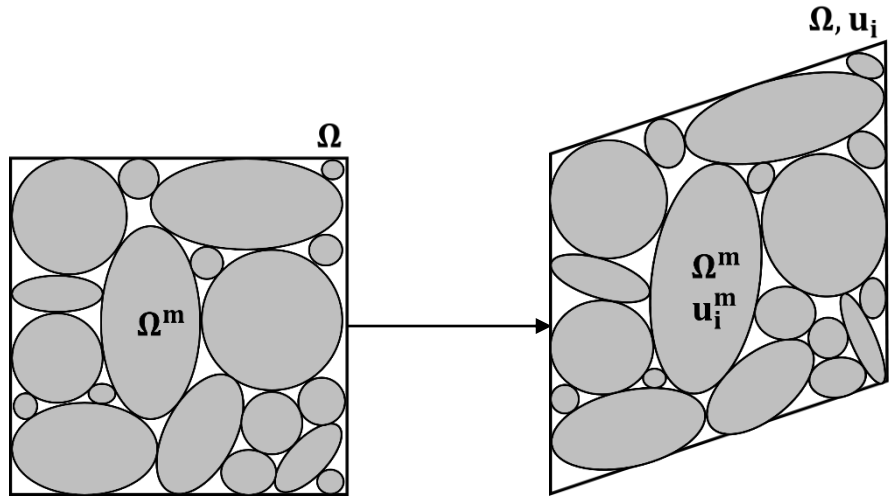

Second gradient H²M model

The rock environment is modelled as

- A multiphasic porous medium
- With strain localisation in the EDZ
- Including transfer properties evolution with strain

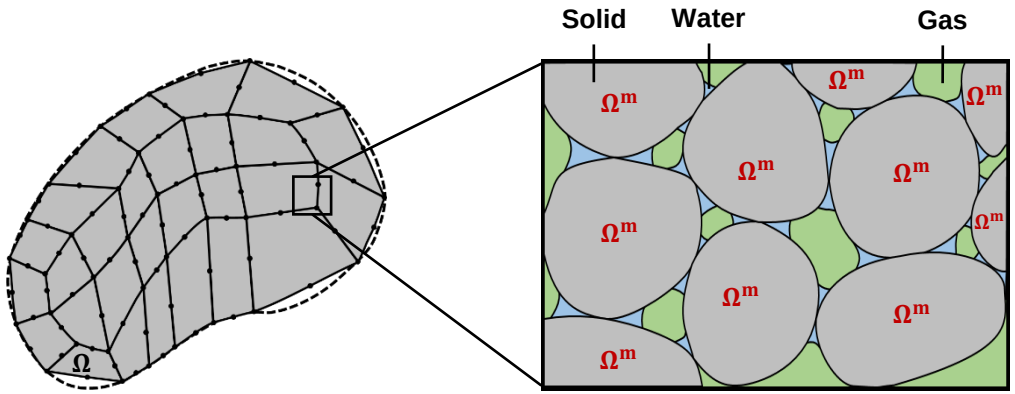

Finite element

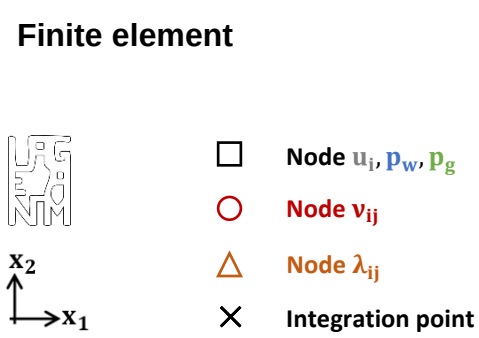

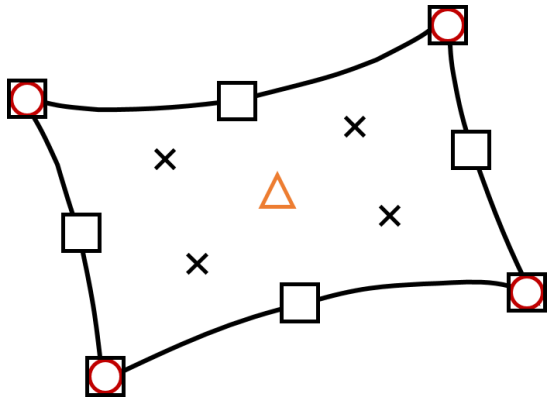

Balance equations

$$\frac{\partial \sigma_{ij}}{\partial x_j} - \frac{\partial^2 \Sigma_{ijk}}{\partial x_j \partial x_k} + \rho_{mix}\, g = 0$$

Microstructure effects

Kinematic restriction ≡ No relative deformation of the microstructure

Field of Lagrange multipliers λ_{ij}

$$\underbrace{\frac{\partial f_{w,i}}{\partial x_i} + \frac{\partial (\rho_w \phi S_{r_w})}{\partial t}}_{\text{Liquid water}} + \underbrace{\frac{\partial f_{v,i}}{\partial x_i} + \frac{\partial \left(\rho_v \phi (1 - S_{r_w})\right)}{\partial t}}_{\text{Water vapour}} = Q_w$$

$$\underbrace{\frac{\partial f_{g,i}}{\partial x_i} + \frac{\partial \left(\rho_g \phi (1 - S_{r_w})\right)}{\partial t}}_{\text{Dry gas}} + \underbrace{\frac{\partial f_{dg,i}}{\partial x_i} + \frac{\partial (\rho_{dg} \phi S_{r_w})}{\partial t}}_{\text{Dissolved gas}} = Q_g$$

$\dot{M}$: Stored fluid quantity f_i : Mass flow of fluid Q : Fluid source term

The second gradient method

- Regularisation method based on the **enrichment of the continuum kinematics** with the **microstructure effects**

	Macro-volume Ω	+	Micro-volumes Ω^m
Displacement	u_i		u_i^m
Deformation	$F_{ij} = \frac{\partial u_i}{\partial x_j}$		$\nu_{ij} = \frac{\partial u_i^m}{\partial x_j}$

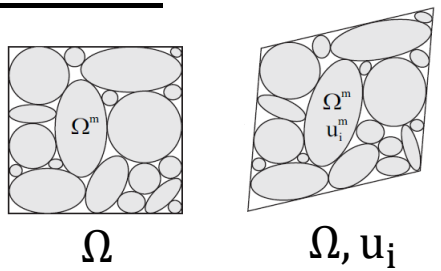

- Principle of **virtual work**: the internal virtual work *(Germain,1973)* = the external virtual work (simplified)

$$W_i^\star = \int_\Omega \left(\sigma_{ij} \frac{\partial u_i^\star}{\partial x_j} + \tau_{ij}\left(\boldsymbol{\nu_{ij}^\star} - F_{ij}^\star\right) + \boldsymbol{\Sigma_{ijk} h_{ijk}^\star} \right) d\Omega \qquad W_e^\star = \int_\Omega G_i u_i^\star \, d\Omega + \int_{\partial\Omega} \left(t_i u_i^\star + \boldsymbol{T_{ij} \nu_{ij}^\star}\right) ds$$

- The **kinematical constraint** $\nu_{ij} = F_{ij}$ implying $\nu_{ij} = \frac{\partial u_i}{\partial x_j}$ is added *(Chambon et al.,1998; Matsushima et al.,2002)*

$$\int_\Omega \left(\sigma_{ij} \frac{\partial u_i^\star}{\partial x_j} + \boldsymbol{\Sigma_{ijk}} \boldsymbol{\frac{\partial^2 u_i^\star}{\partial x_j \partial x_k}} \right) d\Omega = \int_\Omega G_i u_i^\star \, d\Omega + \int_{\partial\Omega} \left(t_i u_i^\star + \boldsymbol{T_{ij} \nu_{ij}^\star}\right) ds$$

- **Finite element formulation**: introduction of Lagrange multiplier fields λ_{ij}

$$\int_\Omega \left(\sigma_{ij} \frac{\partial u_i^\star}{\partial x_j} + \boldsymbol{\Sigma_{ijk}} \boldsymbol{\frac{\partial \nu_{ij}^\star}{\partial x_k}} \right) d\Omega - \int_\Omega \lambda_{ij} \left(\frac{\partial u_i^\star}{\partial x_j} - \nu_{ij}^\star \right) d\Omega = \int_\Omega G_i u_i^\star \, d\Omega + \int_{\partial\Omega} \left(t_i u_i^\star + \boldsymbol{T_{ij} \nu_{ij}^\star}\right) ds$$

$$\int_\Omega \lambda_{ij}^\star \left(\frac{\partial u_i}{\partial x_j} - \nu_{ij} \right) d\Omega = 0$$

The second gradient Finite Element

8 nodes: macro-displacements
pressure fields
temperaure

4 nodes: microkinetic gradient

1 node: Lagrange multiplier

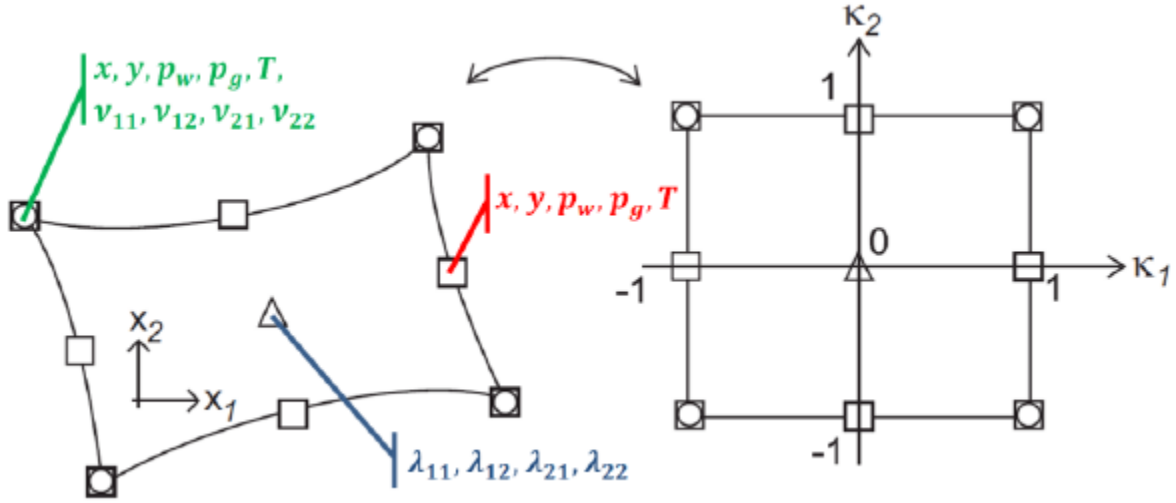

The second gradient mechanical law

$$\tilde{\Sigma}_{ijk} = [D]\frac{\partial \dot{v}_{ij}}{\partial x_k}$$

- The double stress requires a constitutive law
- Isotropic linear relationship *(Mindlin,1965)*
- Only one constitutive parameter D representing the microstructure (internal length scale)

$$\begin{bmatrix} \tilde{\Sigma}_{111} \\ \tilde{\Sigma}_{112} \\ \tilde{\Sigma}_{121} \\ \tilde{\Sigma}_{122} \\ \tilde{\Sigma}_{211} \\ \tilde{\Sigma}_{212} \\ \tilde{\Sigma}_{221} \\ \tilde{\Sigma}_{222} \end{bmatrix} = \begin{bmatrix} D & 0 & 0 & 0 & 0 & \frac{D}{2} & \frac{D}{2} & 0 \\ 0 & \frac{D}{2} & \frac{D}{2} & 0 & -\frac{D}{2} & 0 & 0 & \frac{D}{2} \\ 0 & \frac{D}{2} & \frac{D}{2} & 0 & -\frac{D}{2} & 0 & 0 & \frac{D}{2} \\ 0 & 0 & 0 & D & 0 & -\frac{D}{2} & -\frac{D}{2} & 0 \\ 0 & -\frac{D}{2} & -\frac{D}{2} & 0 & D & 0 & 0 & 0 \\ \frac{D}{2} & 0 & 0 & -\frac{D}{2} & 0 & \frac{D}{2} & \frac{D}{2} & 0 \\ \frac{D}{2} & 0 & 0 & -\frac{D}{2} & 0 & \frac{D}{2} & \frac{D}{2} & 0 \\ 0 & \frac{D}{2} & \frac{D}{2} & 0 & 0 & 0 & 0 & 0 \end{bmatrix} \begin{bmatrix} \frac{\partial \dot{v}_{11}}{\partial x_1} \\ \frac{\partial \dot{v}_{11}}{\partial x_2} \\ \frac{\partial \dot{v}_{12}}{\partial x_1} \\ \frac{\partial \dot{v}_{12}}{\partial x_2} \\ \frac{\partial \dot{v}_{21}}{\partial x_1} \\ \frac{\partial \dot{v}_{21}}{\partial x_2} \\ \frac{\partial \dot{v}_{22}}{\partial x_1} \\ \frac{\partial \dot{v}_{22}}{\partial x_2} \end{bmatrix}$$

Spatial discretisation

- Linear auxiliary problem
  - Linearized equations in matricial form

$$\int_{\Omega^{\tau 1}} \left[U^{\star,\tau 1}_{(x_1,x_2)}\right]^{\mathrm{T}} [E^{\tau 1}] \left[dU^{\tau 1}_{(x_1,x_2)}\right] d\Omega^{\tau 1} = -\Delta_1^{\tau 1} - \Delta_2^{\tau 1} - \Delta_3^{\tau 1} \qquad \textbf{(10)}$$

  - Local stiffness matrix $[E^{\tau 1}]$ and local out-of-balance forces $[f_{OB}^{\tau 1}]$

Global solution

- Linear auxiliary system
  - Assembling the elements

$$[K^{\tau 1}]\left[\delta U^{\tau 1}_{Node}\right] = -[F^{\tau 1}_{OB}] \qquad \textbf{(11)}$$

  - Global stiffness matrix $[K^{\tau 1}]$ and out-of-balance forces $[F_{OB}^{\tau 1}]$

$$[K^{\tau 1}] = \begin{bmatrix} K_{MM(2\times 2)} & K_{WM(2\times 1)} & K_{GM(2\times 1)} & K_{TM(2\times 1)} & K_{\nu M(2\times 1)} & K_{\lambda M(2\times 1)} \\ K_{MW(1\times 2)} & K_{WW(1\times 1)} & K_{GW(1\times 1)} & K_{TW(1\times 1)} & K_{\nu W(1\times 1)} & K_{\lambda W(1\times 1)} \\ K_{MG(1\times 2)} & K_{WG(1\times 1)} & K_{GG(1\times 1)} & K_{TG(1\times 1)} & K_{\nu G(1\times 1)} & K_{\lambda G(1\times 1)} \\ K_{MT(1\times 2)} & K_{WT(1\times 1)} & K_{GT(1\times 1)} & K_{TT(1\times 1)} & K_{\nu T(1\times 1)} & K_{\lambda T(1\times 1)} \\ K_{M\nu(1\times 2)} & K_{W\nu(1\times 1)} & K_{G\nu(1\times 1)} & K_{T\nu(1\times 1)} & K_{\nu\nu(1\times 1)} & K_{\lambda\nu(1\times 1)} \\ K_{M\lambda(1\times 2)} & K_{W\lambda(1\times 1)} & K_{G\lambda(1\times 1)} & K_{T\lambda(1\times 1)} & K_{\nu\lambda(1\times 1)} & K_{\lambda\lambda(1\times 1)} \end{bmatrix} \qquad (12)$$

- Correction of the unknowns fields
  - Updating current unknowns values → Get closer to well-balanced configuration

MAVL Application

Mechanical parameters

	Parameter	Symbol	Value	Unit
Geomechanical	Parallel Young's modulus	$E_{\parallel}$	5	$[GPa]$
	Perpendicular Young's modulus	$E_{\perp}$	4	$[GPa]$
	Poisson's ratio	$\nu_{\parallel\parallel}$	0.24	$[-]$
	Poisson's ratio	$\nu_{\parallel\perp}$	0.325	$[-]$
	Poisson's ratio	$\nu_{\perp\parallel}$	0.26	$[-]$
	Shear modulus	$G_{\parallel\perp} = G_{\perp\parallel}$	1.63	$[GPa]$
	Shear modulus	$G_{\parallel\parallel}$	2.016	$[GPa]$
	Solid grain density	ρ_s	2750	$[kg/m^3]$
	Initial cohesion	c_i	4.1 (0°)	$[MPa]$
	Cohesion parameter	A_{11}	0.117	$[-]$
	Cohesion parameter	b_1	14.236	$[-]$
	Ratio of cohesion softening	ξ_c	5	$[-]$
	Cohesion softening parameter	B_c	0.003	$[-]$
	Cohesion softening shifting	dec_c	0	$[-]$
	Initial compressive friction angle	$\varphi_{c,0}$	10	[°]
	Final compressive friction angle	$\varphi_{c,f}$	23	[°]
	Initial extensive friction angle	$\varphi_{e,0}$	7	[°]
	Final extensive friction angle	$\varphi_{e,f}$	23	[°]
	Friction angle hardening parameter	B_φ	0.001	$[-]$
	Friction angle hardening shifting	dec_φ	0	$[-]$
	Dilatancy angles	$\psi_c = \psi_e$	0.5	[°]
Microstructure	Second gradient elastic modulus	D	14.016	$[kN]$
Viscoplastic	Uniaxial compressive strength	R_c	21	$[MPa]$
	Internal friction coefficient	A^{vp}	2.62	$[-]$
	Cohesion coefficient	C^{vp}	0.03	$[-]$
	Viscoplastic potential parameter	β^{vp}	1.1	$[-]$
	Initial threshold for the VP flow	α_0^{vp}	0.142	$[-]$
	Reference fluidity	γ_0	700	$[s^{-1}]$
	Temperature parameter	γ_1	57×10^3	$[J/mol]$
	Creep curve shape parameter	$\mathcal{N}$	5.0	$[-]$
	VP hardening function parameter	B^{vp}	7.5×10^{-2}	$[-]$

	Parameter	Symbol	Value	Unit
Classic Stuffing	Elastic Young's modulus	E_{CS}	17.5	$[GPa]$
	Poisson'ratio	ν_{CS}	0.25	$[-]$
	Friction angle	φ_{CS}	30	[°]
	Cohesion	c_{CS}	2.94	$[MPa]$
	Density	ρ_{CS}	2300	$[\frac{kg}{m^3}]$
Compressible stuffing	Elastic Young's modulus	E_{ES}	0.1	$[GPa]$
	Poisson's ratio	ν_{ES}	0.0	$[-]$
	Density	ρ_{ES}	2300	$[\frac{kg}{m^3}]$
Arch segments	Elastic Young's modulus	E_{AS}	39	$[GPa]$
	Poisson's ratio	ν_{AS}	0.2	$[-]$
	Friction angle	φ_{AS}	38	[°]
	Cohesion	c_{AS}	14.6	$[MPa]$
	Density	ρ_{AS}	2650	$[\frac{kg}{m^3}]$

MAVL Application

Flow parameters

	Parameter	Symbol	Value	Unit
Hydraulic	Initial porosity	n	0.173	$[-]$
	Initial parallel intrinsic permeability	$k_{w,\parallel,0}$	4×10^{-20}	$[m^2]$
	Initial perp. intrinsic permeability	$k_{w,\perp,0}$	1.33×10^{-20}	$[m^2]$
	Water density	ρ_w	1000	$[kg/m^3]$
	H2 density	ρ_{H2}	0.0794	$[kg/m^3]$
	Water dynamic viscosity	μ_w	0.001	$[Pa.s]$
	H2 dynamic viscosity	μ_{H2}	9×10^{-6}	$[Pa.s]$
	Water compressibility	χ_w^{-1}	5×10^{-10}	$[Pa^{-1}]$
	Henry coefficient	H_{H2}	0.0193	$[-]$
	Air entry pressure (1^{st} coeff. of $S_{r,w}$)	P_r	15	$[MPa]$
	Parameter (2^{nd} coeff. of $S_{r,w}$)	$\mathcal{G}$	1.49	$[-]$
	Parameter (1^{st} coeff. of $k_{r,w}$)	$\mathcal{M}$	0.32886	$[-]$
	Parameter (1^{st} coeff. of $k_{r,g}$)	$\mathcal{N}$	3	$[-]$
	Max. degree of water saturation	S_{max}	1	$[-]$
	Residual degree of water saturation	S_{res}	0.01	$[-]$
	Evolution parameter	β_{perm}	10^{10}	$[-]$
	Tortuosity	τ	0.25	$[-]$

Compressible Stuffing	Initial porosity	n	0.25	$[-]$
	Initial parallel intrinsic permeability	$k_{w,\parallel,0}$	10^{-15}	$[m^2]$
	Initial perp. intrinsic permeability	$k_{w,\perp,0}$	10^{-15}	$[m^2]$
	Air entry pressure (1^{st} coeff. of $S_{r,w}$)	P_r	1	$[MPa]$
	Parameter (2^{nd} coeff. of $S_{r,w}$)	$\mathcal{G}$	1.54	$[-]$
	Parameter (1^{st} coeff. of $k_{r,w}$)	$\mathcal{F}$	0.3507	$[-]$
	Max. degree of water saturation	S_{max}	1	$[-]$
	Residual degree of water saturation	S_{res}	0.01	$[-]$
	Tortuosity	τ	0.25	$[-]$
Compressible Stuffing	Initial porosity	n	0.5	$[-]$
	Initial parallel intrinsic permeability	$k_{w,\parallel,0}$	10^{-10}	$[m^2]$
	Initial perp. intrinsic permeability	$k_{w,\perp,0}$	10^{-10}	$[m^2]$
	Air entry pressure (1^{st} coeff. of $S_{r,w}$)	P_r	0.2	$[MPa]$
	Parameter (2^{nd} coeff. of $S_{r,w}$)	$\mathcal{G}$	1.54	$[-]$
	Parameter (1^{st} coeff. of $k_{r,w}$)	$\mathcal{F}$	0.3507	$[-]$
	Max. degree of water saturation	S_{max}	1	$[-]$
	Residual degree of water saturation	S_{res}	0.01	$[-]$
	Tortuosity	τ	0.25	$[-]$
Arch Segments	Initial porosity	n	0.15	$[-]$
	Initial parallel intrinsic permeability	$k_{w,\parallel,0}$	10^{-18}	$[m^2]$
	Initial perp. intrinsic permeability	$k_{w,\perp,0}$	10^{-18}	$[m^2]$
	Air entry pressure (1^{st} coeff. of $S_{r,w}$)	P_r	5	$[MPa]$
	Parameter (2^{nd} coeff. of $S_{r,w}$)	$\mathcal{G}$	1.54	$[-]$
	Parameter (1^{st} coeff. of $k_{r,w}$)	$\mathcal{F}$	0.3507	$[-]$
	Max. degree of water saturation	S_{max}	1	$[-]$
	Residual degree of water saturation	S_{res}	0.01	$[-]$
	Tortuosity	τ	0.25	$[-]$

MAVL Application

Evolution of convergence

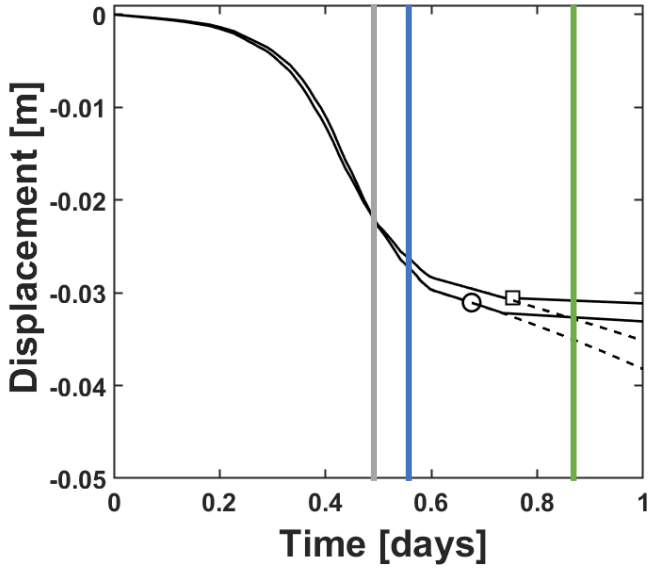

Development of damage in the near field

	80% deconfinement	90% deconfinement	100% deconfinement
Reference case with transfer properties evolution	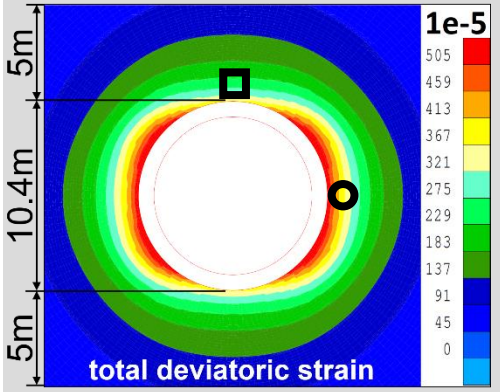	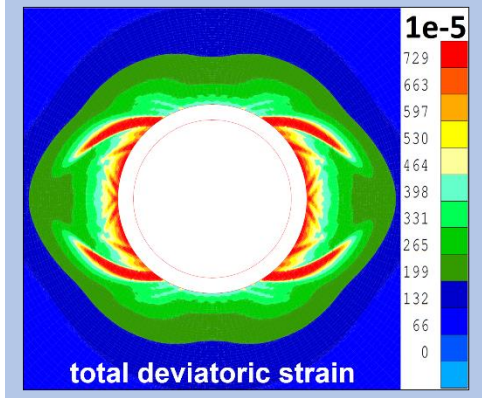	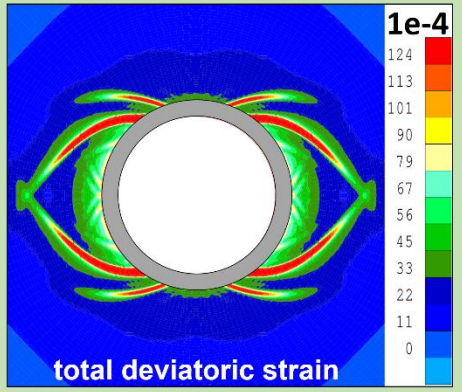
No support	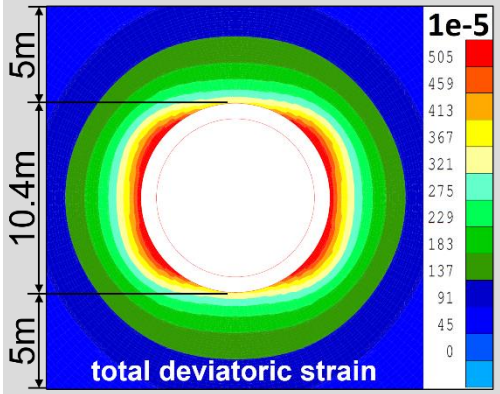	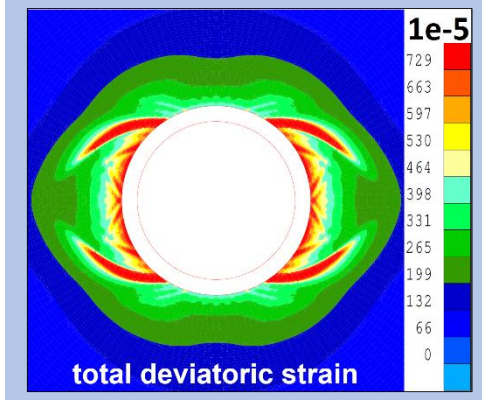	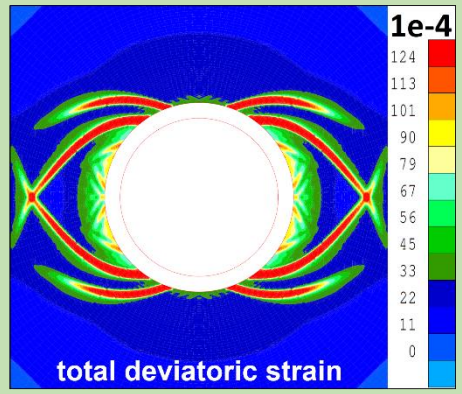

MAVL Application

Evolution of convergence

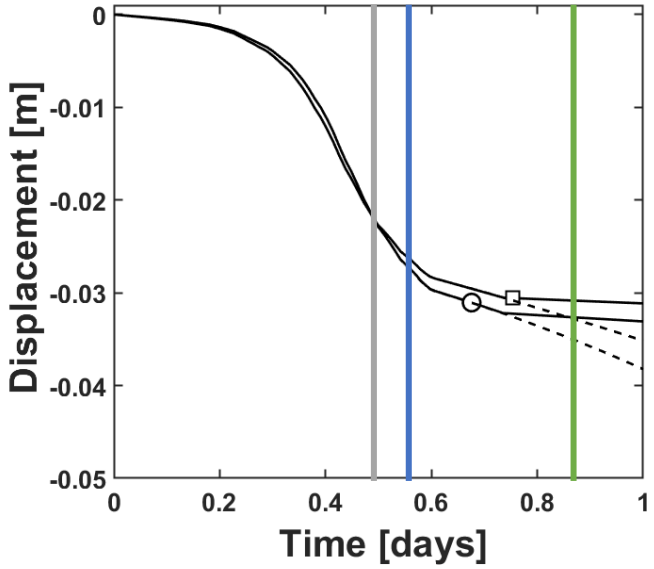

Development of damage in the near field

Reference case with transfer properties evolution

Higher value of D

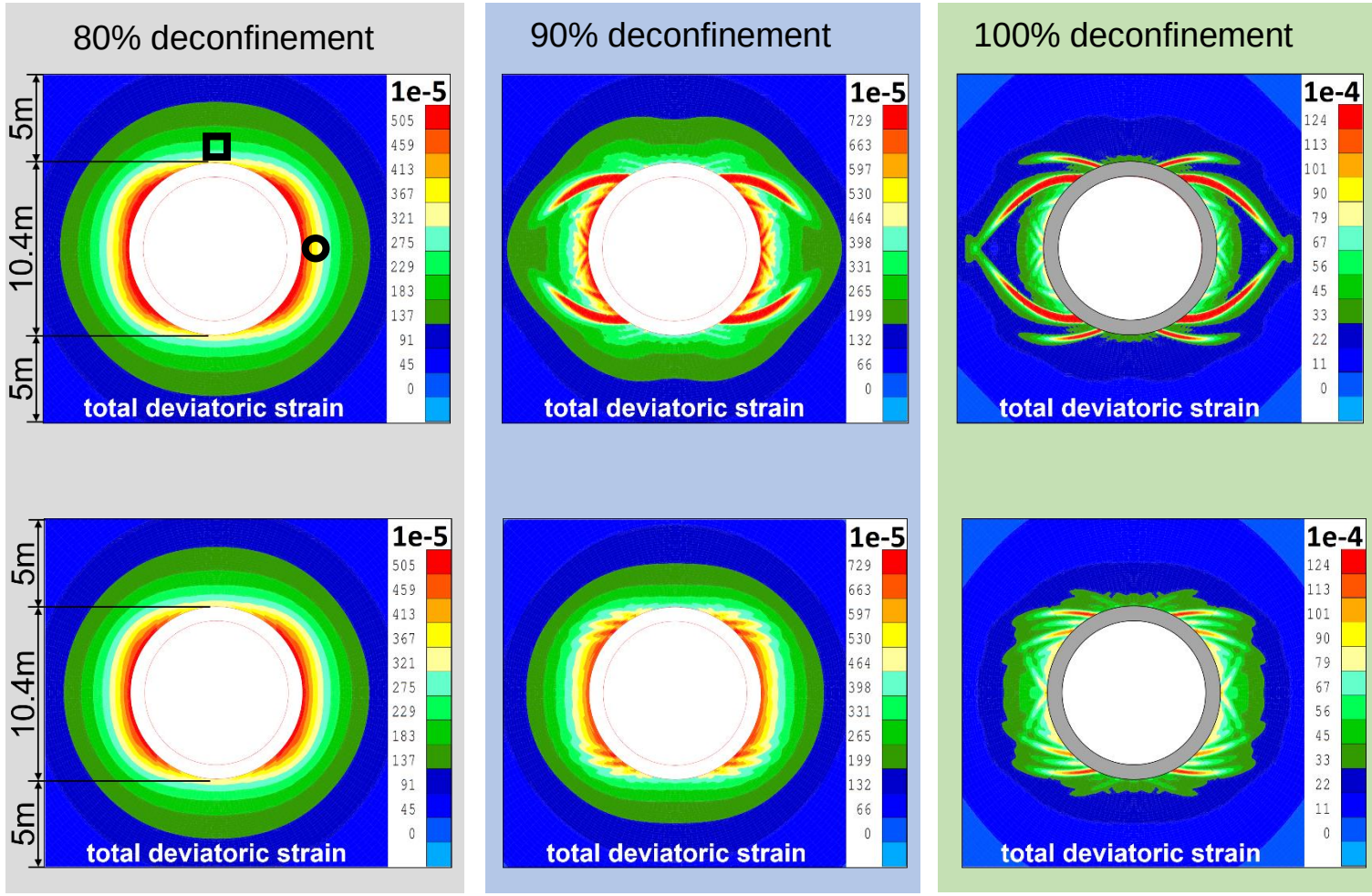

Appendices
Model 2

Representation of microstructure effects

km | m | cm | mm | µm | nm

Repository scale

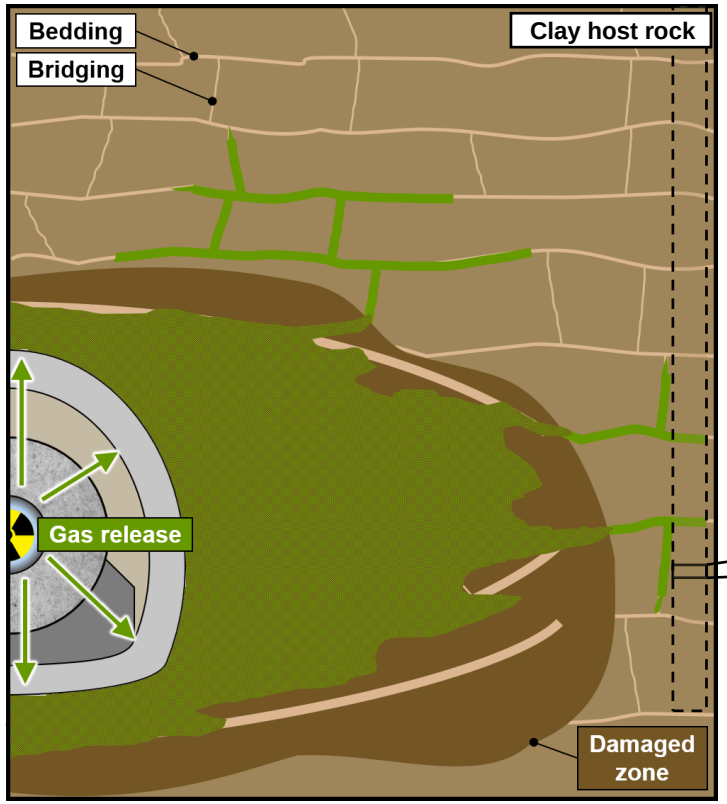

Laboratory scale

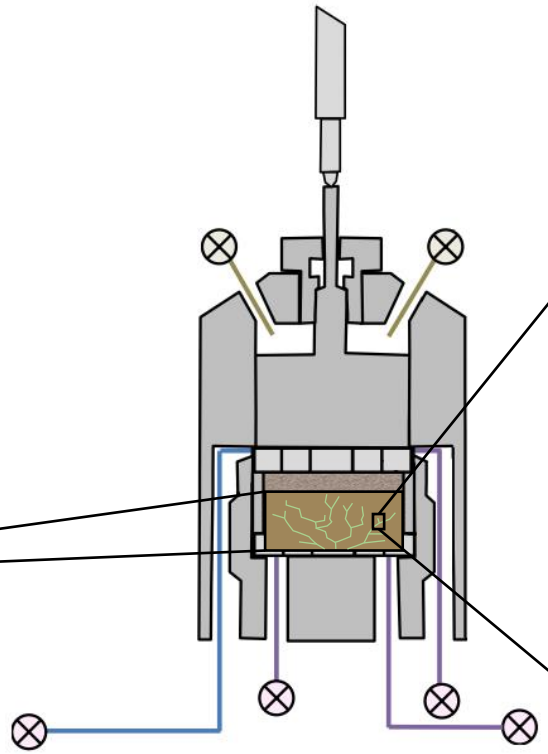

[Gonzalez-Blanco, 2017]

Process scale

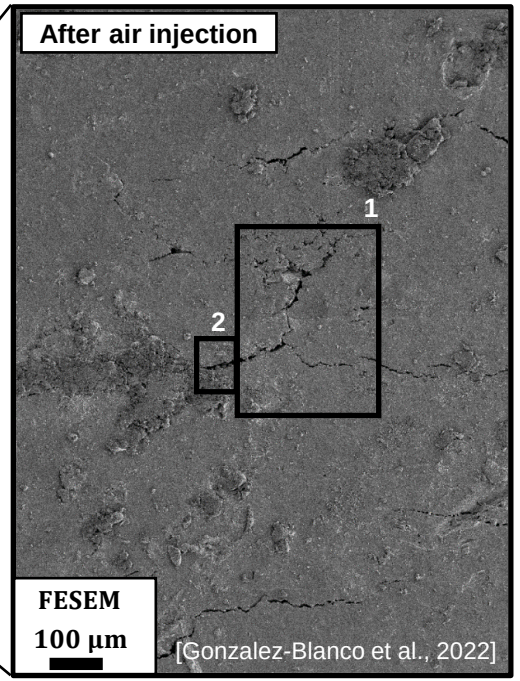

[Gonzalez-Blanco et al., 2022]

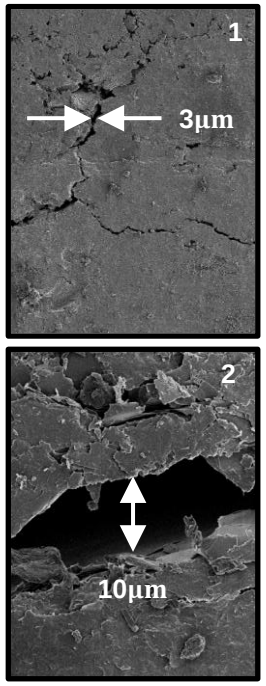

Representation of microstructure effects

km | m | cm | mm | µm | nm

Large-scale models	Intermediate-level multi-scale models	Small-scale models
Repository scale	***Laboratory scale***	***Process scale***
► No direct representation of local phenomena ► Enriched with micro-mechanical effects, *e.g.* embedded fracture model	► Combination of the benefits from both scales ► Explicit description of the constituents on their specific length scale through a REV definition	► Direct modelling of the whole microstructure ► Useful for modelling at the process scale

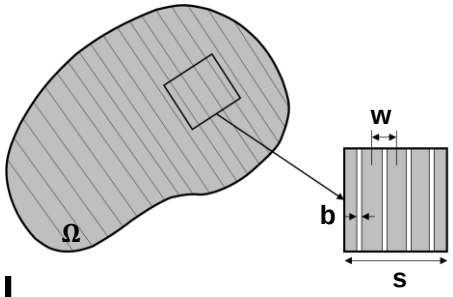

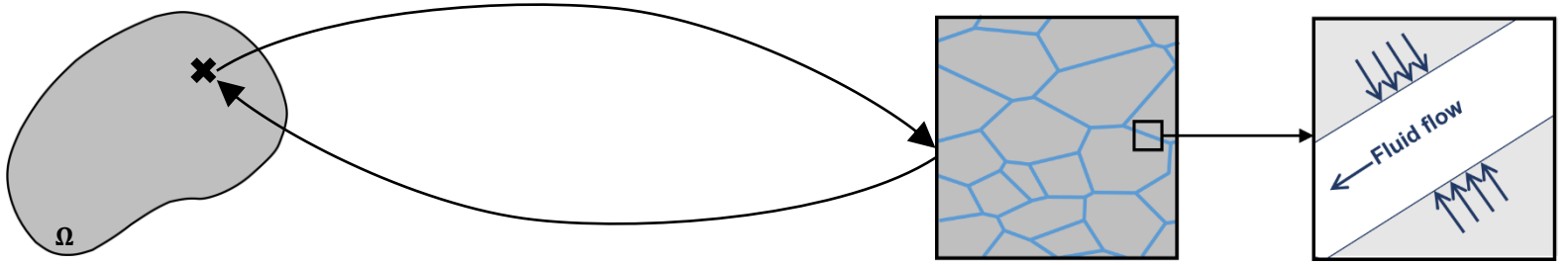

[van den Eijnden et al., 2016]

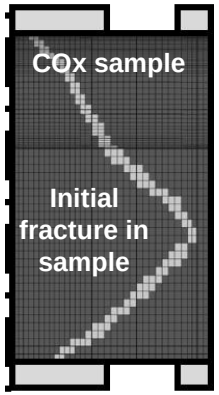

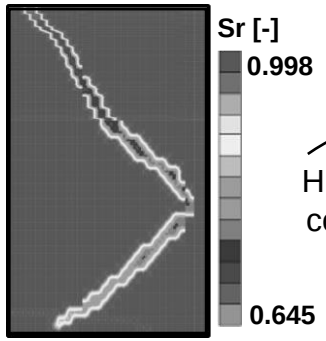

[Gerard et al., 2014]

High computational costs for upscaling

Very limited exploitation of the microstructure potential

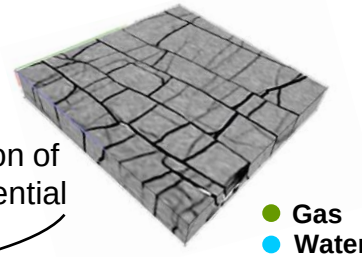

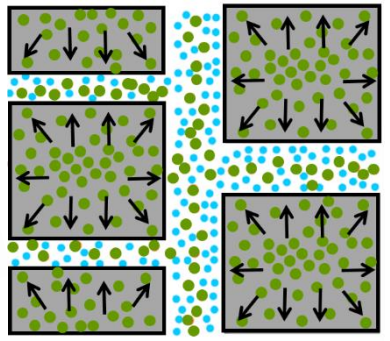

From [Jing et al., 2016] & [Bertrand et al., 2019]

Multi-scale modelling approach

Macro-scale

1. Localisation

Micro-scale

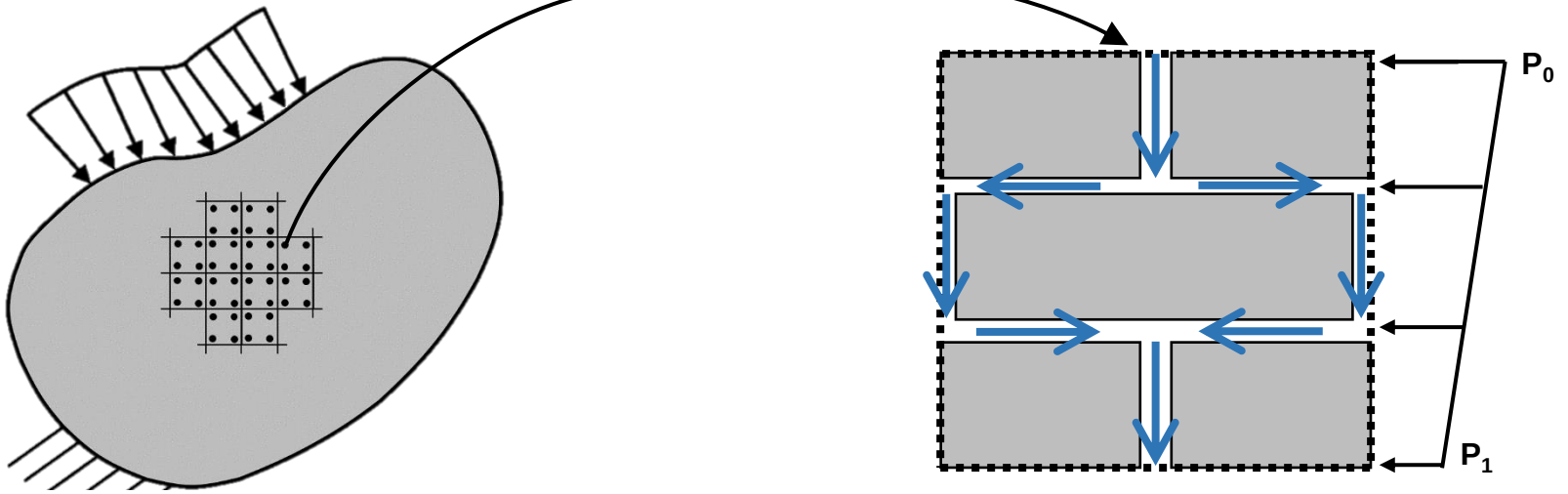

4 Steps

❶ Localisation

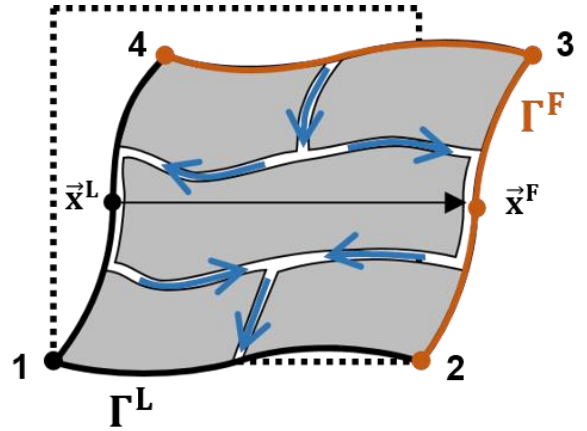

Periodic boundary conditions
Separation of scales

Multi-scale modelling approach

Macro-scale

1. Localisation

Micro-scale

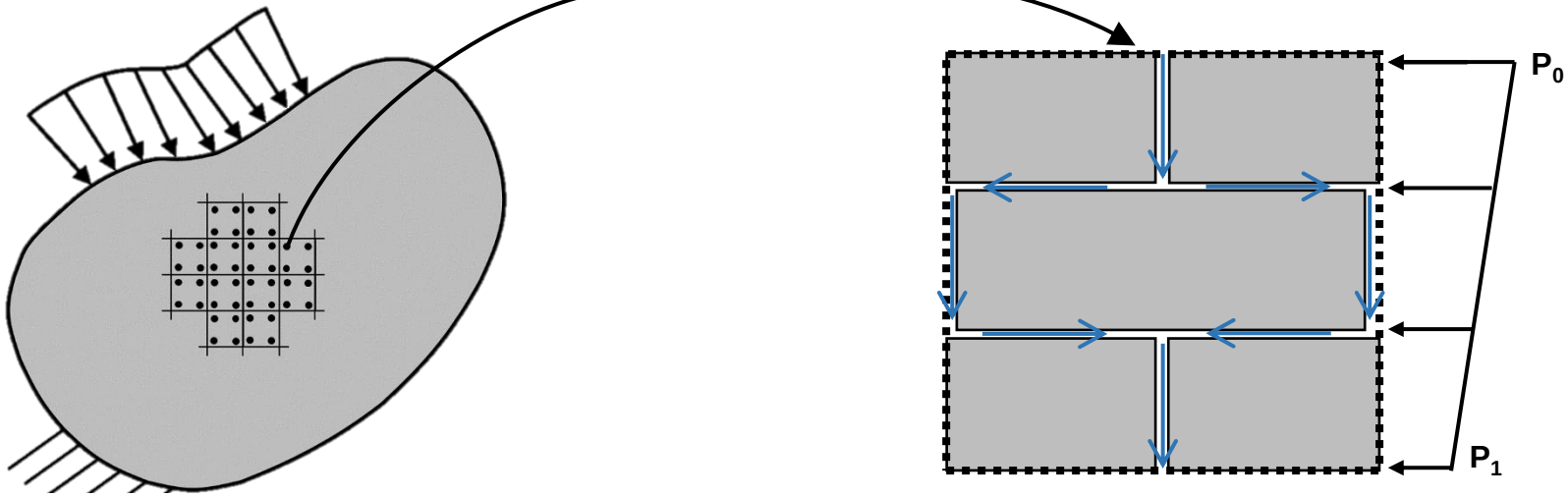

2. Micro-scale computation

4 Steps

1. Localisation
2. Resolution of the problem at the micro-scale

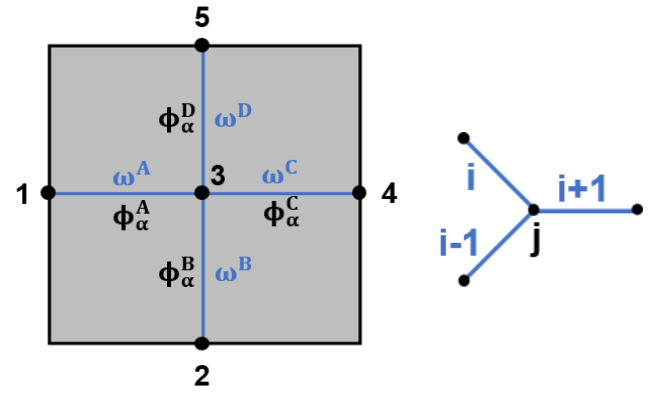

Mass balance on each node:

$$\omega_\alpha^{i-1} + \omega_\alpha^{i} + \omega_\alpha^{i+1}$$

Steady state conditions

Multi-scale modelling approach

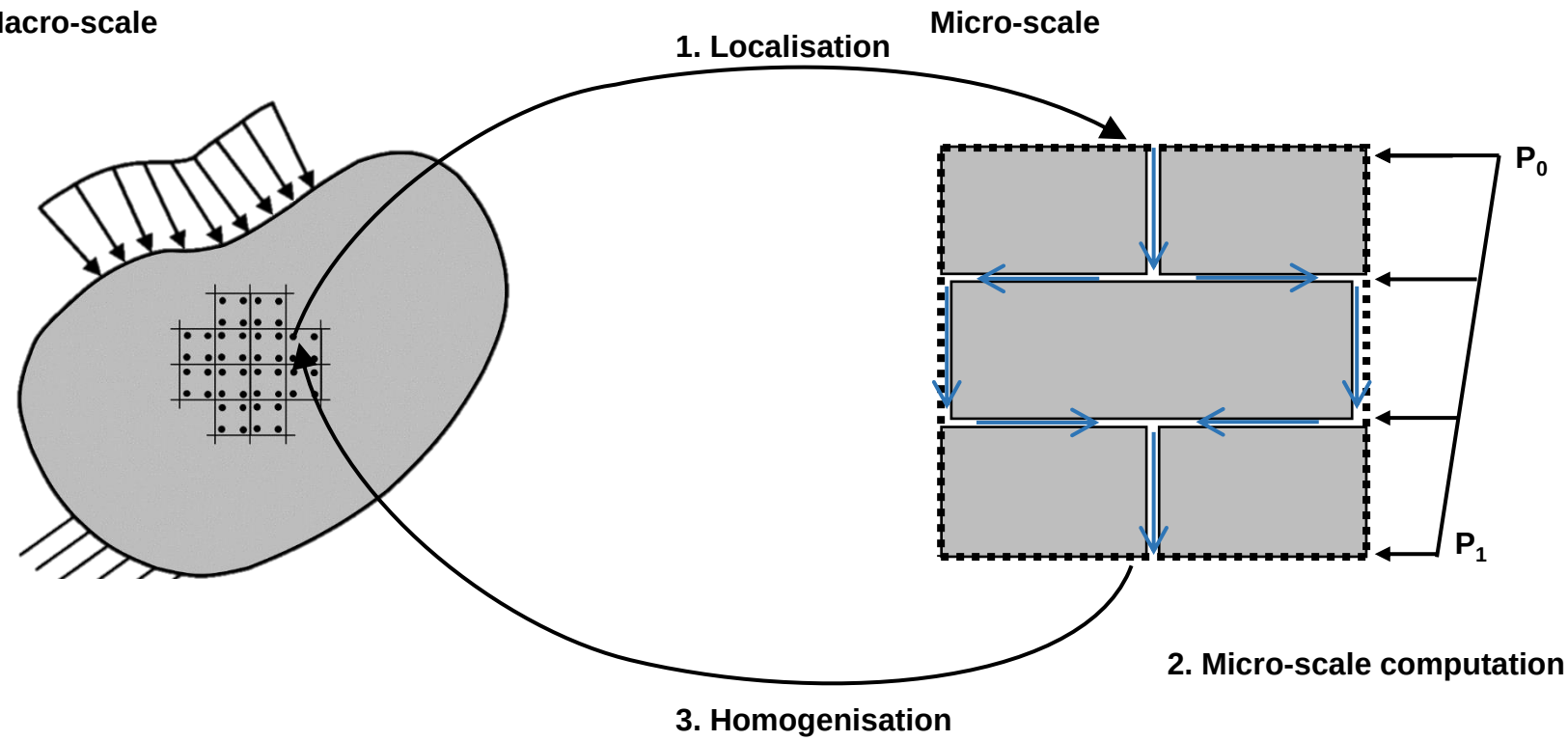

4 Steps

1. Localisation
2. Resolution of the problem at the micro-scale
3. Homogenisation

Average micro-scale work = macro-scale work

[Hill, 1965][Mandel, 1972]

Fluxes
Fluid contents

Multi-scale modelling approach

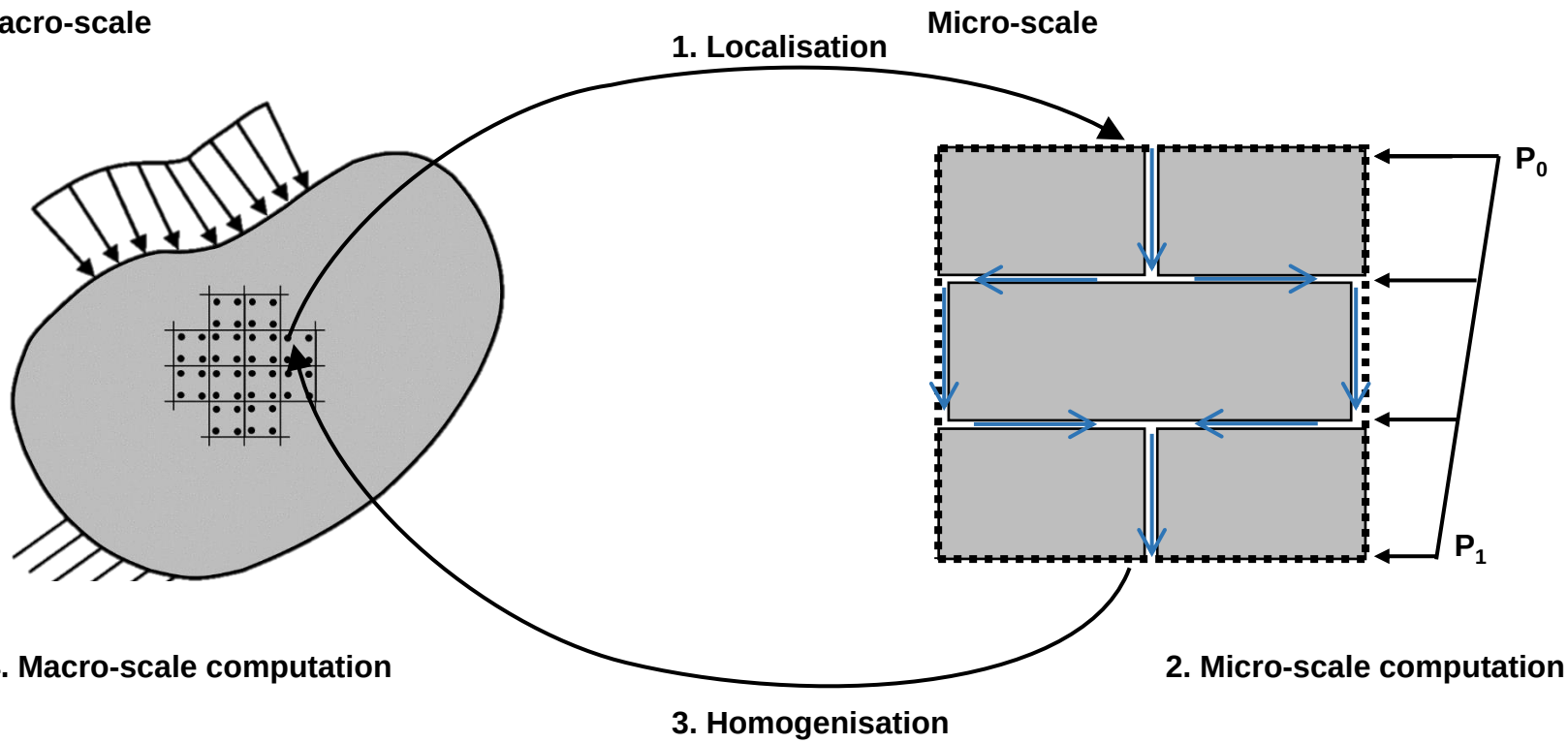

4 Steps

1. Localisation
2. Resolution of the problem at the micro-scale
3. Homogenisation
4. Resolution of the problem at the macro-scale

$$\begin{bmatrix} [\mathbf{E}^{\mathbf{M}}_{\mathbf{MM}}] & [\mathbf{E}^{\mathbf{M}}_{\mathbf{MW}}] & [\mathbf{E}^{\mathbf{M}}_{\mathbf{MG}}] \\ [\mathbf{E}^{\mathbf{M}}_{\mathbf{WM}}] & [\mathbf{E}^{\mathbf{M}}_{\mathbf{WW}}] & [\mathbf{E}^{\mathbf{M}}_{\mathbf{WG}}] \\ [\mathbf{E}^{\mathbf{M}}_{\mathbf{GM}}] & [\mathbf{E}^{\mathbf{M}}_{\mathbf{GW}}] & [\mathbf{E}^{\mathbf{M}}_{\mathbf{GG}}] \end{bmatrix} \begin{Bmatrix} \{\boldsymbol{\delta\varepsilon}^{\mathbf{M}}\} \\ \{\boldsymbol{\delta\nabla p}^{\mathbf{M}}_{\mathbf{w}}\} \\ \boldsymbol{\delta p}^{\mathbf{M}}_{\mathbf{w}} \\ \{\boldsymbol{\delta\nabla p}^{\mathbf{M}}_{\mathbf{g}}\} \\ \boldsymbol{\delta p}^{\mathbf{M}}_{\mathbf{g}} \end{Bmatrix} = \begin{Bmatrix} \{\boldsymbol{\delta\sigma}^{\mathbf{M}}\} \\ \boldsymbol{\delta f}^{\mathbf{M}}_{\mathbf{w}} \\ \boldsymbol{\delta \dot{M}}^{\mathbf{M}}_{\mathbf{w}} \\ \boldsymbol{\delta f}^{\mathbf{M}}_{\mathbf{g}} \\ \boldsymbol{\delta \dot{M}}^{\mathbf{M}}_{\mathbf{g}} \end{Bmatrix}$$

$$[\mathbf{E}^{\mathbf{M}}]_{(10\times10)} \qquad \{\boldsymbol{\delta U}^{\mathbf{M}}\}_{10} = \{\boldsymbol{\delta\Sigma}^{\mathbf{M}}\}_{10}$$

$[\mathbf{E}^{\mathbf{M}}]$ ≡ *Macro-scale stiffness matrix*
$\{\boldsymbol{\delta U}^{\mathbf{M}}\}$ ≡ *Infinitesimal variations of the macro-scale variables*
$\{\boldsymbol{\delta\Sigma}^{\mathbf{M}}\}$ ≡ *Responses of the macro-scale variables*

Multi-scale modelling approach

❶ Localisation (macro- to micro-scale transition)

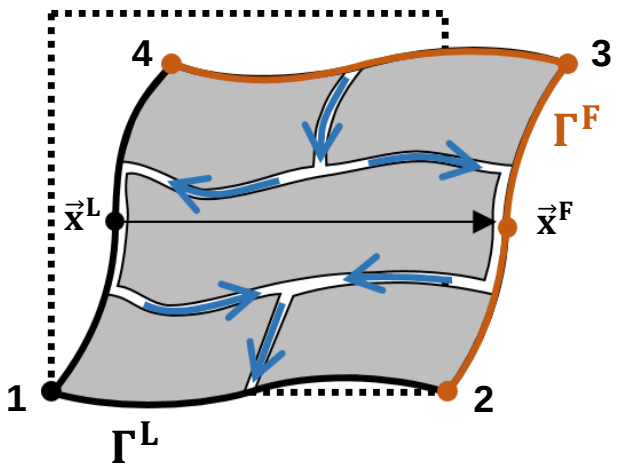

Periodic boundary conditions

Water pressure: $\mathbf{p_w^F = p_w^L + (\nabla p_w)^M (x_j^F - x_j^L)}$

Gas pressure: $\mathbf{p_g^F = p_g^L + (\nabla p_g)^M (x_j^F - x_j^L)}$

Separation of scales: $l_{REV} \ll \dfrac{p^M\ [Pa]}{\nabla p^M \left[\dfrac{Pa}{m}\right]}$

If important macro-solicitation, potentially not satisfied because the difference the left and right boundaries is also very important

❷ Resolution of the micro-scale hydraulic network

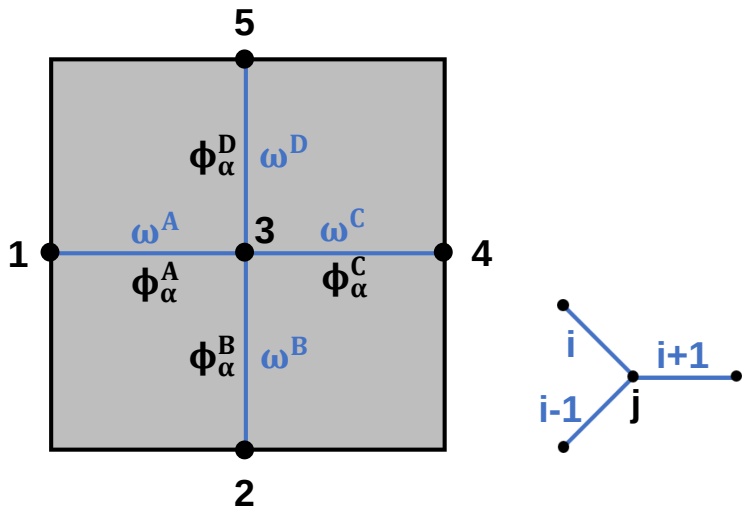

Given mechanical configuration
Steady state conditions

Conditions to be respected

Anti-symmetric boundary fluxes: $\omega_\alpha^A = -\omega_\alpha^C$ $\omega_\alpha^B = -\omega_\alpha^D$ No storage

Macroscopic pressure gradient: $p_4 - p_1 = (\nabla p)_x^M \Delta x$ $p_5 - p_2 = (\nabla p)_y^M \Delta y$

Mass balance on each node $\omega_\alpha^{i-1} + \omega_\alpha^i + \omega_\alpha^{i+1}$ In =out

$\omega_\alpha^i = \phi_\alpha^i (p_j - p_{j-1})$

$\phi_\alpha^i \equiv$ Flow model for the channel i

Multi-scale modelling approach

❸ Homogenisation (micro- to macro-scale transition)

Hill-Mandel macro-homogeneity condition

Average micro-scale work = macro-scale work

[Hill, 1965][Mandel, 1972]

Fluxes: $\mathbf{f}_{\alpha_i}^{\mathbf{M}} = \frac{\mathbf{1}}{\boldsymbol{\Omega}} \int_{\boldsymbol{\Gamma}} \bar{\mathbf{q}}_{\boldsymbol{\alpha}}^{\mathbf{m}} \, \mathbf{x_i} \; \mathbf{d\Gamma}$

Fluid contents: $\mathbf{M}_{\mathbf{w}}^{\mathbf{M}} = \frac{\mathbf{1}}{\boldsymbol{\Omega}} \int_{\boldsymbol{\Omega}_{\mathbf{w}}^{\mathbf{int}}} \boldsymbol{\rho}_{\mathbf{w}} \; \mathbf{d\Omega} = \boldsymbol{\rho}_{\mathbf{w}} \, \mathbf{S}_{\mathbf{r}} \, \boldsymbol{\phi}_{\mathbf{n}}$

$$\mathbf{M}_{\mathbf{w}}^{\mathbf{M}} = \mathbf{M}_{\mathbf{g}}^{\mathbf{m}} + \mathbf{M}_{\mathbf{dg}}^{\mathbf{m}} = \boldsymbol{\rho}_{\mathbf{g}}(\mathbf{1} - \mathbf{S}_{\mathbf{r}}) \, \boldsymbol{\phi}_{\mathbf{n}} + \boldsymbol{\rho}_{\mathbf{dg}} \, \mathbf{S}_{\mathbf{r}} \, \boldsymbol{\phi}_{\mathbf{n}}$$

Fluid mass storage terms: $\dot{M}^{M,t} \approx \frac{M^{M,t} - M^{M,t-\Delta t}}{\Delta t}$

❹ Macro-scale computations

The macro-scale problem is solved using finite elements

under matrix form:

$$\begin{bmatrix} [\mathbf{E}_{\mathbf{MM}}^{\mathbf{M}}] & [\mathbf{E}_{\mathbf{MW}}^{\mathbf{M}}] & [\mathbf{E}_{\mathbf{MG}}^{\mathbf{M}}] \\ [\mathbf{E}_{\mathbf{WM}}^{\mathbf{M}}] & [\mathbf{E}_{\mathbf{WW}}^{\mathbf{M}}] & [\mathbf{E}_{\mathbf{WG}}^{\mathbf{M}}] \\ [\mathbf{E}_{\mathbf{GM}}^{\mathbf{M}}] & [\mathbf{E}_{\mathbf{GW}}^{\mathbf{M}}] & [\mathbf{E}_{\mathbf{GG}}^{\mathbf{M}}] \end{bmatrix} \begin{Bmatrix} \{\boldsymbol{\delta\varepsilon}^{\mathbf{M}}\} \\ \{\boldsymbol{\delta\nabla p}_{\mathbf{w}}^{\mathbf{M}}\} \\ \boldsymbol{\delta p}_{\mathbf{w}}^{\mathbf{M}} \\ \{\boldsymbol{\delta\nabla p}_{\mathbf{g}}^{\mathbf{M}}\} \\ \boldsymbol{\delta p}_{\mathbf{g}}^{\mathbf{M}} \end{Bmatrix} = \begin{Bmatrix} \{\boldsymbol{\delta\sigma}^{\mathbf{M}}\} \\ \{\boldsymbol{\delta f}_{\mathbf{w}}^{\mathbf{M}}\} \\ \boldsymbol{\delta\dot{M}}_{\mathbf{w}}^{\mathbf{M}} \\ \{\boldsymbol{\delta f}_{\mathbf{g}}^{\mathbf{M}}\} \\ \boldsymbol{\delta\dot{M}}_{\mathbf{g}}^{\mathbf{M}} \end{Bmatrix}$$

summarised as:

$$[\mathbf{E}^{\mathbf{M}}]_{(\mathbf{10}\times\mathbf{10})} \{\boldsymbol{\delta U}^{\mathbf{M}}\}_{\mathbf{10}} = \{\boldsymbol{\delta\Sigma}^{\mathbf{M}}\}_{\mathbf{10}}$$

$$f_{w_i}^M \frac{\partial p_w^{\star,M}}{\partial x_i} = \frac{1}{\Omega}\int_\Omega f_{w_i}^m \frac{\partial p_w^{\star,M}}{\partial x_i} d\Omega = \frac{1}{\Omega}\int_\Gamma \bar{q}_w^m p_w^{\star,M} d\Gamma$$
$$= \frac{1}{\Omega}\frac{\partial p_w^{\star,M}}{\partial x_i}\int_\Gamma \bar{q}_w^m x_i d\Gamma$$
$$= \frac{1}{\Omega}\int_\Gamma \bar{q}_w^m x_i d\Gamma$$
$$f_{g_i}^M + f_{dg_i}^M = \frac{1}{\Omega}\int_\Gamma \bar{q}_g^m x_i d\Gamma$$

$$M_w^M = \frac{1}{\Omega}\int_{\Omega_w^{int}} \rho_w d\Omega = \rho_w S_{r_w} \phi_n$$

$$M_g^M = M_g^m + M_{dg}^m = \frac{1}{\Omega}\left(\int_{\Omega_g^{int}} \rho_g d\Omega + \int_{\Omega_w^{int}} \rho_{dg} d\Omega\right) = \rho_g (1 - S_{r_w}) \phi_n + \rho_{dg} S_{r_w} \phi_n$$

Steady state

Perturbation: Numerically compute the derivative terms in the rigidity matrix

$[\mathbf{E}^{\mathbf{M}}]$ ≡ Macro-scale stiffness matrix

$\{\boldsymbol{\delta U}^{\mathbf{M}}\}$ ≡ Infinitesimal variations of the macro-scale variables

$\{\boldsymbol{\delta\Sigma}^{\mathbf{M}}\}$ ≡ Responses of the macro-scales variables

Hydro-mechanical multi-scale model

Macro-scale

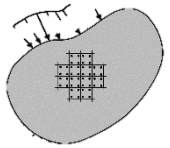

Micro-scale (REV)

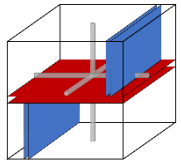

Mechanical model

- Isotropic elastic law
- Elasto-plastic law

$$(\boldsymbol{\sigma}, \boldsymbol{\varepsilon}) = \boldsymbol{f}(\mathbf{E}, \boldsymbol{\nu}, \mathbf{c}, \boldsymbol{\varphi})$$

Hydro-mechanical couplings

- Effective stress definition

[Bishop, 1959]

$$\boldsymbol{\sigma}' = \boldsymbol{\sigma} - \mathbf{p} \qquad \mathbf{p} = \mathbf{S_r} \cdot \mathbf{p_w} + (\mathbf{1} - \mathbf{S_r}) \cdot \mathbf{p_g}$$

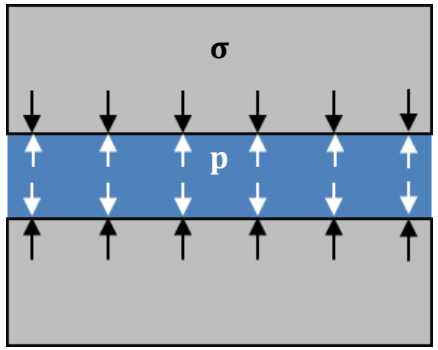

Hydro-mechanical multi-scale model

Macro-scale

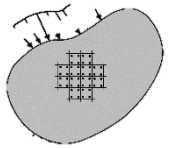

Micro-scale (REV)

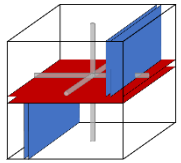

Mechanical model

- Isotropic elastic law
- Elasto-plastic law

$$(\boldsymbol{\sigma}, \boldsymbol{\varepsilon}) = \boldsymbol{f}(\mathbf{E}, \boldsymbol{\nu}, \mathbf{c}, \boldsymbol{\varphi})$$

Hydro-mechanical couplings

- Effective stress definition

[Bishop, 1959]

$$\boldsymbol{\sigma}' = \boldsymbol{\sigma} - \mathbf{p} \qquad \mathbf{p} = \mathbf{S_r} \cdot \mathbf{p_w} + (\mathbf{1} - \mathbf{S_r}) \cdot \mathbf{p_g}$$

Hydraulic model

- Permeability

	Planes	Tubes
	$\mathbf{k_{frac}} = \frac{\mathbf{h_b^2}}{\mathbf{12}} \frac{\mathbf{h_b}}{\mathbf{w}}$	$\mathbf{k_{tube}} = \boldsymbol{\pi} \frac{\mathbf{D_b^4}}{\mathbf{128 w^2}}$
Navier-Stokes equations	between two parallel plates	in a cylinder

Non-slip boundary conditions
Laminar flow
Steady state conditions
No body force

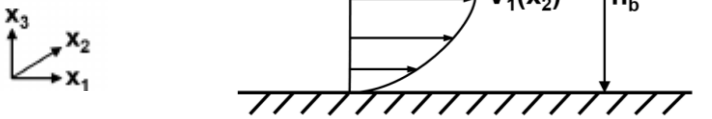

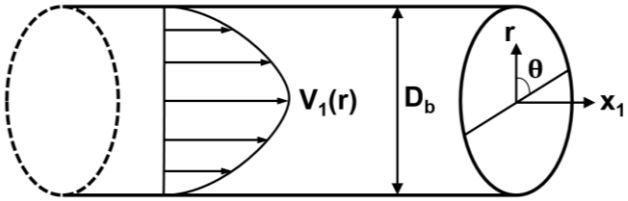

Hydro-mechanical multi-scale model

Macro-scale

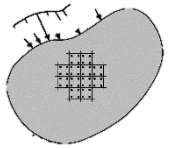

Micro-scale (REV)

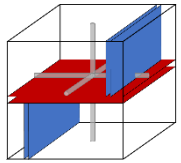

Mechanical model

- Isotropic elastic law
- Elasto-plastic law

$$(\boldsymbol{\sigma}, \boldsymbol{\varepsilon}) = \boldsymbol{f}(\mathbf{E}, \boldsymbol{\nu}, \mathbf{c}, \boldsymbol{\varphi})$$

Hydro-mechanical couplings

- Effective stress definition

[Bishop, 1959]

$$\boldsymbol{\sigma}' = \boldsymbol{\sigma} - \mathbf{p} \qquad \mathbf{p} = \mathbf{S_r} \cdot \mathbf{p_w} + (\mathbf{1} - \mathbf{S_r}) \cdot \mathbf{p_g}$$

Hydraulic model

	Planes	Tubes
► Permeability	$\mathbf{k_{frac}} = \frac{\mathbf{h_b^2}}{\mathbf{12}} \frac{\mathbf{h_b}}{\mathbf{w}}$	$\mathbf{k_{tube}} = \boldsymbol{\pi} \frac{\mathbf{D_b^4}}{\mathbf{128 w^2}}$
► Multi-phase flow [Yuster et al., 1951]	$\mathbf{k_{rw}} = \frac{\mathbf{S_r^{*2}}}{\mathbf{2}}(\mathbf{3} - \mathbf{S_r^*})$	$\mathbf{k_{rw}} = \mathbf{S_r^{*2}}$
	$\mathbf{k_{rg}} = (\mathbf{1} - \mathbf{S_r^*})^{\mathbf{3}}$	$\mathbf{k_{rg}} = (\mathbf{1} - \mathbf{S_r^*})^{\mathbf{2}}$

Integrating Navier-Stokes in each stratum considering that the fluids are flowing simultaneously

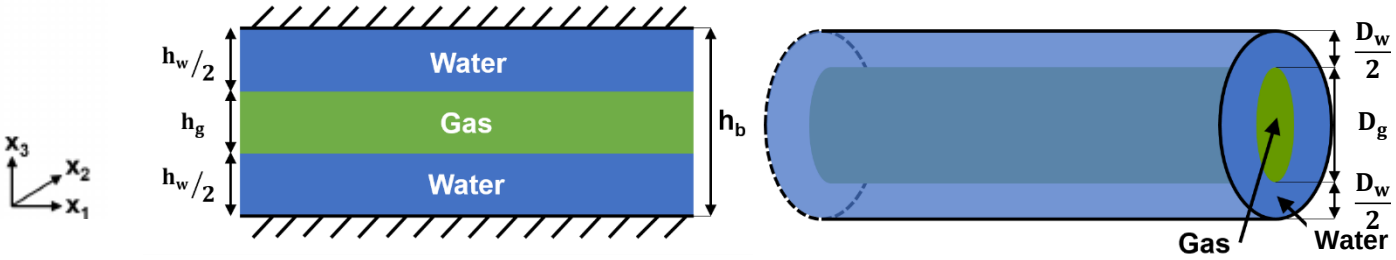

Hydro-mechanical multi-scale model

Macro-scale

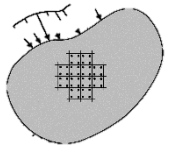

Micro-scale (REV)

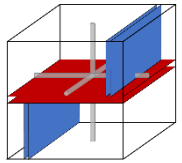

Mechanical model

- Isotropic elastic law
- Elasto-plastic law

$$(\boldsymbol{\sigma}, \boldsymbol{\varepsilon}) = \boldsymbol{f}(\mathbf{E}, \boldsymbol{\nu}, \mathbf{c}, \boldsymbol{\varphi})$$

Hydro-mechanical couplings

- Effective stress definition
  [Bishop, 1959]

$$\boldsymbol{\sigma}' = \boldsymbol{\sigma} - \mathbf{p} \qquad \mathbf{p} = \mathbf{S_r} \cdot \mathbf{p_w} + (\mathbf{1} - \mathbf{S_r}) \cdot \mathbf{p_g}$$

Hydraulic model

	Planes	Tubes
► Permeability	$\mathbf{k_{frac}} = \frac{\mathbf{h_b^2}}{\mathbf{12}} \frac{\mathbf{h_b}}{\mathbf{w}}$	$\mathbf{k_{tube}} = \boldsymbol{\pi} \frac{\mathbf{D_b^4}}{\mathbf{128 w^2}}$
► Multi-phase flow [Yuster et al., 1951]	$\mathbf{k_{rw}} = \frac{\mathbf{S_r^{*2}}}{\mathbf{2}}(\mathbf{3} - \mathbf{S_r^*})$	$\mathbf{k_{rw}} = \mathbf{S_r^{*2}}$
	$\mathbf{k_{rg}} = (\mathbf{1} - \mathbf{S_r^*})^3$	$\mathbf{k_{rg}} = (\mathbf{1} - \mathbf{S_r^*})^2$
► Retention curve [van Genuchten., 1980]	$\mathbf{S_{rw}} = \mathbf{S_{r,res}} + (\mathbf{S_{max}} - \mathbf{S_{r,res}}) \left(\mathbf{1} + \left(\frac{\mathbf{p_c}}{\mathbf{P_r}} \right)^{\mathcal{N}} \right)^{\frac{\mathbf{1}}{\mathcal{N}} - \mathbf{1}}$	
	$\mathbf{P_{r,0}} = \frac{\mathbf{2\sigma \cos \theta}}{\mathbf{h_b}}$	$\mathbf{P_{r,0}} = \frac{\mathbf{2\sigma \cos \theta}}{\mathbf{D_b/2}}$

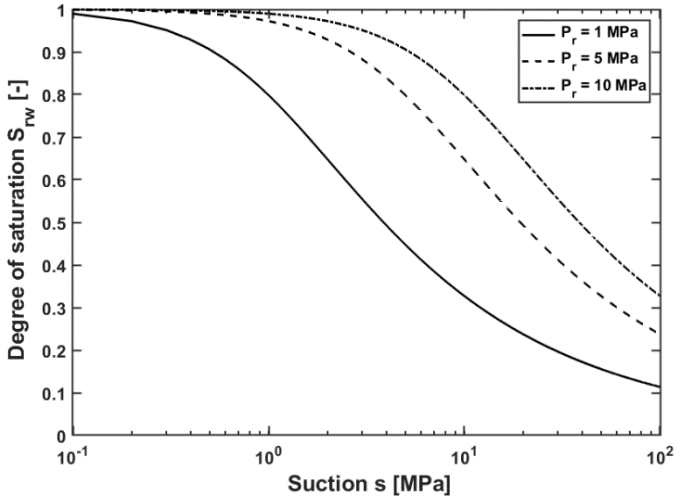

Hydro-mechanical multi-scale model

Macro-scale

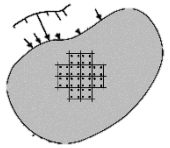

Micro-scale (REV)

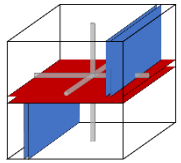

Mechanical model

- Isotropic elastic law
- Elasto-plastic law

$$(\boldsymbol{\sigma}, \boldsymbol{\varepsilon}) = \boldsymbol{f}(\mathbf{E}, \boldsymbol{\nu}, \mathbf{c}, \boldsymbol{\varphi})$$

Hydro-mechanical couplings

- Effective stress definition
  [Bishop, 1959]

$$\boldsymbol{\sigma}' = \boldsymbol{\sigma} - \mathbf{p} \qquad \mathbf{p} = \mathbf{S_r} \cdot \mathbf{p_w} + (\mathbf{1} - \mathbf{S_r}) \cdot \mathbf{p_g}$$

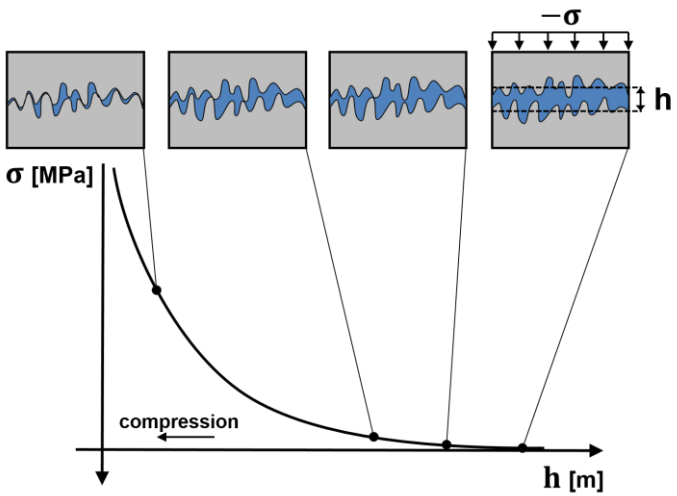

Modified after [Cerfontaine et al., 2015]

Hydraulic model

	Planes	Tubes
► Permeability	$\mathbf{k_{frac}} = \frac{\mathbf{h_b^2}}{\mathbf{12}} \frac{\mathbf{h_b}}{\mathbf{w}}$	$\mathbf{k_{tube}} = \boldsymbol{\pi} \frac{\mathbf{D_b^4}}{\mathbf{128 w^2}}$
► Multi-phase flow [Yuster et al., 1951]	$\mathbf{k_{rw}} = \frac{\mathbf{S_r^{*2}}}{\mathbf{2}}(\mathbf{3} - \mathbf{S_r^*})$	$\mathbf{k_{rw}} = \mathbf{S_r^{*2}}$
	$\mathbf{k_{rg}} = (\mathbf{1} - \mathbf{S_r^*})^{\mathbf{3}}$	$\mathbf{k_{rg}} = (\mathbf{1} - \mathbf{S_r^*})^{\mathbf{2}}$
► Retention curve [van Genuchten., 1980]	$\mathbf{S_{rw}} = \mathbf{S_{r,res}} + (\mathbf{S_{max}} - \mathbf{S_{r,res}}) \left(\mathbf{1} + \left(\frac{\mathbf{p_c}}{\mathbf{P_r}} \right)^{\mathcal{N}} \right)^{\frac{\mathbf{1}}{\mathcal{N}} - \mathbf{1}}$	
	$\mathbf{P_{r,0}} = \frac{\mathbf{2\sigma \cos \theta}}{\mathbf{h_b}}$	$\mathbf{P_{r,0}} = \frac{\mathbf{2\sigma \cos \theta}}{\mathbf{D_b/2}}$

Hydro-mechanical couplings

► Mechanical aperture [Goodman., 1976]	$\dot{\mathbf{h}}_{\mathbf{b(x)}} = \frac{\dot{\boldsymbol{\sigma}}'_{\mathbf{(xx)}}}{\mathbf{K_{n(x)}}}$	$\dot{\mathbf{D}}_{\mathbf{b(x)}} = \frac{\dot{\boldsymbol{\sigma}}'_{\mathbf{(xx)}}}{\mathbf{K_{(x)}}}$
	$\mathbf{K_n} = \frac{\mathbf{K_n^0}}{\left(\mathbf{1} - \frac{\mathbf{h_0} - \mathbf{h}}{\mathbf{h_0}}\right)^{\mathbf{2}}}$	$\mathbf{K} = \frac{\mathbf{2G}}{\mathbf{D_0}}$

Hydro-mechanical multi-scale model

Macro-scale

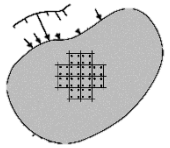

Micro-scale (REV)

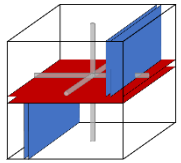

Mechanical model

- Isotropic elastic law
- Elasto-plastic law

$$(\boldsymbol{\sigma}, \boldsymbol{\varepsilon}) = \boldsymbol{f}(\mathbf{E}, \boldsymbol{\nu}, \mathbf{c}, \boldsymbol{\varphi})$$

Hydro-mechanical couplings

- Effective stress definition
  [Bishop, 1959]

$$\boldsymbol{\sigma}' = \boldsymbol{\sigma} - \mathbf{p} \qquad \mathbf{p} = \mathbf{S_r} \cdot \mathbf{p_w} + (\mathbf{1} - \mathbf{S_r}) \cdot \mathbf{p_g}$$

Model implemented in the FE code LAGAMINE

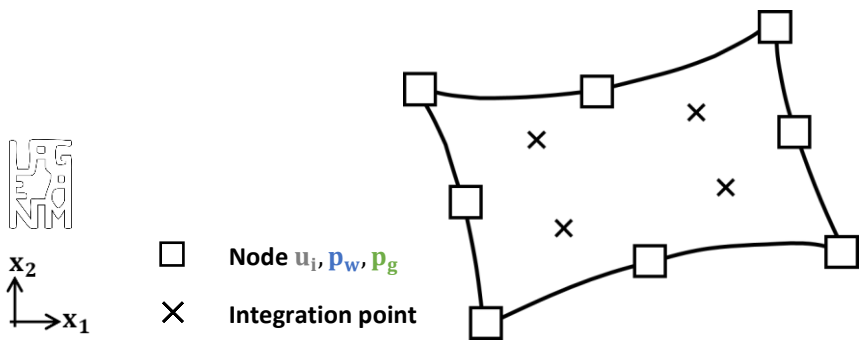

Hydraulic model

	Planes	Tubes
► Permeability	$\mathbf{k_{frac}} = \frac{\mathbf{h_b^2}}{\mathbf{12}} \frac{\mathbf{h_b}}{\mathbf{w}}$	$\mathbf{k_{tube}} = \boldsymbol{\pi} \frac{\mathbf{D_b^4}}{\mathbf{128 w^2}}$
► Multi-phase flow [Yuster et al., 1951]	$\mathbf{k_{rw}} = \frac{\mathbf{S_r^{*2}}}{\mathbf{2}}(\mathbf{3} - \mathbf{S_r^*})$	$\mathbf{k_{rw}} = \mathbf{S_r^{*2}}$
	$\mathbf{k_{rg}} = (\mathbf{1} - \mathbf{S_r^*})^{\mathbf{3}}$	$\mathbf{k_{rg}} = (\mathbf{1} - \mathbf{S_r^*})^{\mathbf{2}}$
► Retention curve [van Genuchten., 1980]	$\mathbf{S_{rw}} = \mathbf{S_{r,res}} + (\mathbf{S_{max}} - \mathbf{S_{r,res}}) \left(\mathbf{1} + \left(\frac{\mathbf{p_c}}{\mathbf{P_r}} \right)^{\mathcal{N}} \right)^{\frac{\mathbf{1}}{\mathcal{N}} - \mathbf{1}}$	
	$\mathbf{P_{r,0}} = \frac{\mathbf{2\sigma \cos \theta}}{\mathbf{h_b}}$	$\mathbf{P_{r,0}} = \frac{\mathbf{2\sigma \cos \theta}}{\mathbf{D_b/2}}$

Hydro-mechanical couplings

	Planes	Tubes
► Mechanical aperture [Goodman., 1976]	$\dot{\mathbf{h}}_{\mathbf{b(x)}} = \frac{\dot{\boldsymbol{\sigma}}'_{\mathbf{(xx)}}}{\mathbf{K_{n(x)}}}$	$\dot{\mathbf{D}}_{\mathbf{b(x)}} = \frac{\dot{\boldsymbol{\sigma}}'_{\mathbf{(xx)}}}{\mathbf{K_{(x)}}}$
	$\mathbf{K_n} = \frac{\mathbf{K_n^0}}{\left(\mathbf{1} - \frac{\mathbf{h_0} - \mathbf{h}}{\mathbf{h_0}}\right)^{\mathbf{2}}}$	$\mathbf{K} = \frac{\mathbf{2G}}{\mathbf{D_0}}$
→Permeability (implicit)		
→Entry pressure (implicit)	$\mathbf{P_r} = \mathbf{P_{r,0}} \left(\frac{\mathbf{h_{b_0}}}{\mathbf{h_b}} \right)^{\mathbf{m}}$	$\mathbf{P_r} = \mathbf{P_{r,0}} \left(\frac{\mathbf{D_{b_0}}}{\mathbf{D_b}} \right)^{\mathbf{m}}$

Applications

Gas injection experiment (lab scale, BC)

Characterisation of the sample

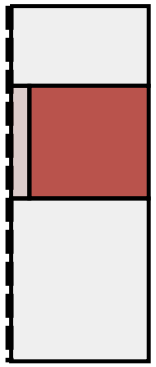

1. **Size of the REV** — Bedding plane separation $\mathbf{w = 300\ \mu m}$

[Gonzalez-Blanco, 2017]

FESEM	µ-CT
150 – 270 μm	410 – 560 μm

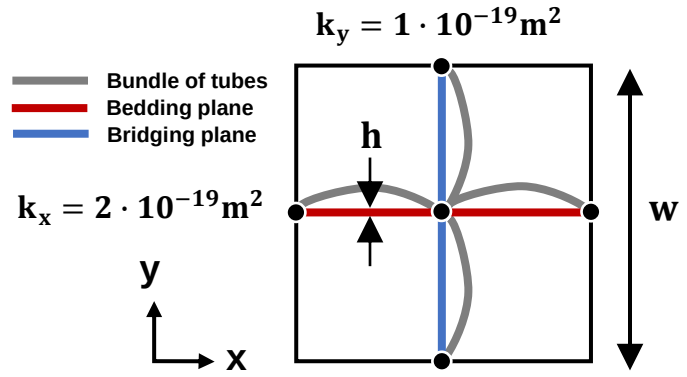

2. **Macro-porosity** — Fitting of the pore size distribution

Effect of small-size pores
(Tortuosity = Calibration factor)

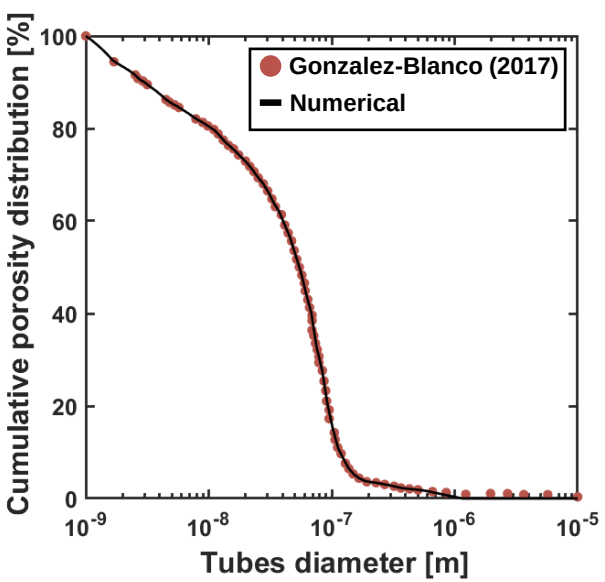

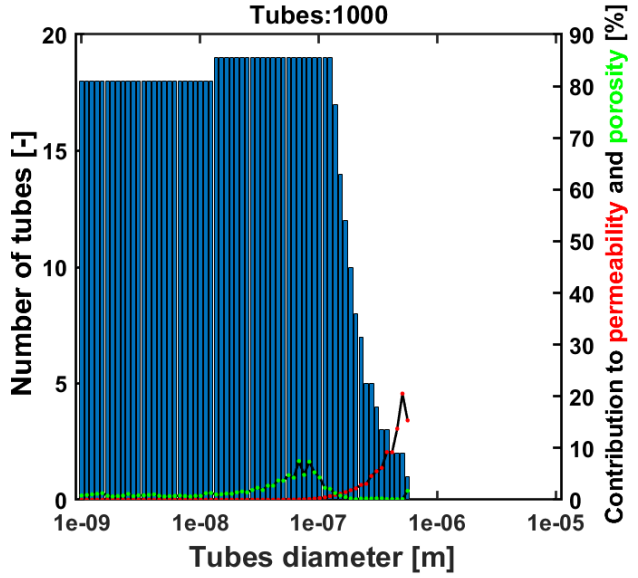

3. **Global permeability** — Effect of large-size pores

Fracture aperture

$$k_{x,frac,0} = 10^{-19} m^2$$

$$\rightarrow h_{b,0} = \sqrt[3]{12\, w\, k}$$

Macro-pores

$$k_x = \frac{\pi}{8}\left(\frac{D_b}{2}\right)^4\left(\frac{1}{w^2}\right) + \overbrace{\frac{h_b^2}{12}\left(\frac{h}{w}\right)}^{k_{x,frac}}$$

$$k_y = \frac{\pi}{8}\left(\frac{D_b}{2}\right)^4\left(\frac{1}{w^2}\right)$$

Applications

Gas injection experiment (lab scale, BC)

Characterisation of the sample

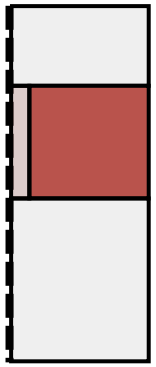

4. Relative permeability curves

[Yuster et al., 1951]

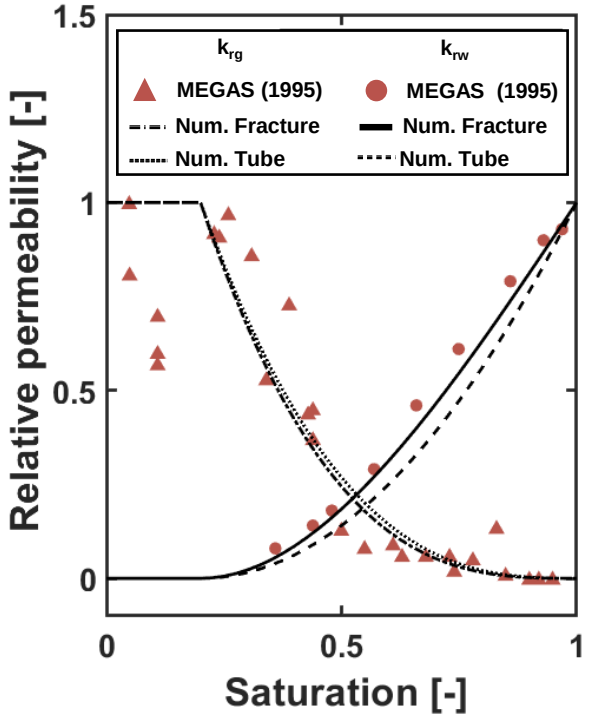

Planes

$$k_{rw} = \frac{S_r^{*2}}{2}(3 - S_r^*)$$

$$k_{rg} = (1 - S_r^*)^3$$

Tubes

$$k_{rw} = S_r^{*2}$$

$$k_{rg} = (1 - S_r^*)^2$$

5. Retention curve

[van Genuchten, 1980]

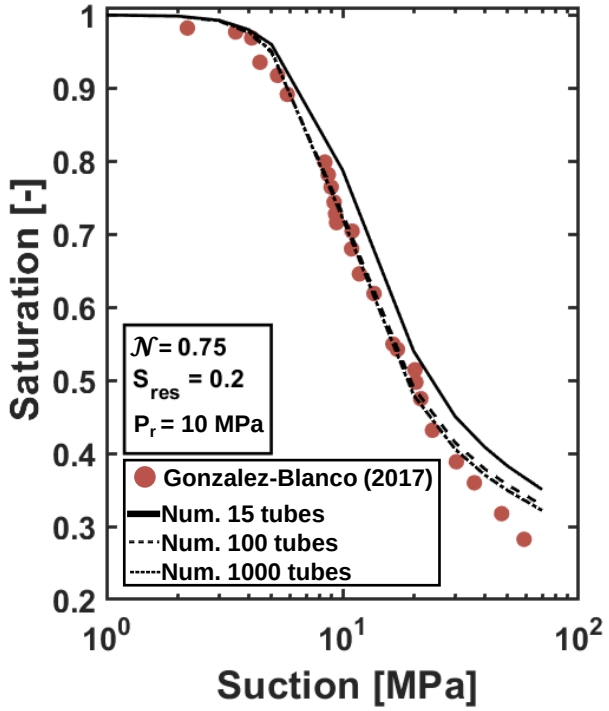

$$S_{rw} = S_{r,res} + (S_{max} - S_{r,res})\left(1 + \left(\frac{p_c}{P_r}\right)^{\mathcal{N}}\right)^{\frac{1}{\mathcal{N}}-1}$$

6. Normal stiffness of the fracture

[Goodman, 1976]

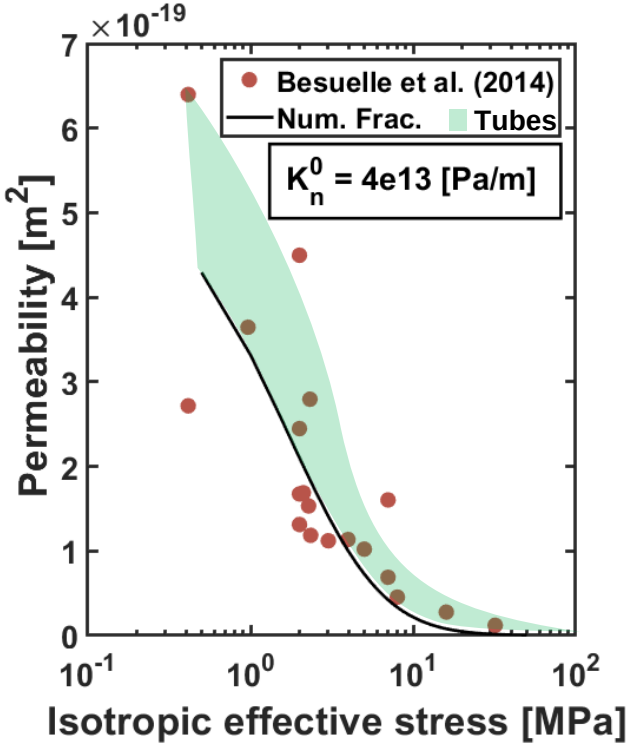

$$\dot{h}_{b(x)} = \frac{\dot{\sigma}_{(xx)}}{K_{n(x)}} \qquad K_n = \frac{K_n^0}{\left(1 - \frac{h_0 - h}{h_0}\right)^2}$$

Applications

Gas injection experiment (lab scale, BC)

Characterisation of the ZFD

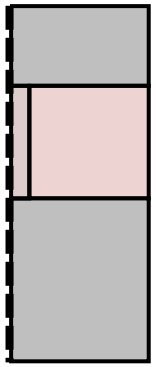

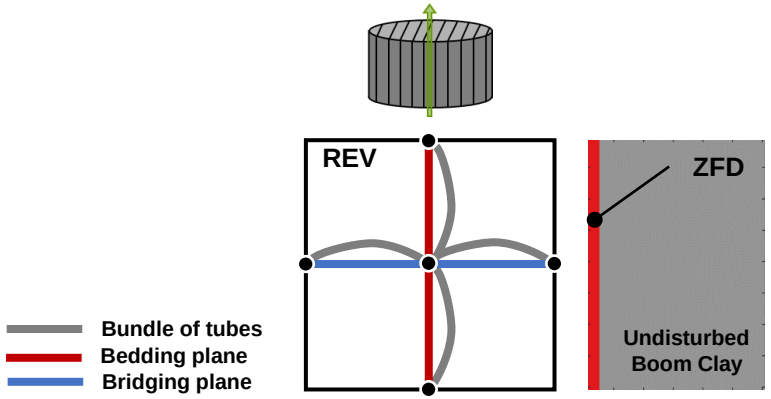

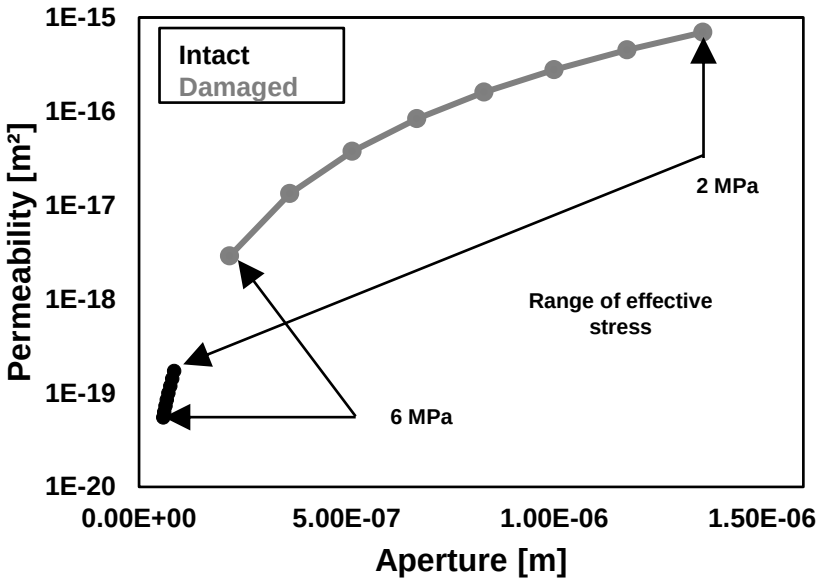

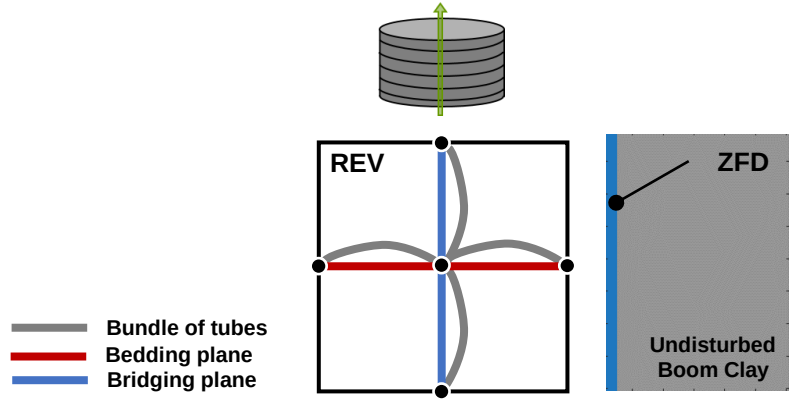

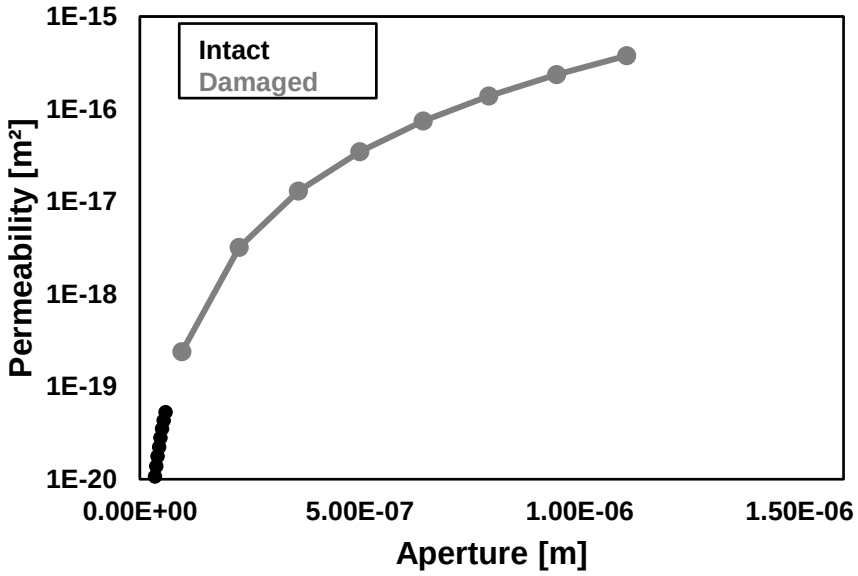

Characterisation of the reservoirs

Stiff elements with a high conductivity and a flat retention curve

Multi-scale application

Geometry and boundary conditions

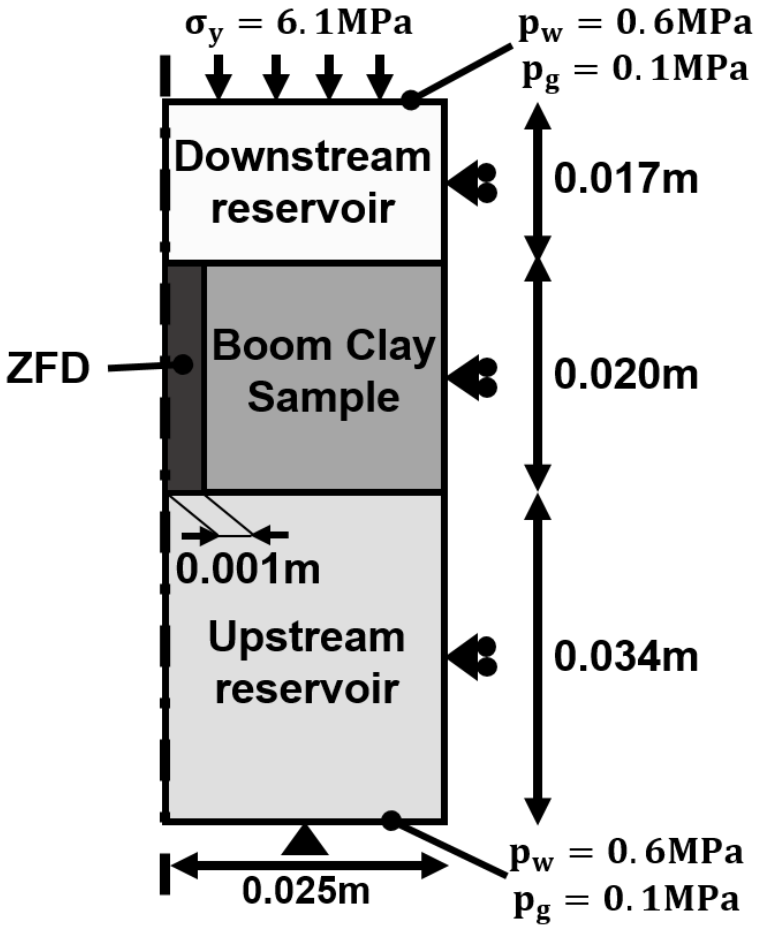

Parameters

Reservoirs

- Stiff elements: $E = 10000MPa$ $\nu = 0.3$
- Highly conductive: $n = 0.5$ $k = 10^{-10}m^2$
- Flat retention curve: $P_{entry} = 0.01MPa$

Boom Clay matrix

- Mechanical: $E = 200 - 400MPa$ $\nu = 0.33$
- Hydraulic:
  - Initial aperture: $0.80 - 1.27 \cdot 10^{-7}m$
  - Initial permeability: $2.0 - 4.0 \cdot 10^{-19}m^2$
  - Initial porosity: 0.363

Boom Clay Zone of Fracture Development (ZFD)

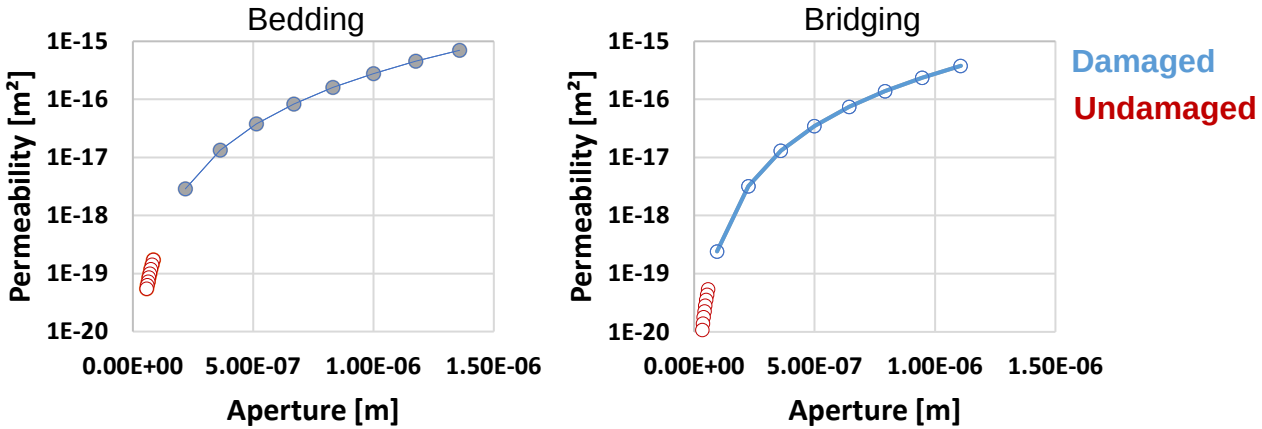

Multi-scale application

Fracture aperture

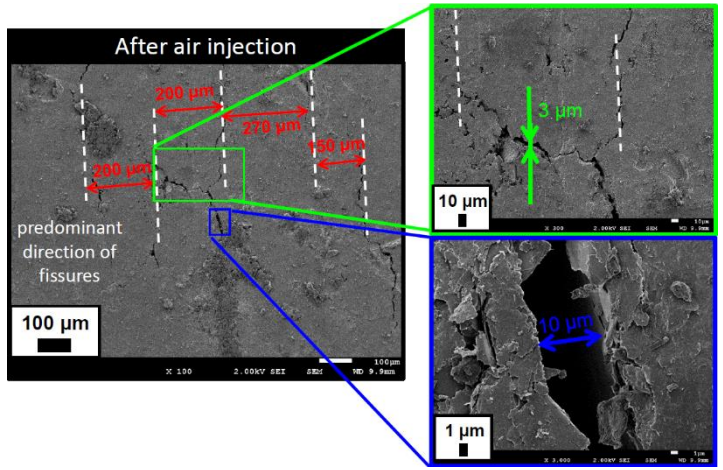

Experimental observations: Opened fractures after injection

Gonzalez-Blanco & Romero (2022)

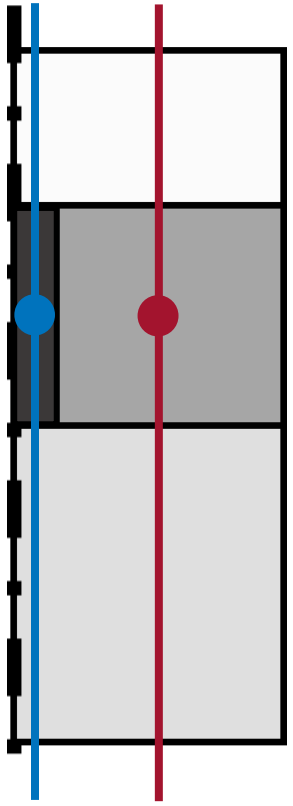

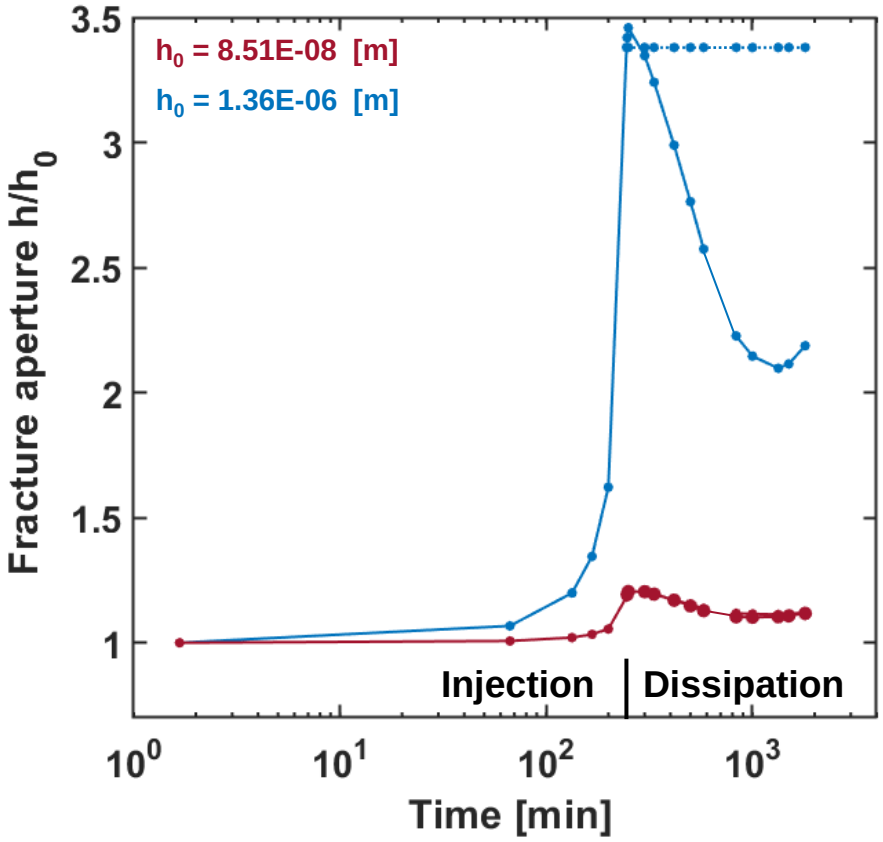

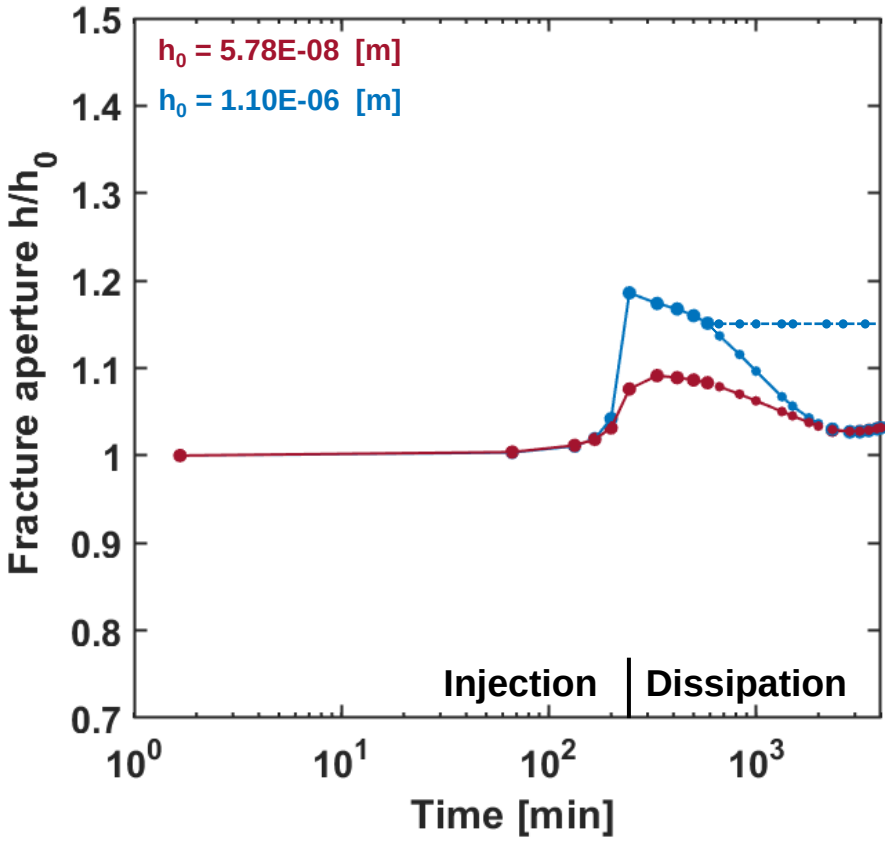

Multi-scale application

Fracture aperture

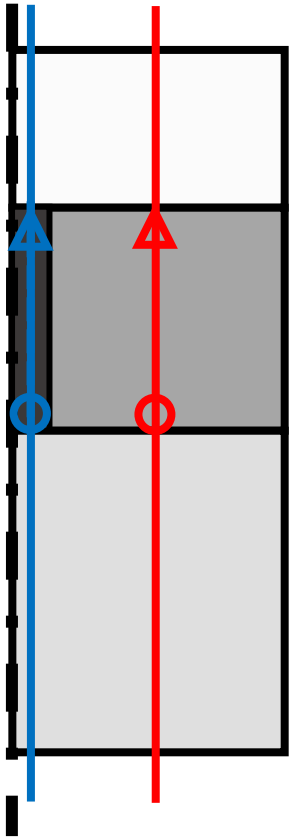

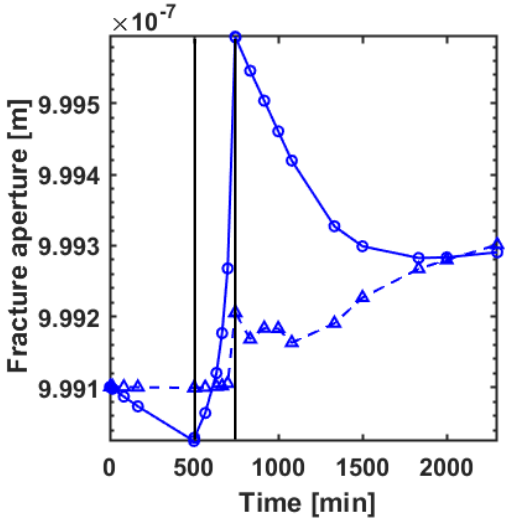

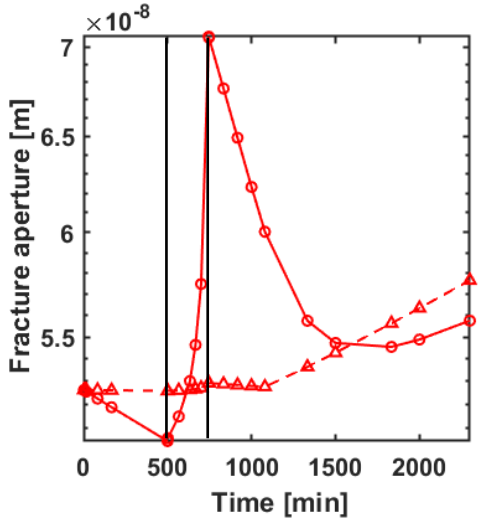

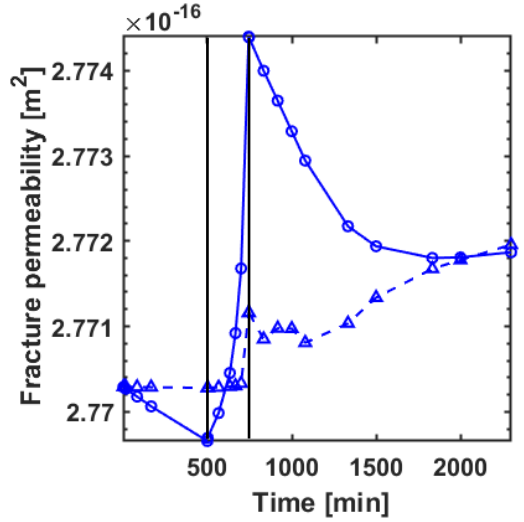

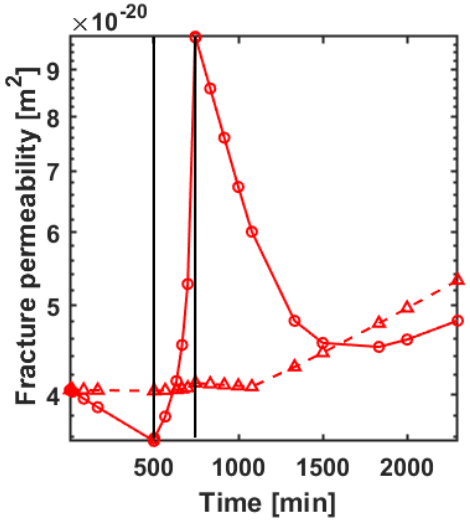

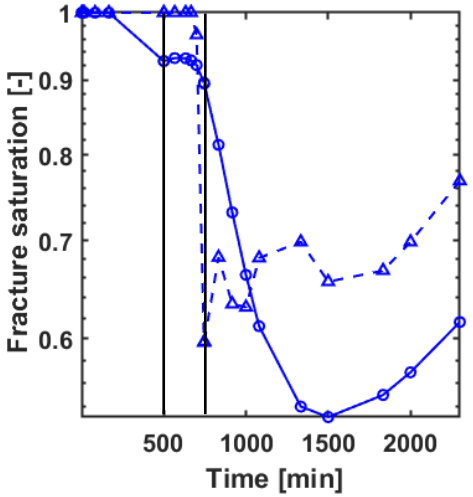

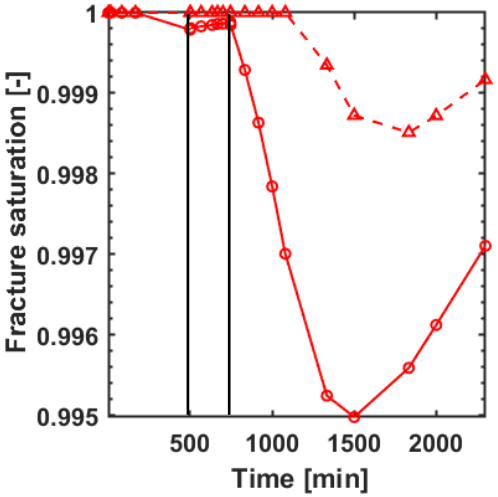

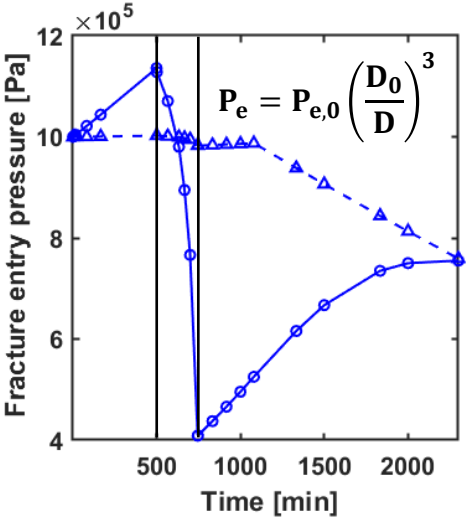

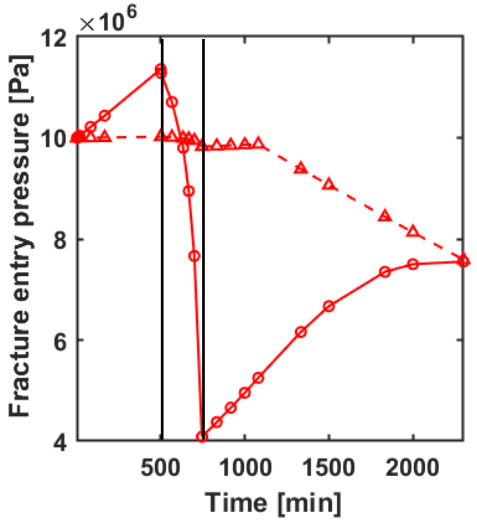

Original contributions

Second gradient H^2M model [Corman et al., 2022]

- A new degree of freedom for **gas**
- A **biphasic fluid transfer model** into the second gradient framework.
- **HM couplings** between the transfer properties and the deformations
- **Small-scale** and **large-scale applications** to assess the impact of the HM couplings inherent to the EDZ on gas flows

Multi-scale HM model [Corman et al. 2024] (under review)

- **Microstructure** (tube and fracture), and related parameters for clay rocks
- **HM couplings** between the transfer properties (micro-scale) and the stress state (macro-scale)
- Mechanism of **diffusion of dissolved gas** within the liquid phase
- **Lab-scale** gas injection tests and of **up-scaled configurations**, to assess the potential development of gas preferential pathways

Perspectives

Integration of the models

- **3D modelling**
- **Stochastic approach**
- **Predictability**

- Improve the fracture modelling
  - Integrate other types of fractures
  - Investigate the onset of strain localisation
- Improve the coupled processes modelling
  - Thermal effects
  - Self-sealing capacity

- Improve the coupled processes modelling
  - Macroscopic fractures
  - Self-sealing capacity
- Improve the integration of heterogeneity and variability